ULTRAHARMONIC IVUS IMAGING OF MICROVASCULARIZATION

David Maresca

2013

Financial support for the publication of this thesis was kindly provided by:

- Infraredx, Inc. (Burlington, MA, USA)
- Cardialysis BV (Rotterdam, the Netherlands)

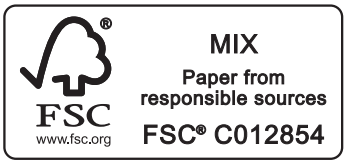

Cover design by Marie Maresca.

Editing by Emmanuel Fombaron.

ISBN 978-94-6108-466-8

Ultraharmonic IVUS Imaging of Microvascularization

Ultraharmonische IVUS beeldvorming van microvasculatuur

Thesis

to obtain the degree of doctor from the
Erasmus University Rotterdam
by command of the Rector Magnificus

Prof.dr. H.G. Schmidt

and in accordance with the decision of the Doctoral Board.

The public defense shall be held on
Tuesday June 18, 2013 at 15.30 hours by

David Maresca
born in Paris, France

Doctoral Committee

Promotors:	Prof.dr.ir. A.F.W. van der Steen
	Prof.dr.ir N. de Jong
Other members:	Prof.dr. A. van der Lugt
	Dr. E.S. Regar
	Dr. E. Stride
Copromotor:	Dr. G. van Soest

à Paul

TABLE OF CONTENTS

1.

Introduction

CORONARY ARTERY ANATOMY

The coronary arteries are major blood vessels branching along the heart surface to convey nutrients and oxygen carried in the blood to the heart muscle cells. In turn, the heart ensures the perpetual transportation of blood throughout the other organs of the circulatory system. Coronary arteries comprise the right and left coronary artery. Both originate from the root of the aorta. The left main coronary artery (LCA) gives off the left circumflex artery (LCX) and continues its descent as the left anterior descending coronary artery (LAD). The LCX runs around the left border of the heart to reach the posterior surface where it supplies the left ventricle muscle. The LAD and its branches supply two thirds of the anterior heart surface. The right coronary artery (RCA) descends along the border of the right atrium and the right ventricle to supply the right ventricle muscle. A simplified representation of the coronary artery anatomy is represented in Figure 1.

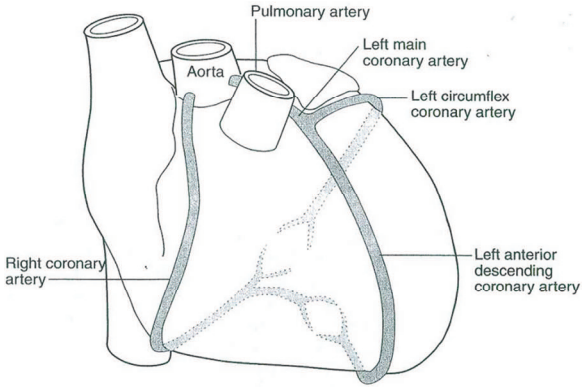

Figure 1. Simplified representation of the coronary artery anatomy. Intra-coronary catheters are inserted from the root of the aorta either in the right or left coronary artery. [1]

CORONARY ATHEROSCLEROSIS AND THE VULNERABLE PLAQUE

Atherosclerosis is a systemic chronic disease of the arterial wall [2, 3]. As late atherosclerosis developmental stages can become erratic and lead to ischemia, development of the disease in a major nutrient vessel such as a coronary artery can set the stage for a heart attack. Coronary atherosclerosis is one of the leading causes of premature death worldwide and results in the loss of productive life years for society.

Over the past 20 years, physicians' vision and understanding of atherosclerosis drastically evolved [4]. Atherosclerosis was perceived as the passive accumulation of cholesterol on the arterial wall, leading to total vessel occlusion and the subsequent loss of the organ function. Research efforts in the vascular biology of atherosclerosis have since revealed dynamic cellular mechanisms that start within the arterial wall, where inflammation adversely supports atherosclerotic lesions progression (referred to as plaques) from onset till occasionally rupture. The current view is that most adverse cardiac events result from the rupture of an atherosclerotic plaque [5] rather than from plaque growth until total vessel occlusion. It is the anomalous encounter of plaque content with luminal blood that leads to ischemia via thrombogenesis (blood clot formation).

In 1989, Dr. James Muller and colleagues introduced the term "Vulnerable Plaque" to describe a plaque at high risk of disruption that leads to coronary thrombosis [6]. The identification of vulnerable coronary atherosclerotic plaques, susceptible to rupture and therefore candidates for intervention remains today a central issue in cardiac imaging. The terminology of high-risk and vulnerable coronary artery plaques was further specified in 2004 [7] but a medical debate on their adequate treatment is ongoing [8]. Plaque vulnerability is known to be related to composition, mechanical stress distribution, and inflammation state. Several markers of plaque vulnerability were identified [8, 9] and are represented in Figure 2 (schematic). In particular, the proliferation inside a plaque of nutrient microvessels (the vasa vasorum) is increasingly recognized as critical to plaque progression and may constitute an independent marker of vulnerability [3]. The cross section of a vulnerable human coronary atherosclerotic plaque is displayed in Figure 2.

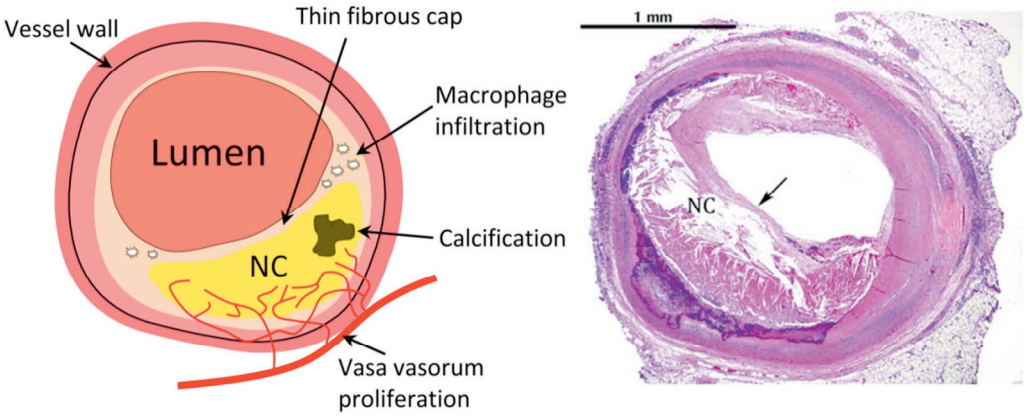

Figure 2. (Left) Markers of plaque vulnerability [10]. (Right) Histology of a human coronary artery vulnerable plaque (thin-cap fibroatheroma). Such a plaque configuration, that exhibits a large lipid pool covered by a thin fibrous cap (arrow), is associated with a high risk of rupture. The lumen appears white. NC stands for necrotic core (lipid rich region). [11]

CORONARY ATHEROSCLEROSIS MONITORING AND INTERVENTION

The standard procedure to visualize the entire coronary anatomy is coronary angiography. The technique consists in the real-time acquisition of X-ray images of the heart (angiograms) after the release of an X-ray contrast fluid by means of an intracoronary catheter. Angiography provides two dimensional projections of intracoronary blood volume which enables the localization of obstructed blood flow as well as the quantification of the degree of stenosis at these locations. It is important to realize that because it visualizes blood, coronary angiography informs on the luminal geometry of coronary arteries. Coronary angiography has a spatial resolution of 200 μm and temporal resolution of 5 ms [12]. In some case, coronary angiography can be ambiguous in detecting atherosclerotic plaques. Glagov et al. reported in 1987 that "many persons have an adequate, if not normal, lumen cross-sectional area in the presence of advanced atherosclerosis and that such a possibility should be taken into account in evaluating the extent and severity of disease with angiography" [13]. These observations demonstrated the need for techniques capable of imaging the coronary wall with a high resolution, as illustrated in Figure 3.

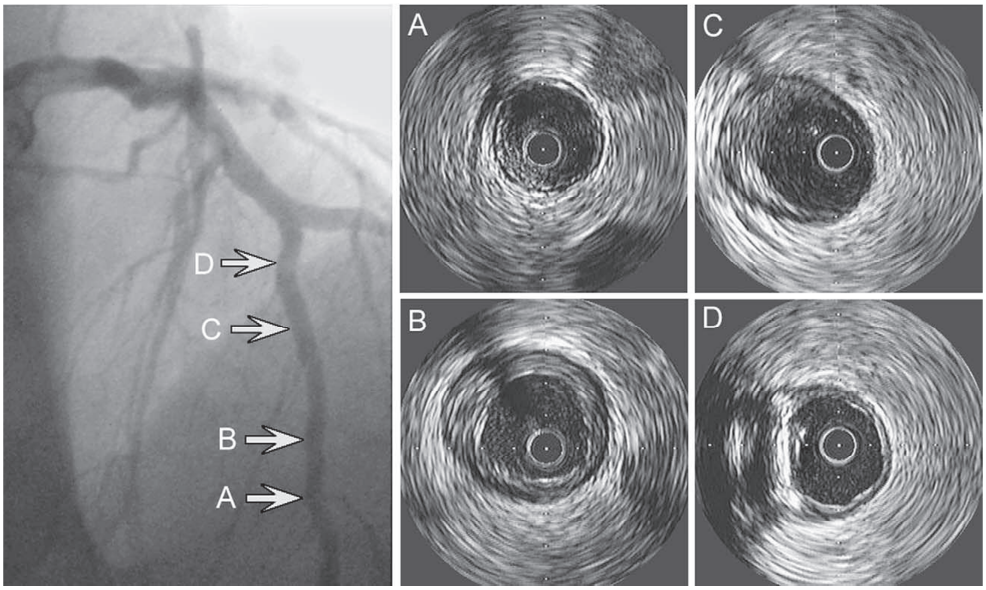

Figure 3. Local intravascular ultrasound images (A to D) detect the presence of coronary atherosclerosis plaques in the arterial wall, invisible in coronary angiography (left). [15]

The standard procedure for the treatment for symptomatic coronary atherosclerosis is to perform a percutaneous coronary intervention (PCI). A stent folded at the tip of a catheter is navigated under coronary angiography guidance to the coronary artery stenosis site. A stent is released in contact with the arterial wall in order to maintain the artery lumen open, which restores the impaired blood flow and prevents ischemia. Recently, bioresorbable stents (or scaffolds) were introduced to limit post-treatment complications such as late stent thrombosis observed with metal stents [14].

INTRAVASCULAR ULTRASOUND (IVUS)

Intravascular ultrasound (IVUS) is a catheter-based echocardiography modality that was invented at Erasmus MC in 1972 [16]. Twenty years later, IVUS was developed for its capacity to image the coronary artery wall with high resolution. IVUS technology consists in a miniaturized echography unit mounted at the tip of a catheter that is either made of a single piezoelectric transducer (40 to 60 MHz range) or of a 64 transducers circular array (20 MHz). IVUS catheters are side looking devices that display radial images perpendicular to the catheter axis. Single transducer IVUS images are acquired by mechanically rotating the transducer over 360 degrees while in circular array IVUS the ultrasound beam is steered electronically. IVUS image resolution is of the order of 100 μm in the axial direct (frequency dependent) and 300 μm in the lateral direction (transducer diameter dependent). In clinical practice, catheters are advanced through the groin until the root of the aorta and entered directly into the left or right coronary artery to inspect the status of the arterial wall. In vivo images of inner artery wall structures such as atherosclerotic plaques are created this way (Figures 2 and 3). IVUS has been used initially to ensure a more accurate local diagnosis of coronary atherosclerosis, since X-ray angiography can be ambiguous. Later on, IVUS played an important role in the standardization of balloon angioplasty and stent treatments. To date, prominent interventional cardiologists advocate IVUS guided PCI interventions [17]. IVUS provides plaque morphology, plaque burden, luminal diameter before intervention and helps defining optimal stent dimensions. After intervention, proper stent apposition can be controlled and potential complications can be assessed using IVUS (e.g. thrombus formation). IVUS technology also proved to be very useful in clinical trials. Since plaque progression and regression can be accurately measured with IVUS, the efficacy of new cardiovascular drugs can be assessed. The most valued IVUS functions are the estimation of the total plaque burden [18] (thanks to the delineation of the external elastic membrane) as well as calcium detection (Figure 4). Furthermore, IVUS penetration depth is sufficient to image side branches and large vessel diameters such as the left main coronary artery.

Yet, to predict the risk for future acute cardiovascular events, the knowledge of plaque composition is critical [20] but is not provided by conventional IVUS. Several modalities have been derived from IVUS radiofrequency signal analysis to enhance the detection and characterization of high risk coronary artery plaques, notably IVUS flow and IVUS palpography. The principle of IVUS flow is based on the analysis of decorrelation of the IVUS radiofrequency signals [21]. Red blood cells flowing in the ultrasound beam cause a decorrelation of successively received signals.

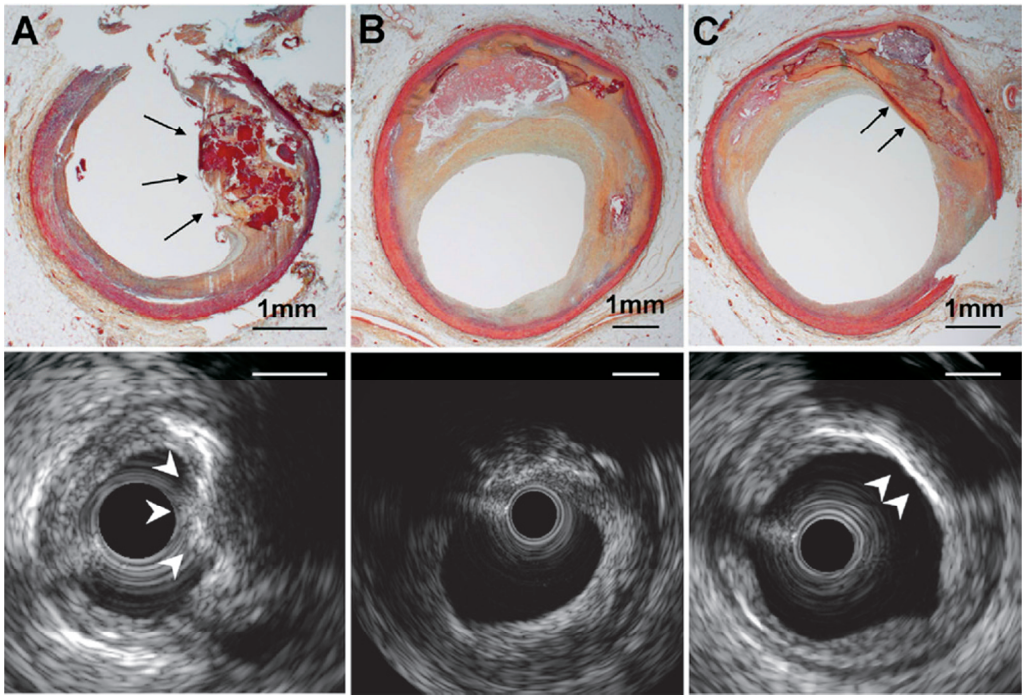

Figure 4. (A) An example of calcified nodule, (B) fibroatheroma, and (C) calcified fibrosis (non-nodular calcium) by pathology *(top)* and IVUS *(bottom)*. (A) Pathology of calcified nodule (Movat pentachrome stain) shows calcified nodule *(dark brown)* with accumulated fibrin *(red)* protruding into the lumen through a disrupted thin fibrous cap *(arrow)*. IVUS of the calcified nodule shows a convex and irregular (nonsmooth and lumpy) luminal surface *(arrowhead)*. (B) Pathology of late fibroatheroma shows luminal narrowing with necrotic core. (C) Pathology of non-nodular calcium shows a lump of calcium *(dark purple, arrow)*. IVUS shows a smooth concave luminal/calcified surface with high echogenicity *(arrow)*. [19]

The principle of IVUS flow is based on the analysis of decorrelation of the IVUS radiofrequency signals [21]. Red blood cells flowing in the ultrasound beam cause a decorrelation of successively received signals. The rate of decorrelation is proportional to the local blood flow velocity. These are then converted into color maps representing local instantaneous blood flow velocity in the arterial cross section. A color scheme is used, going from dark red (10 cm/s) to yellow (100 cm/s). Flow velocities are measured at 100 angular positions, with a depth resolution of 160 μm (Figure 5). Blood velocity and volumetric flow are valuable criteria to assess the severity of a stenosis.

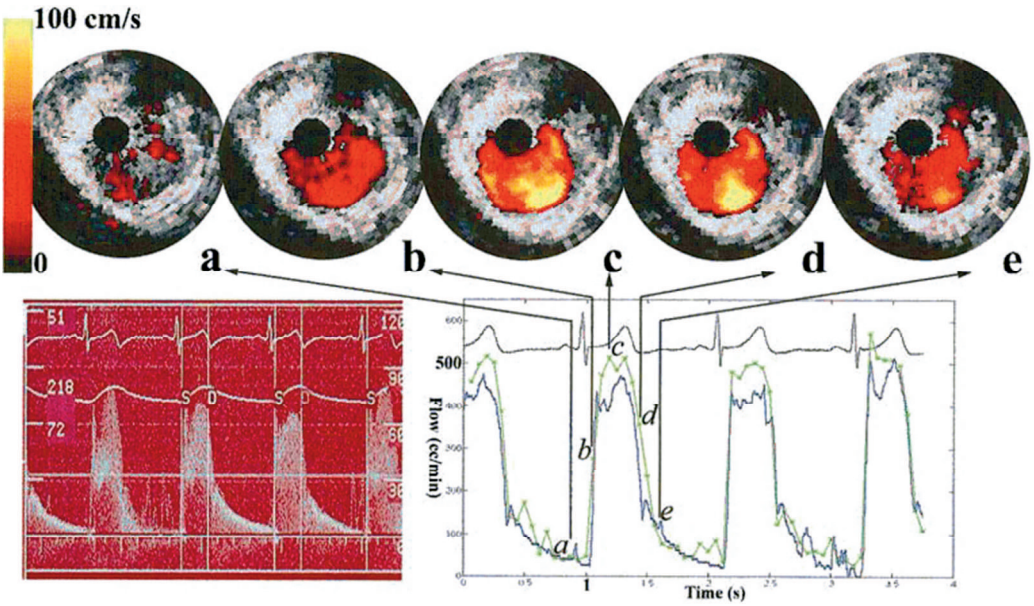

Figure 5. IVUS flow in the renal artery of a human patient [22]. Blood flow is mapped is red at different phases of the heart cycle. IVUS volumetric flow (green curve) was found is good agreement with Doppler volumetric flow (blue curve).

IVUS palpography capitalizes on the arterial wall deformation induced by the pulsatile intraluminal cardiac pressure. Since the strains in the radial and circumferential direction are the principal directions, there is a great benefit of using intravascular catheters; the ultrasound beams are more or less in the radial direction whereas the circumferential strain can be determined from displacements perpendicular to the ultrasound beams. For acquiring an intravascular elastogram, an IVUS catheter is inserted in a coronary artery and radiofrequency signals are recorded for the full circumference at low and high intraluminal pressure. Radial displacements are calculated by applying cross-correlation technique to each separate ultrasound line. From the displacements, the strain is calculated and plotted next to the IVUS echograms (Figure 6).

Strain information can also be visualized by overlaying simply the inner ring of strain values (the eventually rupture prone region) in IVUS image at the lumen vessel wall boundary [24]. Such an image is referred to as a palpogram and can be used to differentiate vulnerable plaques from stable ones. The IBIS-2 clinical trial reported that patients with vulnerable plaques that were treated with the inhibitor of an enzyme associated with inflammation activity showed a significant decrease in strain values in 12 months' time [25].

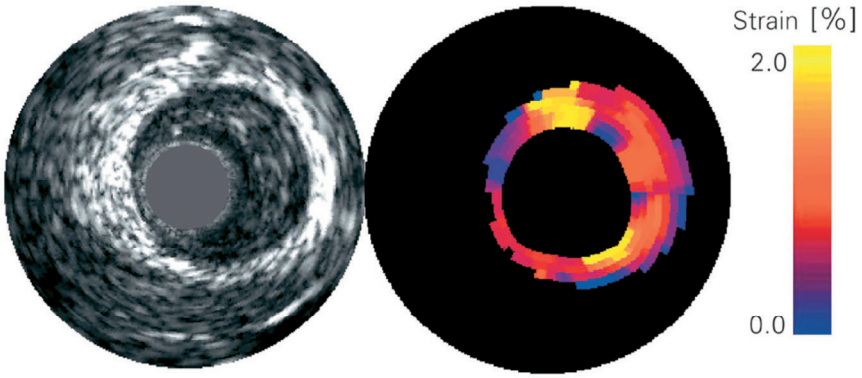

Figure 6. *In vivo* IVUS image of a human coronary plaque and corresponding elastogram. The elastogram reveals that the plaque has deformable edges with non-deformable surrounding tissue. High strain regions at the shoulders of a plaque are an indication of vulnerability, often related to the infiltration of macrophages. [23]

IVUS DETECTION OF INTRAPLAQUE VASA VASORUM

Larger blood vessels such as the coronary arteries require their own blood supply. It is provided by a network of microvessels that penetrate the inner layers of the arterial wall. This microvascular network is referred to as the vasa vasorum [26]. It is increasingly recognized that the progression of atherosclerotic plaques is associated with the development of neovascular vasa vasorum through the process of angiogenesis. This hypothesis was recently supported by 3D micro-CT images of ex vivo coronary arteries [27] as shown in Figure 7. To date however, there is no established clinical technique capable of imaging coronary vasa vasorum in vivo.

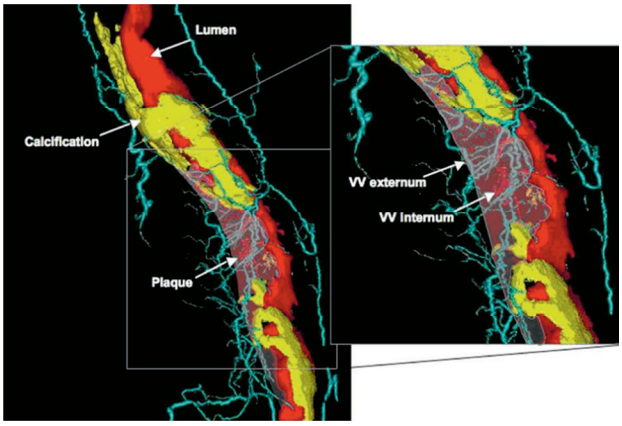

Figure 7. 3D micro computed tomography image of an ex vivo human coronary artery plaque. Vasa vasorum proliferation is visible in the plaque area. [28]

Exploratory work combining IVUS with an ultrasound contrast agent laid the foundation for what could be a unique clinical tool for coronary artery vasa vasorum imaging. An ultrasound contrast agent is a suspension of high molecular weight gas microbubbles encapsulated by thin lipid shells. Bubbles are typically designed to be of a size (1-10 μm) that passes through capillary beds and are acoustically active at diagnostic ultrasound frequencies. The primary advantages of using ultrasound contrast agents are the improvement of the signal strength from blood, which becomes bright in echographic images (a parallel can be drawn with bright blood pulse sequences in magnetic resonance imaging), and the detection of slow microvascular flow in the presence of tissue motion. Several studies reported extra-luminal image enhancement following the bolus injection of contrast agent, which has been attributed to the presence of vasa vasorum [29, 30]. The basis of this approach was to compare post-contrast injection images with a baseline image derived from a single point in the cardiac cycle. While these results were promising, the sensitivity and robustness of this method ultimately relied upon the assumption of similarity between images acquired at the same point in the cardiac cycle and, as such, was susceptible to acyclical catheter-vessel motion or non-uniform rotation velocity of the IVUS transducer. Nonetheless, this work motivated the development of contrast IVUS detection techniques based on bubble-specific signatures. Goertz et al. demonstrated the feasibility of nonlinear contrast IVUS for vasa vasorum imaging using a prototype IVUS transducer with a double frequency peak [31, 32]. Contrast mode images of blood circulation could be displayed by isolating the nonlinear second harmonic or subharmonic echoes backscattered by the ultrasound contrast agent as shown in Figure 8.

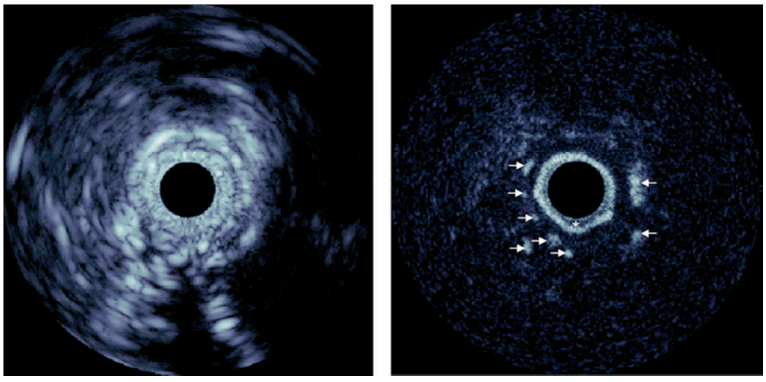

Figure 8. *In vivo* contrast IVUS image of an atherosclerotic rabbit aorta using decanted Definity. Left: fundamental mode at 20 MHz, 10 s after injection, in which changes in adventitial enhancement are not evident. Right: at 10 s after injection, the harmonic mode (transmit at 20 MHz, receive at 40 MHz) shows significant adventitial enhancement, consistent with the detection of adventitial microvessels. The white dots are contrast microbubbles in the vasa vasorum (white arrows), and the bright ring, contrast microbubbles inside the lumen (asterisk). Scale of images is 12 mm across. The dynamic range of the fundamental and harmonic image is 40 and 25 dB, respectively.

While these initial results were very promising, a great deal of work remains before contrast-enhanced IVUS imaging can be adopted in the clinic. Despite a good sensitivity, the prototype transducer utilized by Goertz et al. suffered from a lower spatial resolution than conventional clinical IVUS, because of the narrow bandwidth of its two frequency peaks (two-way 30% -6 dB relative bandwidth). It also became evident that existing IVUS catheters are far from optimal for the primary goal of vasa vasorum imaging. The bandwidth and sensitivity of commercial IVUS transducers is not adequate for second harmonic and subharmonic imaging (a -6 dB relative bandwidth of the order of 70% is required). In addition, nonlinear ultrasound propagation in biological tissue generates second harmonics that impair the specificity of second harmonic contrast imaging [32]. And subharmonic contrast IVUS imaging, which has been demonstrated with a tailored contrast agent size distribution, still needs to be evaluated with a commercial ultrasound contrast agent distribution.

THESIS OUTLINE

This thesis gathers in a comprehensive unit the principal contributions to the field of intravascular ultrasound vasa vasorum imaging that were achieved as a part of the Simon Stevin Meester grant 2007. The ambition was to develop and validate robust quantitative contrast IVUS imaging techniques able to establish the microvascular status of coronary atherosclerotic plaques. Furthermore, research efforts should be directed towards translation into clinical practice.

Chapter 2 presents a single transducer technique that capitalizes on the behavior of individual ultrasound contrast microbubbles at IVUS frequency to estimate the size distribution of an ultrasound contrast agent acoustically. It could help studying the retention of microbubbles that occurs *in vivo* in organs as the lungs and the kidneys.

Chapter 3 reports the 3D reconstruction of a vasa vasorum phantom using a commercial ultrasound contrast agent in combination with commercial IVUS equipment. This short study was thought as a tutorial that highlights the limitations of current IVUS systems in terms of nonlinear contrast imaging. Since the IVUS catheter bandwidth did not allow second harmonic or subharmonic imaging, the system was operated at the fundamental frequency. A non-diluted bolus of ultrasound contrast agent was needed to differentiate microbubbles from tissue. The drawback was that the contrast agent signal was saturated, rendering any quantitative hemodynamic assessments impossible.

Chapter 4 introduces chirp IVUS imaging and discusses its potential for both tissue and contrast imaging. Higher signal to noise ratios were achieved at equal peak negative pressure than conventional imaging pulses, translating into superior IVUS penetration depth and thus enhanced plaque burden assessment capabilities. Moreover, a chirp specific contrast imaging mode was successfully implemented on a conventional bandwidth-limited IVUS transducer.

Chapter 5 compares the performance of two novel narrowband contrast IVUS vasa vasorum imaging techniques, chirp reversal IVUS and ultraharmonic IVUS, that can operate within the bandwidth limitations of commercial IVUS transducers.

Chapter 6 reports the first in vivo IVUS image of a microvascular network and compares its accuracy to an optical reference measurement. The approach combines the superior sensitivity of chirp excitations with the specificity of ultraharmonics to deliver a robust artifact-free contrast-enhanced IVUS modality capable of detecting microvasculature invisible in conventional intracoronary imaging. Ultraharmonic IVUS has emerged as a promising method for the detection of coronary plaque neovascularization in humans.

Chapter 7 confronts the IVUS biomedical engineering research exposed in this thesis to the results of a sociology study of IVUS innovation. A representative network of experts with experience in IVUS was surveyed, comprising cardiologists, engineers, industry leaders and funders. We discuss the potential of IVUS technology and its future in light of the controversies conveyed by this international network of experts.

Chapter 8 concludes this thesis and suggests possible technological advances in the field of IVUS.

2.

Acoustic Sizing of an Ultrasound Contrast Agent

Based on the publication by D. Maresca, M. Emmer, P. L. van Neer, H. J. Vos, M. Versluis, M. Muller, N. de Jong, A. F. van der Steen, **Acoustic Sizing of an Ultrasound Contrast Agent**. *Ultrasound in Medicine & Biology* **36**, 1713-1721 (2010).

ABSTRACT

Because the properties of ultrasound contrast agent populations after administration to patients are largely unknown, methods able to study them noninvasively are required. In this study, we acoustically performed a size distribution measurement of the ultrasound contrast agent Definity®. Single lipid-shelled microbubbles were insonified at 25 MHz, which is considerably higher than their resonance frequency, so that their acoustic responses depended on their geometrical cross sections only. We calculated the size of each microbubble from their measured backscattered pressures. The acoustic size measurements were compared with optical reference size measurements to test their accuracy. Our acoustic sizing method was applied to 88 individual Definity® bubbles to derive a size distribution of this agent. The size distribution obtained acoustically showed a mean diameter (2.5 μm) and a standard deviation (0.9 μm) in agreement within 8% with the optical reference measurement. At 25 MHz, this method can be applied to bubble sizes larger than 1.2 μm in diameter. It was observed that similar sized bubbles can give different responses (up to a factor 1.5), probably because of shell differences. These limitations should be taken into account when implementing the method in vivo. This acoustic sizing method has potential for estimating the size distribution of an ultrasound contrast agent noninvasively.

INTRODUCTION

Encapsulated gas microbubbles, the constituents of medical ultrasound contrast agents (UCAs), are increasingly used clinically because they showed strong potential for organ perfusion diagnostics, capillary networks imaging and local therapy including drug or gene delivery and sonothrombolysis [33-35]. Commercial UCAs consist of bubble populations ranging from 0.5-10 μm in size and usually exhibit a mean diameter of 1-3 μm. Ultrasound contrast imaging techniques rely largely on the nonlinear scattering of contrast microbubbles [36, 37]. Bubble size has a great impact on the generation of higher harmonic energy scattered by an UCA [38, 39]. Microbubbles enhance echo contrast the most at their individual resonance frequencies. As an example, Definity® contrast bubbles (Lantheus Medical Imaging, Inc., North Billerica, MA, USA) are estimated to have a resonance frequency of 75 MHz for a bubble diameter of 0.5 μm, 27 MHz for a diameter of 1 μm and 10 MHz for a diameter of 2 μm [40]. Thus, ultrasound contrast imaging techniques benefit from different sized groups of an agent population depending on the frequency of the ultrasound field applied [41]. Contrast echocardiography or contrast liver imaging work in the 1-7 MHz range [42, 43], whereas contrast intravascular ultrasound [31, 32, 44] works in the 20-40 MHz range. Therefore, it is important to know the size distribution of an UCA. Standard particle size analyzers used to measure an UCA size distribution in vitro can be based on to the change of electric conductance of particles in a solution (Coulter principle), on laser diffraction of these particles (e.g., Mastersizer 2000, Malvern Instruments Ltd., Worcestershire, UK) or on the optical scanning of an agent population using a microscope [45]. However, the size distribution of UCA populations after human administration is unknown. Factors such as the gas concentration of the bubbles inside the body, the temperature elevation to 37°C [46] and the lung filtering of the largest bubbles [47, 48] make comparison with in vitro size distribution measurements unreliable. It is therefore of interest to offer experimental methods to measure UCA size distributions noninvasively [49]. Newhouse and Mohana Shankar [50] presented an ultrasound based double-frequency method of sizing bubbles, already envisioning the study of contrast agents for echocardiography as a potential application. Gas bubbles respond to a dual-frequency excitation by returning a signal at plus and minus the two frequencies, at resonance only. From the knowledge of the resonance frequency of a gas bubble, the radius can be readily determined. This idea was developed further [51] and an instrument to size and analyze bubbles with this technique was built and tested [52]. However, this double-frequency technique needs at least two transducers and was applied to size bubbles bigger than 30 μm only. Leighton et al. [53] suggested to size bubbles using ultrasound by applying eight different ultrasound methods simultaneously (e.g., broadband scattering, fundamental or harmonic scattering, two frequencies mixing at resonance). The limitations and advantages of the different methods compensate each other, providing

a sharper size estimation. The approach was successfully applied to a single gas bubble of radius 0.9 mm. None of these studies used high-frequency ultrasound (>10 MHz). Unfortunately, the resonance frequency of an encapsulated bubble is not an unambiguous determinant of its size because of the shell influence. Other research groups developed methods to determine the size distribution of lipid-shelled bubble clouds in vitro by fitting attenuation or backscattering simulations to their experimental acoustic pulse attenuation or scattering measurements [54, 55]. In this study, we suggest inspecting bubbles high above their resonance frequencies. In this condition, bubble responses depend on their geometrical cross section only, quasi-independent from their shell elasticity and viscosity [56]. Our objective was to take advantage of this feature to measure single bubble radii using ultrasound in pulse-echo mode. Such a noninvasive method can potentially be exploited to estimate the size distribution of an UCA in vivo. An acoustic sizing method was developed in our laboratory and applied to a population of 88 individual Definity® bubbles. The result is compared with an optical size measurement of the same bubbles. The theoretical background of this method is introduced and particular attention is given to the measurement system and its calibration, which enabled the derivation of the size of an UCA bubble from its echo amplitude.

THEORETICAL BACKGROUND

In this section, we are going to derive the equation to determine a bubble radius out of the acoustic pressure impinging on that bubble, the acoustic pressure scattered back by the bubble and the bubble-transducer distance. A gas bubble of radius R, insonified by an ultrasound wave of wavelength λ, scatters an omnidirectional pressure wave if $R << \lambda$ is assumed. The power scattered by the bubble, Ps, relates to the incident wave intensity, I_i, as $Ps = \sigma I_i$, where σ is the acoustic scattering cross section [57]. The intensity scattered by a point source is equal to the quotient of the scattered power and the spherical surface at distance z. For a spherical gas bubble, the incident and scattered intensities relate as:

$$I_s = \frac{\sigma I_i}{4\pi z^2} \tag{1}$$

where I_s is the scattered intensity. For harmonic plane waves, the intensity can be formulated as the quotient of the acoustic pressure squared divided by twice the acoustic impedance. Thus equation (1) can be rewritten as:

$$p_s = \frac{1}{z}\sqrt{\frac{\sigma}{4\pi}}p_i \tag{2}$$

where p_i is the incident pressure that hits the bubble and p_s the pressure scattered by the bubble. Medwin [57] has shown that the acoustic scattering cross section of a gas bubble in a liquid environment is expressed in the linear regime as:

$$\sigma(R,f)=\frac{4\pi R^2}{\left\{\left(\frac{f_0(R)^2}{f^2}\right)-1\right\}^2+\delta(R,f)^2} \tag{3}$$

where f is the frequency of the applied ultrasound field, f_0 the resonance frequency of the bubble and δ the total damping. This equation is also valid for encapsulated bubbles in the linear regime. The damping δ^2 for the microbubbles in this study is assumed to be much smaller than 1 [40, 58]. It follows that for $f >> f_0$, the acoustic scattering cross section becomes a function of R only:

$$\sigma(R,f)=4\pi R^2 \tag{4}$$

Combining eqns (2) and (4) at the bubble wall leads to:

$$p_s(R)=p_i(R) \tag{5}$$

The scattered pressure is equal to the incident pressure at the bubble wall. As $R << \lambda$, the pressure distribution over the bubble wall is homogeneous and the pressure wave is scattered equally in every direction. The pressure scattered at a distance z can be calculated using energy conservation in a lossless medium:

$$p_s^{\,2}(z)=\frac{4\pi R^2}{4\pi z^2}\,p_s^{\,2}(R) \tag{6}$$

Combining eqns (5) and (6), the bubble radius is expressed as:

$$R=z\,\frac{p_s(z)}{p_i(R)} \tag{7}$$

Equation (6) states that, for $f >> f_0$, the radius of a bubble can be derived from its backscattered pressure once the distance and the pressure impinging on the bubble wall are known. This holds for lipid-shelled bubbles as well as gas bubbles.

METHODS

Measurement system overview | The combined optical and acoustic single-bubble size measurement setup (Fig. 1) consisted of an arbitrary waveform generator (AWG520, Tektronix, Beaverton, OR, USA) and a 60 dB RF linear power amplifier (LPI-10, ENI, Rochester, NY, USA) linked to generate and amplify the transmit pulses (25MHz, 30% bandwidth Gaussian pulses). A low-noise amplifier (Miteq, Hauppauge, NY, USA) amplified the received signals by 60 dB. These were then digitized at 200 MHz by a 12 bit A/D PCIcard (DP310, Acqiris, Geneva, Switzerland). A 25 MHz single-element focused transducer (Panametrics NDT, 1-inch focus, 54% -6 dB bandwidth; Olympus NDT, Waltham, MA, USA) was mounted to a water tank. The UCA Definity® was injected with a syringe in a 200 μm diameter cellulose capillary (Spectrum Laboratories Inc., 132294, Breda, The Netherlands), which crossed the transducer beam focus inside the water tank. The tank holding the transducer and the capillary was placed on the translation stage of a microscope (Olympus BH-2 research microscope, Olympus Corporation, Zoeterwoude, The Netherlands) equipped with a water immersion objective lens (Olympus LUMPLFLN 40XW, N.A. 0.8) focused on the capillary tube. A charge-coupled device (CCD) camera (Lm165M, Lumenera Corporation, Ottawa, ON, Canada) was mounted on the microscope and used to record images of the capillary region of interest, where both the microscope and the acoustic beam were in focus. An optical fiber was fixed below the water tank to illuminate the microscope focal plane with a continuous light source.

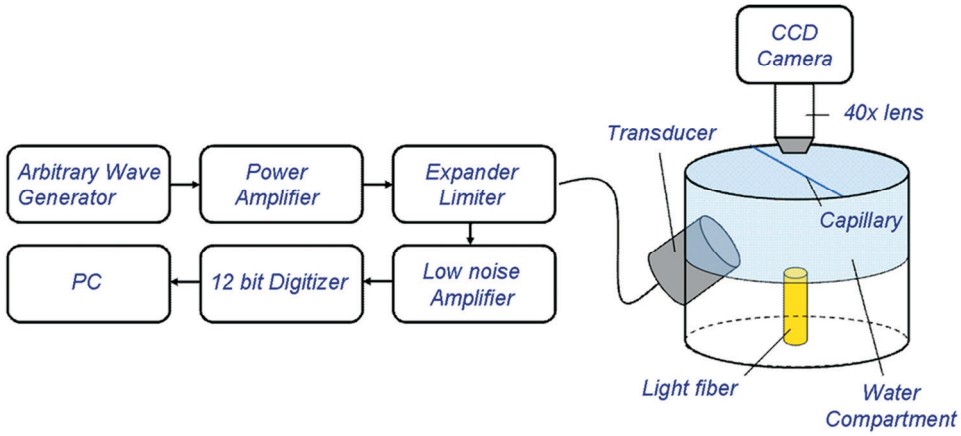

Figure 1. Schematic overview of the experimental setup for optical and acoustical sizing of microbubbles, using an acoustically and optically transparent capillary tube.

Transducer calibration | To measure the incident pressure received by a bubble at the transducer focus, as well as the pressure backscattered by the same bubble on the transducer surface, the transducer was

carefully calibrated both in emission and in reception. This complete characterization was performed at 25 MHz based on two independent measurements. First, a calibrated hydrophone setup (75 μm polyvinylidene fluoride needle hydrophone, Precision Acoustics Ltd., Dorchester, Dorset, UK) was used to measure the pressure at focus and to determine the transmit transfer function of the transducer [59]. For our experimental conditions, we measured a pressure at focus of 390 kPa and a transmit transfer function of 3.2 kPa/V. The uncertainty of the hydrophone at 25 MHz was ±12%. Note that the calculation of this transmit transfer function was done using a transducer gain corrected for water attenuation. Our transducer had a focal distance of 2.6 cm that resulted in an attenuation in water of 3.3 dB at 25 MHz. Second, a pulse-echo setup, using a flat aluminum reflector at the transducer focus, enabled the measurement of the product of the transmit transfer function and the receive transfer function of the transducer [59]. By combining the results of these two measurements, we derived the receive transfer function, which was 26.0 μV/Pa. The knowledge of the receive transfer function, R_r, at 25 MHz made the conversion of the digitized backscattered bubble echoes into pressure values possible. To determine the pressure variation near the focal spot of the transducer beam, we performed a lateral beam profile at focus. The measurement was compared with a Field II simulation [60]. Figure 2 shows both the simulation and the experiment. The pressure drops by 1 dB 80 μm away from the absolute focus. Because the hydrophone chosen for this study exhibits a diameter in the order of a wavelength at 25 MHz, we calculated the spatial averaging that will affect the incident pressure field estimates. Following the theory detailed by Radulescu et al. [61], together with our Field II simulated pressure values, we obtained a pressure drop at focus of 0.12 dB because of spatial averaging. Thus, we concluded that spatial averaging has a negligible impact on our study.

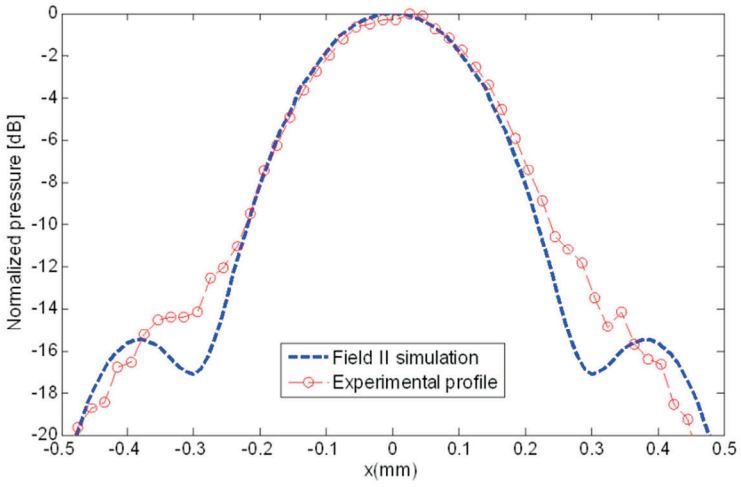

Figure 2. Comparison of the experimental lateral beam profile at focus of the 25-MHz transducer (dotted circled curve) with its simulated profile (dotted curve).

Circuit characterization in reception | The transducer receive transfer function, R_t, was defined [59] as:

$$R_t = \frac{V_{Open}^{Tx}}{p_s} \tag{8}$$

where V^{Tx}_{open} is the open circuit voltage produced by the transducer and p_s the pressure backscattered by a bubble on the transducer surface. To obtain V^{Tx}_{open}, the received amplitudes have to be converted from digitizer voltages to open circuit voltages. The receive chain of the circuit consisted of the transducer connected to the expander/limiter, the low-noise amplifier, a band-pass filter (3 to 35 MHz, fifth-order Butterworth) and the digitizer. The reception circuit is represented in Fig. 3. We can link the backscattered pressure, p_s, to the digitizer voltage, V_d, by:

$$p_s = \frac{1}{R_t}\left(\frac{Z_T + Z_C}{Z_C}\right)\frac{V_d}{T_{V_d \to V_c}} \tag{9}$$

where Z_T is transducer electric impedance, Z_c the receive circuit impedance, V_c the received signal voltage before amplification and $T_{Vd \to Vc}$ the transfer ratio accounting for amplification, the filter and the coaxial cables. We measured with a vector impedance meter (4193A, Hewlett Packard, Yokogawa, Japan) Z_T and Z_C and found 46.9 Ohms and 40.7 Ohms, respectively. $T_{Vd \to Vc}$ was measured by linking the reception circuit to the AWG520 and simulating a received pulse of 1.1 mV amplitude. We found a corresponding voltage of 200 mV. We derived from these measures that $T_{Vd \to Vc}$, which is equal to the ratio of V_d over V_c, and obtained a value of 182. The knowledge of Z_T, Z_c, $T_{Vd \to Vc}$ and R_t fully characterized the circuit in reception and allowed the exact conversion of the digitized bubble echoes from voltage amplitudes into real pressures.

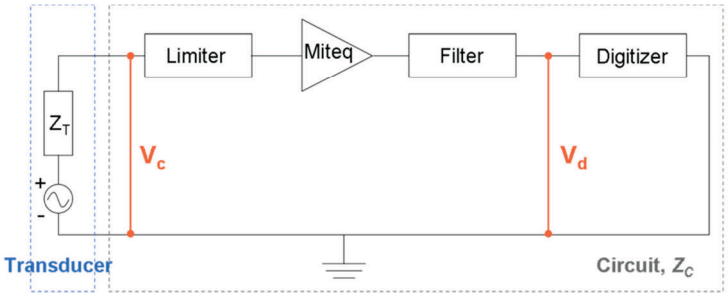

Figure 3. Schematic overview of the receive circuit. V_d is the voltage at the digitizer leads and V_c the voltage at the input. Z_T is transducer impedance and Z_C the receive circuit impedance.

Optical and acoustic size measurements | A low concentration of Definity® microbubbles was injected into the capillary using a syringe, to have no more than one bubble per capillary section of 200 μm. The flow in the capillary was controlled using a manual syringe pump. Thanks to that flow control, single bubbles were kept one by one in the capillary region of interest, where both the transducer beam and the microscope are focused. For each single bubble studied, 64 RF signals were recorded. Simultaneously, an image of the corresponding bubble was captured with the CCD camera. The size of the bubble of interest was determined from the microscope image using a minimum-cost algorithm that delimits the contour of the bubble by finding the steepest grayscale gradient in a box set around the bubble (Fig. 4). The optical observation of the diameters before and after insonification revealed no alteration of the bubble sizes. The systematic error on the optical size measurement of a bubble was estimated by using a calibrated grid displaying dot patterns (DA020, Max Levy Autograph, Philadelphia, PA, USA). The algorithm was used to measure the size of 20 calibrated dots from the grid, and the variation of the results was investigated. The random error was estimated by sizing the same bubble on different images. Combining the random and the systematic error, we quantified the uncertainty of the optical size measurement to be 0.2 μm. The acoustic sizing was based on the accurate knowledge of the distance between the bubble of interest and the transducer, the pressure at the transducer focus (390kPa) and the pressure backscattered by that bubble on the transducer surface. The bubble-transducer distance was derived from the time of flight of the digitized bubble echoes. The backscattered pressures were determined as follows. For each bubble studied, 64 RF signals were acquired. Because the capillary flow could not be completely stopped, the bubbles of interest were moved back and forth around the highest echo position using the manual syringe pump. This movement had a typical amplitude of 50 μm. Among the 64 signals acquired per bubble, one had the highest amplitude. That signal was chosen because it corresponds to the closest position of a given bubble from the exact transducer beam focal point. These selected backscattered amplitudes were converted into a pressure value knowing the receive transfer of the transducer. We evaluated the uncertainty of the acoustic size measurement to be 24% of the estimated bubble diameter, which corresponds to an error of 0.7 μm for a bubble of 3 μm. It originates from the 12% uncertainty of the incident and scattered pressure values. The uncertainty of the bubble transducer distance was negligible.

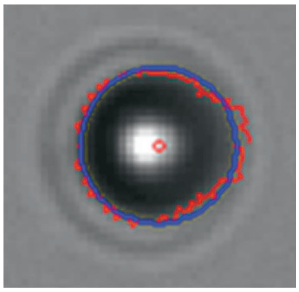

Figure 4.
Contour detection of a contrast bubble for optical sizing. The red curve corresponds to the steepest color gradient detection and the blue contour is the best circular fit from the red contour.

RESULTS

Experimental and simulated basckattered pressures | A set of 88 Definity® microbubbles was characterized both optically and acoustically. The experimental backscattered pressure values were plotted as a function of the optical reference diameters and compared with theory (Fig. 5). We calculated the time responses of individual bubbles using the nonlinear Marmottant model [62] and derived the theoretical backscattered pressure values from these time responses. The input for the simulation were Definity® shell parameters determined in our frequency range [40] combined with our experimental settings (25 MHz, 390 kPa at transducer focus, transducer-tobubble distance of 2.6 cm). The experimental data points showed the linear trend expected above resonance from the simulation. Note that for a given bubble diameter, the amplitude of the scattering varied up to a factor 1.5, which is in agreement with previous findings [63].

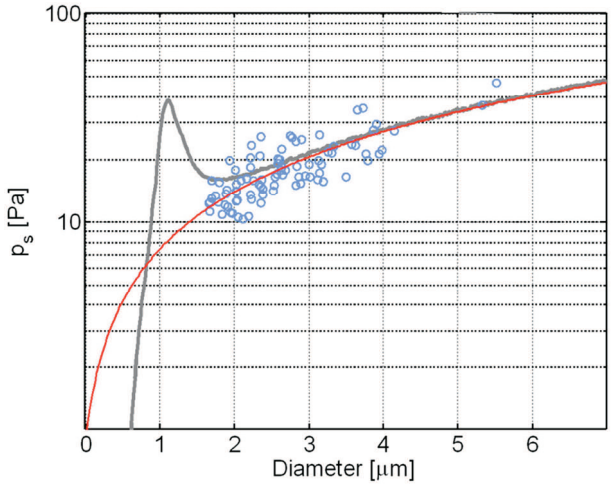

Figure 5. Comparison of the theoretical and experimental backscattering of individual Definity® microbubbles as a function of their diameters. The blue circles represent the 88 experimental data points, the red curve is the linear fit of the experimental data and the gray curve is the behavior predicted by the nonlinear Marmottant model.

Size distributions | The size distribution obtained with our acoustic method resulted in a mean diameter of 2.45 µm and a standard deviation of 0.85 µm. As a comparison, the optical characterization of the same 88 microbubbles featured a mean diameter of 2.67 µm and a standard deviation of 0.78 µm. In terms of medians, the acoustic distribution exhibits a value of 2.22 µm and the optical one a value of 2.55 µm (Table 1). The maximum diameter measured acoustically was 6.2 µm and corresponds to an optical diameter of 5.5 µm. The minimum acoustic diameter measured was 1.4 µm and the optical one

measured 1.7 μm. As a comparison, Lantheus Medical Imaging claims for Definity® a mean diameter range of 1.1-3.3 μm and a percentage of bubbles showing a diameter inferior to 10 μm of 98%. The acoustic diameters and the optical ones are compared in Fig. 6, showing a correlation coefficient of 0.9. The optical and acoustic size distributions are represented in Fig. 7. The diameter range of the optical distribution was divided into 20 columns, resulting in a bin size of 0.20 μm. The same bin size was used for the acoustic size distribution.

Table 1. Comparison of the optical and acoustic size measurement of 88 Definity® microbubbles

88 Definity® bubbles study	Optical characterization (reference)	Acoustic characterization	Variation between measurements
Mean diameter (μm)	2.67	2.45	8%
Median diameter (μm)	2.55	2.22	13%
Standard deviation (μm)	0.78	0.85	8%

DISCUSSION

The individual microbubble diameters measured acoustically show a very good agreement with the diameters measured optically, which validates our acoustic sizing method. The experimental data follows the expected linear scattering trend above resonance. The agreement with the Marmottant model, using Definity® shell parameters in the frequency range 12-28 MHz, is excellent. This work also exhibits an unexpected spread of the data points that is not predicted by the current model. We observed a maximum deviation of a factor 1.5 relative to the model. For the smallest bubbles measured, which have a resonance frequency close to 25 MHz [40], the data confirms that lipid-shelled gas bubbles of equal size show scattering variations in amplitude [63]. Our sizing approach would benefit from the development of lipidshelled bubbles that have equal scattering properties at a given size, contrary to the bubbles used in this study. Moreover, the choice of the ultrasound frequency of investigation will determine the smallest bubbles that can be sized accurately, because bubbles smaller than a certain size will violate the linear scatterer assumption. For Definity® and at 25 MHz, we can establish sizes greater than 1.2 μm diameter [40]. By increasing the ultrasound frequency of investigation, smaller bubble sizes can be measured. The acoustically determined size distribution is comparable in shape with the optical one. The acoustic size distribution appears slightly wider in terms of diameter range and shifted towards the lower radii by 8%. The ±12% uncertainty of the hydrophone used to calibrate the transducer is thought be one of the reasons for the observed global shift, because the calibration of the transducer sensitivity in reception governs the bubble size estimation.

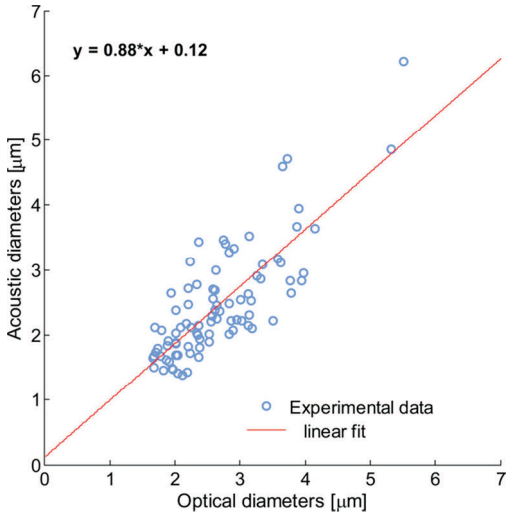

Figure 6. Correlation between the acoustic and the optical diameters determined experimentally.

The total damping, which was neglected in this study, can also have a small impact on the distribution because its contribution increases with bubble size. For Definity® bubble diameters of 1.3 μm and 6 μm, which are the boundaries of our size measurement range, the total damping squared was estimated, respectively, to be 0.02 and 0.1 using the equations used by Goertz et al. [40]. Local disparities between the two distributions partly originate from the scattering variations of lipid-shelled microbubbles for a given size. If a bubble is not scattering at its full potential, it will "sound" like a smaller one. Other factors may explain the remaining differences between these two measurements. First, a tube made of cellulose was used because this material absorbs a large amount of water and is expected to have an acoustic impedance matching reasonably well with water. However, the capillary influence on the pressure value measured with the hydrophone at the transducer focus is not accurately known. Each ultrasound pulse travels twice through the cellulose wall of the capillary (transmission and reception), which may cause an attenuation of the ultrasound waves and which would tend to globally shift the acoustic distribution toward lower radii. Second, the pressure amplitude along the cross section of the capillary tube is not distributed homogeneously. To verify that experimentally, we inserted a 30 μm tungsten wire in a 200 μm cellulose capillary and compared the amplitude of the echo backscattered by the system wire plus capillary with the echo amplitude of the tungsten wire alone. We measured an increase in amplitude of a factor 1.9, with 20 MHz Gaussian pulses of 50% bandwidth for the system wire plus capillary. Others such as Qin et al. [64] simulated for different tube materials that the peak pressure within the tube can rise up to 300% of the incident pressure amplitude. As a consequence, the bubbles might have been excited at higher or lower pressures than 390 kPa, depending on their exact position in the tube during

data acquisition. Another parameter difficult to control was the position of the bubble under consideration along the tube axis. Each candidate was kept in the transducer focal region but the position of the bubble was not stable during the acoustic data acquisition. If the bubble of interest was not located at the focal point where the pressure was measured with the hydrophone, it received an incident pressure slightly lower than the pressure expected at focus. Experimentally, the beam profile of the transducer tells us that at a lateral distance of 80 μm from the focus, the pressure amplitude drops by 1 dB only. We solved this problem by selecting the highest echo amplitude out of the 64 acquired per bubble, because the maximal scattering will occur at the transducer focal point. Experimentally, the bubble of interest was kept in the ultrasound beam focal region using a manual syringe pump and going back and forth around the maximum scattering position. The acoustic bubble sizing method presented in this study proved to be competitive in determining the size distribution of an UCA. It benefits from the usual advantages of ultrasound imaging techniques, e.g., potentially real-time, noninvasive, harmless for the patient and affordable.

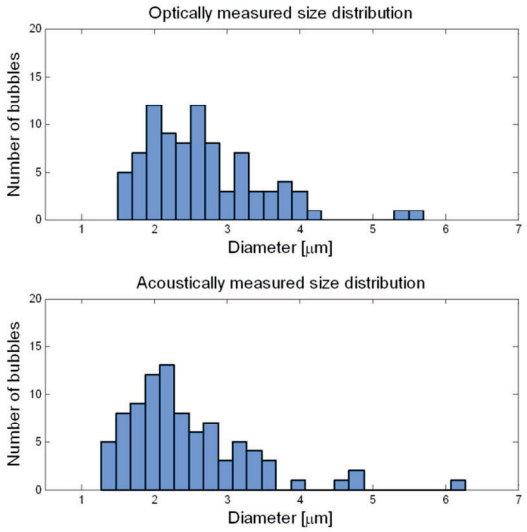

Figure 7. Optical (top) and acoustic (bottom) size distributions of the same population of 88 Definity® bubbles.

Despite the current work focused on studying a lipid-shelled ultrasound contrast agent, the technique could be applied to any type of gas bubbles, independent of the nature of their shell because only the geometric scattering of these microspheres is important. This method could be the core principle running an "acoustic Coulter counter" instrument and used to test UCA filtrations before administration to patients. The next step envisioned is to analyze UCA populations in superficial arteries (e.g., carotid artery) because the method is noninvasive. Such an examination would give extra

information on the change in the size parameters that an UCA population experiences after patient administration and it would help designing microbubble size distributions dedicated to a given clinical application. However, to apply our sizing approach in vivo, some challenges will have to be overcome. Working at high frequencies limits the penetration depth because of tissue and blood attenuation. As a consequence, some bubbles may see their signals lost in the system noise. It is possible to use clinical scanners to image single bubbles as shown by Klibanov et al. [65]. This was achieved at lower frequencies, emitting at 1 MHz and receiving at 3 MHz. On the basis of our experimental results - pressure values of single Definity® bubbles are >10 Pa - we believe that high-end scanners (signal-to-noise ratio <1 Pa) working at our frequency range should also be able to detect single bubbles. A single bubble flowing in the carotid artery (2.5 cm deep, 0.5 dB/cm/MHz attenuation) should give a response above the noise level if the incident pressure is increased to the MPa range (e.g., 4MPa) to compensate for attenuation. An absolute size distribution measurement in vivo would require the exact knowledge of the tissue attenuation. However, even without that knowledge, a relative measurement of the standard deviation of a bubble population could be performed. Another issue is the calibration of the ultrasound beam and the possible presence of resonant bubbles depending on the frequency of the imaging modality (e.g., 15 MHz for 3D carotid imaging). Moreover, the success of this technique depends on single bubbles passing through the focus one by one; otherwise, their size might be significantly underestimated. A solution would be to use two frequencies of the same transducer. To determine a bubble position with respect to the acoustic axis, two consecutive pulses of 20 and 30 MHz can be transmitted, taking advantage of the beam profile differences at both frequencies. A bubble is considered on axis when the difference in backscattered amplitudes at the two frequencies is minimal. The knowledge of the bubble positions, required to estimate their size acoustically, could be determined using a 3D probe. Although temperature elevation to 37°C and viscosity change in the bloodstream may affect the shell properties of UCAs, the acoustic sizing method presented here should still provide meaningful statistical results because it relies on the microspheres' geometry.

Acknowledgements | Funding for this work was provided by the Simon Stevin grant 2007 of the Dutch Technology Foundation (STW). The agent Definity® was provided by Lantheus Medical Imaging. We thank Geert Springeling and Robert Beurskens for their contribution to the experimental setup, Klazina Kooiman for her suggestions on microbubble handling, Frits Mastik for discussion and support with contour detection of bubbles for optical sizing and Mike Danilouchkine for his guidance with lateral beam profile measurements.

3.

IVUS Reconstruction of a Coronary Vasa Vasorum Model

Based on the publication by D. Maresca, M. Emmer, G. Springeling, F. Mastik, G. van Soest, N. de Jong, A. F. van der Steen, **Contrast-enhanced intravascular ultrasound 3D reconstruction of a vasa vasorum mimicking model**. Ultrasonics Symposium (IUS), 2010 IEEE, pp. 2364-2367.

ABSTRACT

The development of newly formed microvessels within a coronary atherosclerotic plaque was associated with an increased risk of plaque rupture. To date, contrast-enhanced intravascular ultrasound (contrast IVUS) is the only technique that demonstrated potential for intracoronary vasa vasorum imaging *in vivo*. The present study aimed at evaluating the capacity of contrast IVUS to reconstruct in 3D a vasa vasorum model with a clinical IVUS catheter. We designed a polyvinyl alcohol based model, exhibiting a vasa vasorum mimicking branch pattern with cross sectional diameters ranging from 200 down to 100 μm. We perfused the vasa vasorum model with a commercial ultrasound contrast agent and performed a manual pullback that generated 93 IVUS images evenly spaced by steps of 200 μm. We segmented ultrasound contrast agent perfused areas in each IVUS image and successfully reconstructed in 3D the vasa vasorum model. We compared the segmented IVUS data with 10 μm thick microscopic slices of the vasa vasorum model at two co-registered pullback positions. The vasa vasorum mimicking micro channel diameters estimated with contrast IVUS agreed within 30 % with the microscopic slice diameters. The feasibility of contrast IVUS imaging of vasa vasorum was demonstrated *in vivo*, and the technique might play a central role in vulnerable plaque detection. Fast *in vivo* pullbacks could be complementarily used to reconstruct vasa vasorum networks in three dimensions.

INTRODUCTION

Major blood vessels such as the coronary arteries require their own blood supply. Blood is provided to the inner layers of the arterial wall by a network of microvessels referred to as the vasa vasorum (VV) [26]. The progression of atherosclerotic plaques is associated with the development of neovascular VV through the process of angiogenesis [7]. A first function of intra-plaque neovasculature is to sustain growth of the plaque beyond the diffusion limits of the existing blood supply. Neovascularization also fosters intra-plaque inflammation, which is linked with plaque instability [66]. There is therefore clinical interest in investigating VV as a potential marker of plaque vulnerability. Studying coronary VV requires sensitive, robust and quantitative imaging techniques capable of detecting and spatially resolving small regions of vascularity and their location relative to the plaque structure (e.g. at base and 'shoulders' of lesions). The small vessel sizes, slow blood flow, and the presence of substantial coronary wall motion, pose considerable problems for imaging modalities to overcome. Currently, there is no established clinical technique capable imaging VV in the coronary arteries of humans. 3D micro-CT images of *ex vivo* coronary arteries have shown the role of angiogenic vasa vasorum (VV) in plaque growth and progression [28]. Goertz et al. [31] reported *in vivo* recordings of VV in a rabbit atherosclerotic aorta using contrast IVUS. Unfortunately, the results could not be compared to the exact microvasculature anatomy.

To tackle this problem, several research groups developed capillary flow phantoms, notably to assess contrast agent replenishment kinetics [67]. The present work aimed at demonstrating the feasibility of a contrast IVUS reconstruction of a coronary vasa vasorum model in 3D, via a controlled phantom experiment. The goal of this study was double: first, evaluate qualitatively the capacity of contrast IVUS to reconstruct a simple vasa vasorum size microchannel pattern. Second, to assess the accuracy of the VV microchannel diameters reconstructed with contrast-enhanced IVUS imaging.

METHODS

Coronary artery vasa vasorum model | The use of tissue substitutes is an established method in ultrasound imaging [68]. In order to evaluate in a controlled manner the capacity of contrast-enhanced IVUS imaging to detect and reconstruct VV-like structures, we designed a coronary artery vasa vasorum model. The model exhibited a central channel with a constant luminal diameter of 3 mm that simulated a human coronary artery lumen. To simulate arterial wall microvasculature, we included a branching microchannel structure running parallel to the central channel at a distance of 1 mm. The microchannel diameter was equal to 200 μm before bifurcation and 100 μm after bifurcation.

The phantom material was made of a 10% by weight solution of polyvinyl-alcohol (PVA) mixed with enamel paint droplets (1.0% by weight of the total solution) to increase scattering. The solution was frozen and thawed in three cycles of 2 hours at least to attaint acoustic properties similar to tissue [69]. We measured a speed of sound of 1511m/s at 25 MHz and an attenuation coefficient of 2.46 dB/mm at room temperature. Literature reports that coronary arteries show an approximate acoustic attenuation coefficient at 30 MHz of 2dB/mm [70]. A syringe connector was glued to the 200 μm entrance of the VV mimicking microchannel to enable perfusion of the model with an ultrasound contrast agent (Figure 1).

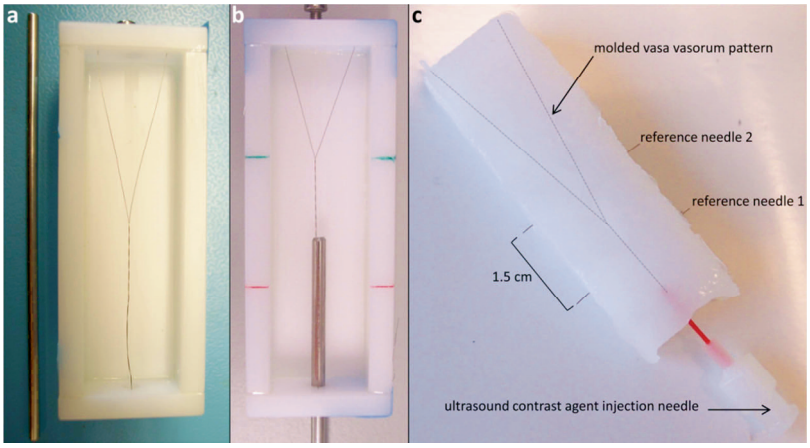

Figure 1. Coronary artery vasa vasorum model. (a, b) PVA mold. A rigid metallic rod of 3 mm diameter was used to create the lumen. A 100 um metallic wire was winded up in a V pattern and fixed at the mold ends. The PVA solution was poured thereafter. (c) PVA model utilized for the pullback experiment. Reference needles were inserted perpendicular to the channels. An injection needle was glued at the entry of the microchannel, enabling perfusion of the ultrasound contrast agent.

Contrast-Enhanced Intravascular Ultrasound | A clinical IVUS catheter (UltraCross 2.9 Coronary imaging catheter, Boston Scientific, Freemantle, USA) transmitted 30 MHz 80% bandwidth Gaussian modulated sine-bursts. We acquired 256 radio frequency (RF) lines per catheter rotation along a manual pullback consisting of 93 steps of 200 μm (Figure 2). The received RF data were bandpass filtered from 18 to 43 MHz. The envelopes of the radiofrequency lines were computed, log compressed with a dynamic range ranging from 0 to 40 dB and scan converted.

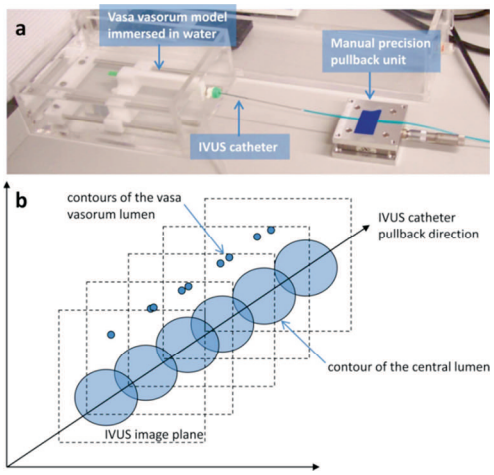

Figure 2. (a) Contrast IVUS pullback setup. The IVUS catheter was inserted in the central lumen of the vasa vasorum model before to be pulled-back in a controlled manner using a precision stage after ultrasound contrast agent injection. (b) Schematic showing the principle for 3D vasa vasorum reconstruction. 2D IVUS images are acquired at evenly spaced pullback locations, enabling the detection of the central channel and VV-mimicking microchannel contours.

As the commercial IVUS system utilized did not offer contrast mode capabilities, we perfused the VV mimicking channel with a native concentration of the ultrasound contrast agent Definity™ (Lantheus Medical Imaging, MA, USA). Even in the absence of a contrast mode, we expected to detect in fundamental images the response of submicron Definity™ bubbles that resonate at 30 MHz [40]. In order to evaluate the accuracy of contrast IVUS VV detection, we compared IVUS images at two registered locations with 10 μm thick microscopic slices of the VV model of the same locations. In the contrast IVUS images, the perfused VV contours were detected by applying a threshold in the intensity scale (set at 30dB). For reference, the lumen intensity, were no contrast agent was injected, was 3dB (Figure 3).

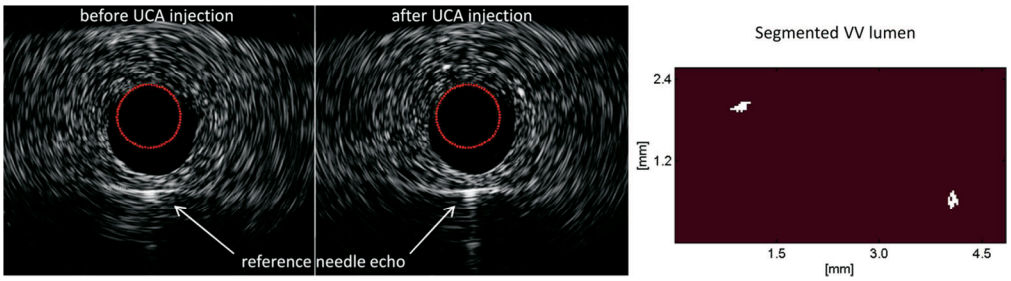

Figure 3. 40 dB IVUS images at the second registered location were identified thanks the reference needle echo, which is visible at the bottom. Left, IVUS image before contrast injection. The 100 μm diameter vasa vasorum cross sections are invisible, below conventional IVUS resolution. Middle, IVUS image after ultrasound contrast agent injection. The vasa vasorum lumina are detected, appearing bright in the image. Right, zoom in IVUS image after thresholding at 30 dB, revealing the perfused microchannel areas only.

The model slices were imaged with a microscope (Visio 200, Tesa Technology, Renens, Switzerland) and the VV diameters were measured with the microscope software (Figure 4).

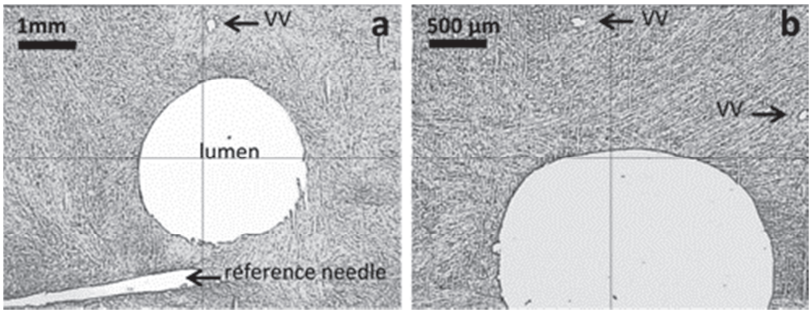

Figure 4. Microscopic cross section at the two reference locations. The needle position is revealed by a hollow cavity perpendicular to the central lumen. Microchannel cross sections were identified and their dimensions estimated with the microscope software.

3D reconstruction | All 93 pullback images processed with a 30 dB threshold to extract perfused microchannel areas. As consecutive contrast IVUS frames showed angular misalignment, a realignment scheme was applied. Angular variations between consecutive pullback frames were estimated by means of frame to frame subtraction. IVUS frame number *i+1* is rotated along 360 degrees and iteratively subtracted to the previous IVUS pullback frame *i*. The minimum of the subtraction curves indicated the angular correction to apply to realign frame *i+1* with frame *i* (Figure 5). After having realigned the 93 contrast IVUS pullback frames, the 3D reconstruction of the vasa vasorum model was performed by meshing the 30 dB iso-surfaces corresponding to the ultrasound contrast agent filled microchannel areas. The 3D volume obtained was smoothed using a Gaussian filter. All processing steps were performed using Matlab.

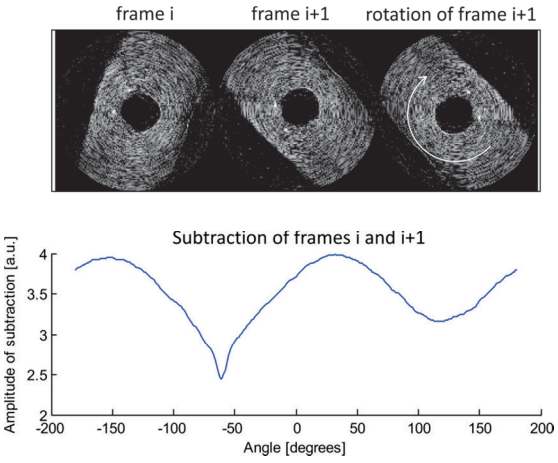

Figure 5. Correction of the frame to frame angular variations. Frame i+1 is rotated along 360 degrees and iteratively subtracted to reference frame i. The minimum of the subtraction curve indicates the correction angle. In this example, the correction angle was -61 degrees.

RESULTS

The phantom microchannel was successfully perfused and the ultrasound contrast agent Definity ™ could be detected in all 30 MHz IVUS images despite the lack of a contrast mode. The VV mimicking channel diameters were estimated at the two needle locations (Figure 1). Microscope measurements of the model slices provided microchannel diameter values of 201 μm at location 1 (before bifurcation), and 151 μm and 127 μm at location 2 (after bifurcation). In the corresponding contrast IVUS image the microchannel perfused area corresponded to 35 pixels at location 1, leading to a diameter estimation of 208 μm in good agreement with the microscope measurement. At location 2, we counted 25 pixels for both microchannel perfused areas, corresponding to a diameter of 176 μm (Figure 3), showing a lesser agreement with the microscope measurement. Pixel counts to diameter conversions were achieved under the assumption that detected pixel areas were circular. Knowing the pixel resolution (1 pixel length equaled 31.25 μm), we estimated microchannel diameters.

We successfully reconstructed the VV mimicking model in three dimensions (Figure 6). The single channel design followed by a bifurcation is clearly discernible. The registration of IVUS images locations allowed the combined visualization of the coronary model morphology and the 3D microvasculature structure.

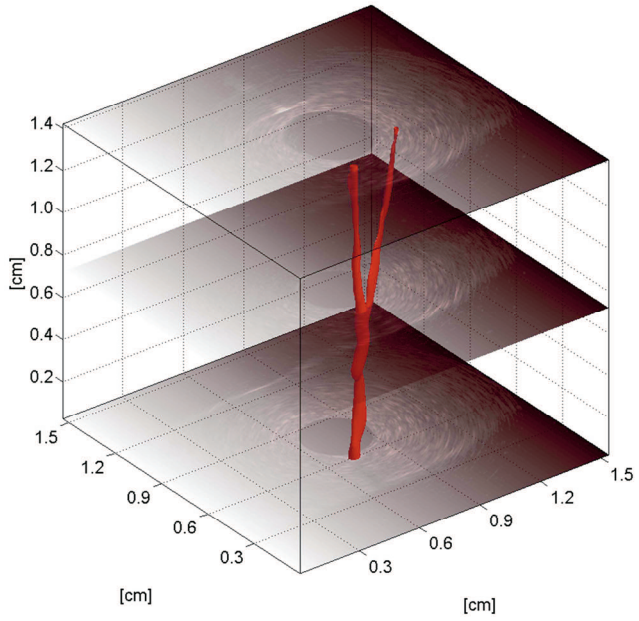

Figure 6. 3D reconstruction of the vasa vasorum model superimposed with three IVUS pullback frames. The branching structure of the vasa vasorum model was clearly identified.

DISCUSSION

We have shown that contrast-enhanced intravascular ultrasound enabled the 3D reconstruction of a controlled microvasculature structure embedded in a coronary artery model. VV networks are invisible in conventional *in vivo* IVUS imaging but we showed that structures of similar dimensions could be reconstructed using contrast IVUS. The axial resolution of our 30MHz clinical catheter (measured on a sub-wavelength 30 μm thick tungsten wire) was 133 μm. Consequently, the 100 μm channels of the vasa vasorum model lay below the system's resolution. The use of contrast IVUS made their detection possible but their diameters were nonetheless overestimated.

The PVA coronary artery model designed proved to be a successful substitute for a controlled contrast IVUS experiment. The lumen and the vasa vasorum mimicking microchannel were molded using a metallic rod and two interleaved metallic wires that were pulled back from the model once it reached proper acoustic properties. This procedure prevented the use of artificial capillaries, which present unrealistic acoustic properties at IVUS frequency.

The irregularities in the 3D volume obtained are thought to be caused by the distribution of the contrast agent, the surface roughness following the wire extraction and the discrepancy between axial and lateral IVUS resolution. Refined contour detection techniques (e.g. steepest intensity gradient detection in the area of interest) could be used to improve the contour detection of contrast filled areas.

The experiment was performed with a conventional catheter used in the clinical practice and a commercial ultrasound contrast agent. If the result is encouraging, it also highlighted important hurdles for vasa vasorum imaging using clinical IVUS systems. The clinical translation of 3D vasa vasorum imaging will require further developments in contrast IVUS imaging. The non-diluted ultrasound contrast agent dose used in this study is not compatible with medical guidelines. Therefore, the development of sensitive IVUS contrast imaging techniques and their implementation on existing catheters is necessary. Harmonic techniques such as second harmonic and subharmonic IVUS imaging were successfully tested [71] but since they require ultra-wideband IVUS transducers, feasibility relied on prototype IVUS transducers that are not commercially produced [72]. Novel bandwidth-limited contrast IVUS methods are therefore desirable to transfer IVUS vasa vasorum imaging into clinical practice. Nevertheless, as IVUS imaging can be carried out *in vivo*, contrast IVUS could play a critical role in percutaneous coronary interventions or clinical trials in helping identifying vulnerable coronary plaques.

Acknowledgement | We would like to thank the Dutch Technology Institute STW for funding. We particularly thank Kim van Gaalen for slicing the coronary artery model. We thank Robert Beurskens and Jan Honkoop for their support with electronics and Frits Mastik, Krista Jansen and Charles Lancée for discussion.

4.

Intravascular Ultrasound Chirp Imaging

Based on the publication by D. Maresca, K. Jansen, G. Renaud, G. Van Soest, X. Li, Q. Zhou, N. De Jong, K. K. Shung, A. F. W. Van Der Steen, **Intravascular Ultrasound Chirp Imaging**. *Appl. Phys. Lett.* **100**, (2012).

ABSTRACT

We demonstrate the feasibility of intravascular ultrasound chirp imaging as well as chirp reversal ultrasound contrast imaging at intravascular ultrasound frequency. Chirp excitations were emitted with a 34 MHz single crystal intravascular transducer and compared to conventional Gaussian-shaped pulses of equal acoustic pressure. The signal to noise ratio of the chirp images was increased by up to 9 dB relative to the conventional images. Imaging of contrast microbubbles was implemented by chirp reversal, achieving a contrast to tissue ratio of 12 dB. The method shows potential for intravascular imaging of structures in and beyond coronary atherosclerotic plaques including the vasa vasorum.

INTRODUCTION

Atherosclerosis is a chronic systemic disease of the arterial wall and a leading cause of premature death worldwide. Most cardiac adverse events result from the rupture of a vulnerable atherosclerotic plaque and subsequent thrombosis in the coronary vascular tree [7]. It is recognized that the formation of new microvessels in the arterial wall is critical to the progression of plaques due to red blood cell leakage and constitutes an important marker of plaque vulnerability [73]. These networks of microvessels, ranging in diameter from 200 μm down to 5 μm, are referred to as vasa vasorum (VV).

As of today, clinically available tools are unable to detect coronary artery VV. *Goertz et al.* [31] demonstrated the feasibility of VV imaging in a rabbit aorta, using intravascular ultrasound (IVUS) in combination with an experimental micron sized ultrasound contrast agent (UCA). By exciting UCA-specific nonlinear resonances with IVUS pulses, contrast infused areas can be disentangled from tissue signals. This method allowed for the detection of arterial wall microvasculature lying below the resolution limit of conventional IVUS. Unfortunately, these results were achieved with a prototype dual frequency IVUS transducer and are not implementable on existing clinical IVUS systems due to frequency bandwidth limitations.

In this Letter, we develop chirp IVUS, with the dual objective of extending the viewing depth, and implementing chirp reversal contrast imaging in a manner that is applicable on a conventional bandwidth-limited IVUS transducer. At a given mechanical index (MI) and frequency bandwidth, chirp excitations can be used to carry more energy than conventional short imaging pulses. The higher energy converts into a higher signal to noise ratio in medical ultrasound images and permits the visualization of deeper structures in the body. Furthermore, specific chirp compression processing can be used to retrieve a good imaging resolution. To date, ultrasound chirp imaging was implemented in noninvasive clinical imaging only [74].

Chirps are also beneficial for UCA detection purposes, as the transient resonant response of microbubbles close to resonance differs for insonification with up and down frequency sweeps [75, 76]. Capitalizing on this asymmetry, we present a contrast imaging mode that provides good contrast to tissue ratio (CTR) at clinically approved concentrations of UCA.

The first part of this study, we investigated the performance of IVUS chirp imaging on several phantoms, as well as an atherosclerotic human coronary artery *ex vivo*. In the second part, we evaluated chirp reversal contrast IVUS imaging using a channel phantom perfused with a commercial UCA.

B-mode IVUS imaging | The experimental intravascular imaging system consisted of a mechanically rotated single element IVUS transducer (single-crystal lead magnesium niobate-lead titanate; PMN-PT [77], active surface 0.5 x 0.5 mm^2, center frequency 34 MHz, -6 dB bandwidth 60%, 2 mm natural focus) mounted in a catheter assembly with a 0.9 mm outer diameter. A photograph of the transducer is shown in Figure 1.

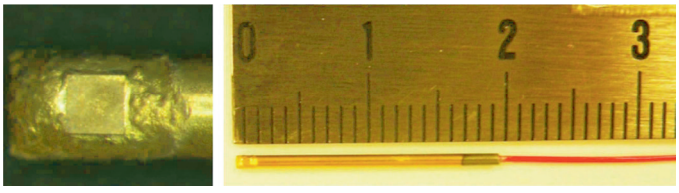

Figure 1. 0.5 x 0.5 mm IVUS transducer mounted in a 0.9 mm diameter rigid catheter assembly. (Left) zoom on the square transducer surface. (Right) Experimental IVUS probe.

We transmitted interleaved Gaussian envelope sine wave pulses and chirp excitations of equal peak negative pressure using an arbitrary waveform generator (Tabor Electronics WW2571A) at 1° angular position steps using a motorized rotary stage (Steinmeyer GmbH). The Gaussian modulated pulses were emitted at the transducer center frequency with a 60% -6 dB bandwidth. The chirp excitations $chirp(t)$ were formulated as $chirp(t)=a(t)\cos(2\pi\varphi(t))$, where $a(t)$ is the envelope and $\varphi(t)$ the phase. In order to minimize the side lobe level after chirp compression, we selected a quasi-linear phase $\varphi(t)$, defined in relation to the instantaneous frequency $f_i(t)$ as

$$f_i(t)=\frac{1}{2\pi}\frac{d\varphi(t)}{dt}=f_1\beta^t \quad with \quad \beta=\left(\frac{f_2}{f_1}\right)^{\frac{1}{T}}, \tag{1}$$

where f_1 is the initial chirp frequency, f_2 the final chirp frequency and T the signal duration. All chirp excitations were apodized using an 11% tapered Tukey window. The ultrasound radio-frequency (RF) data was digitized at 350 MHz (Acqiris DP-310) and band-pass filtered. The received chirp RF lines were compressed by cross-correlation with the emitted chirp signal. The chirp envelope after compression was simulated and compared to the Gaussian sine-wave pulse envelope for our set of transmission parameters (Figure 2).

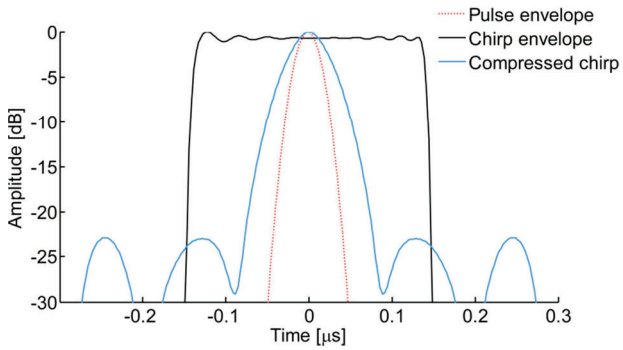

Figure 2. Simulation of the chirp envelope after compression in comparison with the Gaussian pulse envelope

The narrowing of the main lobe which is observed translates into an improved in axial resolution. Simultaneously, sidelobes appear at a level of -23 dB. The short pulse at the transducer center frequency is still providing the highest resolution. Experimentally, the axial resolution and signal to noise ratio (SNR) were determined from the echoes of 15 µm thick platinum/iridium wires at distances of 1.5, 3, 5 and 7 mm from the probe, mounted in a hollow cylinder. Additionally, a cylindrical agar-based phantom [78], with a lumen of 3 mm diameter and three parallel 2 mm channels at distances of 3, 5, and 7 mm off-axis, was designed in order to assess tissue penetration depth. Intravascular ultrasound chirp imaging of human coronary atherosclerosis was performed *ex vivo*. The artery was provided by the Pathology Department of

the Erasmus Medical Center according to local Medical Ethics Committee regulations. The tissue was snap frozen at -80°C within an hour after autopsy. Before imaging, the specimen was thawed in phosphate buffered saline (PBS), mounted in a PBS filled tank and pressurized to 100 mmHg to keep the lumen open. The chirp excitations used for the wire phantom measurement had a temporal length of 0.3 μs, a frequency sweep ranging from 25 to 42.5 MHz and an MI of 0.19 (Figure 3).

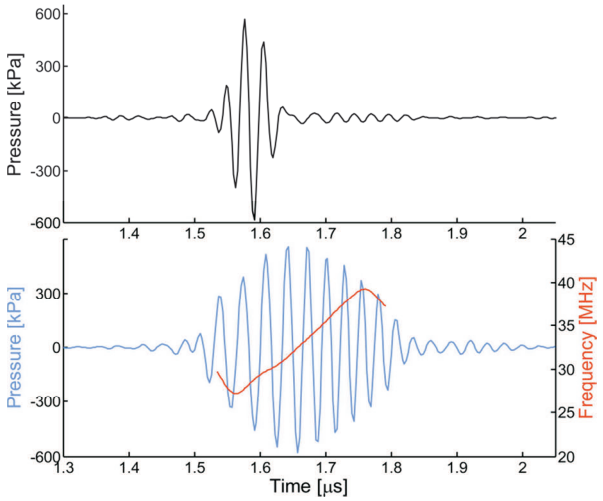

Figure 3. Gaussian modulated sine wave (top) fc = 34 MHz, -6 dB bandwidth 60% and chirp coded excitation (bottom), 25 to 42.5 MHz sweep, 11% tapered Tukey window, pulse length = 0.3 μs. The chirp instantaneous frequency sweep is plotted in red.

Using chirps, we measured a gain in SNR of 8 dB for the closest wire and 9 dB for the other three compared to the conventional imaging pulse. The axial resolution (-6 dB point spread function) at the wire closest to the focus was 106 μm for the pulse and 153 μm for the chirp excitation after compression while the lateral resolution was 272 μm for both. The sidelobe level in the compressed chirp image was at -23 dB relative to the main lobe (Figure 4).

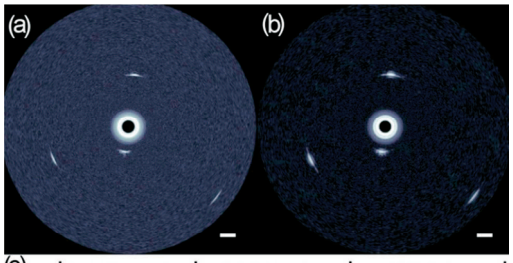

(c)

	Axial resolution	Sidelobe level	SNR Gain
Pulse	106 μm	–	–
Chirp	153 μm	-23 dB	+ 9 dB

Figure 4. Subwavelength wire phantom imaged using pulses (a) and chirps (b). The dynamic range is 55 dB. The scalebar represents 1 mm. (c) Comparative performance of conventional IVUS *versus* chirp IVUS.

Chirp imaging was applied to the tissue-mimicking phantom, and compared to the pulse image, as displayed in Figures 5a and 5b. The third side channel appears at 8 o'clock in the chirp image only. Based on the SNR gain of 8 dB, an imaging depth extension of 1.9 mm, from 5.6 mm to 7.4 mm was achieved. With the ex vivo human coronary artery, a gain in SNR of 7 dB was measured in the chirp image compared to the pulse image (Figure 5c, d).

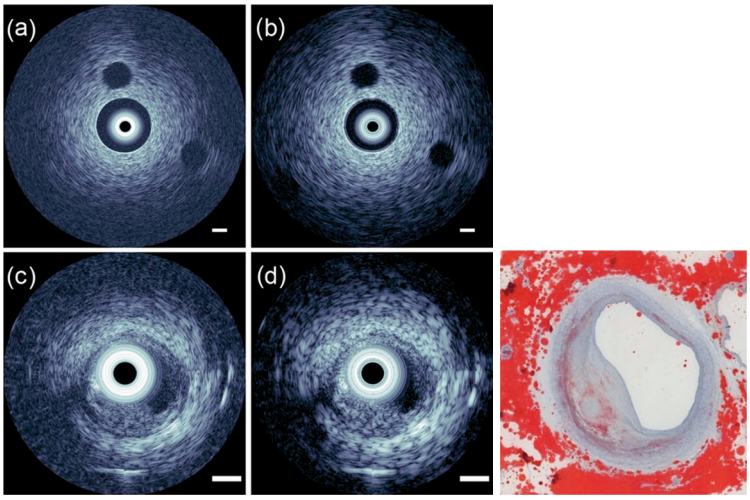

Figure 5. (a) Channel phantom image using pulses and chirps (b). The dynamic range is 55 dB. (c) Human coronary artery image using pulses and chirps (d). The dynamic range is 48 dB. The scalebar corresponds to 1 mm. (e) Histology at corresponding location.

CONTRAST-ENHANCED IVUS IMAGING

Chirp based contrast imaging was evaluated for its potential to detect VV. The UCA used was Definity® (Lantheus Medical Imaging, North Billerica, MA). We first simulated the pressure scattered by a 1 μm diameter bubble in response to an up and down sweep chirp (duration 0.5 μs, frequency sweep 22 to 46 MHz, MI 0.19) with a visco-elastic shell model using the UCA high frequency shell parameters as described by de Jong [79]. Next, for the experiment, the UCA was activated and decanted for 15 to 30 minutes to extract the smallest contrast bubbles which resonate at IVUS frequencies. With this method, the mean bubble diameter was less than 2 μm [40]. Finally, a 1:1000 dilution was prepared. Chirp reversal contrast measurements were performed by filling the lumen and the first two channels of the tissue mimicking phantom with the UCA while the third one was filled with water. A two step pulsing scheme excited the UCA, first with a down sweep chirp and then with an up sweep chirp transmitted at 10 μs intervals.

The simulation results clearly show the asymmetry between the bubble echoes of a down and up sweep chirp (Figure 6c and 6d). A one micron diameter UCA bubble resonates at 25 MHz [40]. The bubble response is enhanced when the driving frequency is close to its resonance frequency, which happens at the beginning for the up sweep chirp and at the end for the down sweep chirp. In addition, a ringdown effect elongates the bubble response to the down sweep chirp compared to the driving excitation. Therefore, the subtraction of the compressed bubble echoes gives a residual contrast signal. Experimentally, the chirp reversal contrast image had a CTR of 12 dB (ratio of mean bubble and tissue signal amplitudes) achieved at clinically approved concentration of this UCA (Figure 6f). Bubbles could be detected up to a depth of 5 mm.

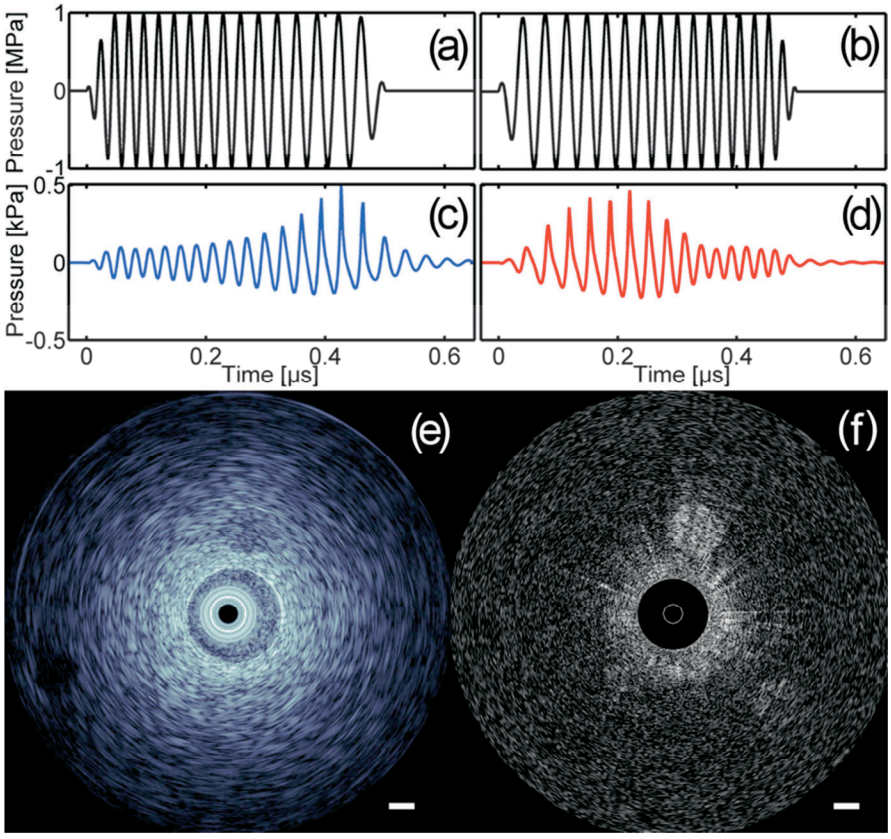

Figure 6. Simulated incident down (a) and up sweep (b) chirps sent a micron size UCA bubble and corresponding scattered acoustic pressures (c, d). (e) Down sweep chirp image and (f) contrast image of the channel phantom perfused with the UCA. The dynamic range is 54 dB for the left image and 21 dB for the contrast image.

DISCUSSION

These results demonstrate the feasibility of intravascular ultrasound chirp imaging of human coronary atherosclerosis at intravascular ultrasound frequencies. A significant SNR gain was achieved, leading to an extension of signal penetration of 1.9 mm, at some cost in axial resolution and limited appearance of side lobes. High-frequency chirp reversal contrast imaging was achieved. This IVUS contrast mode has the potential to image VV in a clinical setting, using commercially available UCAs in a low dose. Reliable *in vivo* quantification of VV holds promise for plaque vulnerability imaging.

The gain in SNR for coded excitations is equal to the time-bandwidth product, and as a result, chirp imaging benefits from long pulses. The duration of chirp excitations in IVUS is limited, however, because image targets are immediately adjacent to the transducer (Figure 5b, c). Theoretically, the SNR can be further enhanced, and the sidelobe level can be reduced, using mismatched filtering [80]. IVUS is the clinical standard to assess the geometry and size of coronary plaques *in vivo*. Image interpretation and segmentation, often ambiguous tasks for trained evaluators at present, may benefit from the SNR gain, allowing for sharper contour detection.

Chirp IVUS will complement conventional IVUS methods by providing extended imaging depth, allowing for imaging deep into and beyond the plaque. Using chirp reversal, it adds a promising method for contrast-enhanced IVUS, imaging plaque vulnerability by quantifying plaque microvessels with low dose clinically approved UCAs, and with conventional frequency-band limited IVUS catheters.

5.

Contrast-Enhanced Intravascular Ultrasound Pulse Sequences for Bandwidth-Limited Transducers

Based on the publication by D. Maresca, G. Renaud, G. van Soest, X. Li, Q. Zhou, K. K. Shung, N. de Jong, A. F. W. van der Steen, **Contrast-Enhanced Intravascular Ultrasound Pulse Sequences for Bandwidth-Limited Transducers**. *Ultrasound in Medicine & Biology* **39**, 706-713 (2013).

ABSTRACT

We demonstrate two methods for vasa vasorum imaging using contrast-enhanced intravascular ultrasound, which can be performed using commercial catheters. Plaque neovascularization was recognized as an independent marker of coronary artery plaque vulnerability. IVUS-based methods to image the microvessels available to date require high bandwidth (26 dB relative frequency bandwidth >70%), which are not routinely available commercially. We explored the potential of ultraharmonic imaging and chirp reversal imaging for vasa vasorum imaging. In vitro recordings were performed on a tissue-mimicking phantom using a commercial ultrasound contrast agent and a transducer with a center frequency of 34 MHz and a -6 dB relative bandwidth of 56%. Acoustic peak pressures, 500 kPa were used. A tissue-mimicking phantom with channels down to 200 μm in diameter was successfully imaged by the two contrast detection sequences while the smallest channel stayed invisible in conventional intravascular ultrasound images. Ultraharmonic imaging provided the best contrast agent detection.

INTRODUCTION

The identification of vulnerable coronary atherosclerotic plaques remains a central issue in cardiac imaging [81]. As with malignant tumors, intraplaque formation of new microvessels is critical to the progression of atherosclerosis and may constitute an independent marker of vulnerability [3, 66], a hypothesis recently supported by a 3D micro-computed tomographic study of ex vivo coronary arteries [28]. There is a clear role in both studies of atherosclerosis and diagnostic imaging for methods capable of detecting and visualizing the microvascular networks within the arterial wall, also referred to as "vasa vasorum" (VV). VV diameters reported in human diseased arteries range from 2–200 μm [82]; however, the clinical tools to image coronary artery VV in vivo do not exist. Intravascular ultrasound (IVUS) is an established minimally invasive diagnostic tool that provides high-resolution intravascular images of the vessel wall and atherosclerotic plaques [83, 84]. It has been shown that IVUS combined with an ultrasound contrast agent (UCA) has the capacity to detect VV in the arterial wall [31, 32, 85]. Pulse inversion schemes proved to be efficient in cancelling fundamental signals and therefore detecting subharmonic or second harmonic responses from UCAs [37, 71]. In a step toward harmonic IVUS imaging of VV, an IVUS transducer having two frequency peaks at 22 and 40 MHz was designed [31, 32, 86, 87]. Despite a good sensitivity, this transducer suffered from a lower spatial resolution than conventional clinical IVUS because of the narrow bandwidth of the two frequency peaks (two-way 30%, -6 dB relative bandwidth) and is not produced commercially. Alternatively, harmonic IVUS imaging could be performed with single-frequency peak IVUS transducers presenting a -6 dB relative frequency bandwidth of 70% or more [72]. Such a frequency bandwidth allows one to transmit at the inferior or superior limit of the -6 dB frequency bandwidth and receive the response of UCA at the second harmonic frequency or the subharmonic frequency with adequate sensitivity. These broadband IVUS transducers have not progressed beyond the prototype stage to date, and they remain far from application in routine clinical devices. In this study, we investigated the performance of two contrast-enhanced intravascular ultrasound pulse sequences for VVimaging functioning with conventional IVUS transducer bandwidths (<60%), chirp reversal IVUS imaging [44] and ultraharmonic IVUS imaging. Chirp reversal capitalizes on the asymmetric resonant response of UCAs to upsweep and downsweep chirp excitations. Ultraharmonic imaging presents two advantages over subharmonic imaging. First, a 40% -6 dB relative bandwidth is sufficient to capture it, whereas the second harmonic or subharmonic require 70%. In addition, the lateral resolution of ultraharmonic imaging is expected to be superior to subharmonic and fundamental imaging [88]. Like the subharmonic response, the ultraharmonic response is a UCA-specific response that is not generated by tissue, thus providing a contrast signal more specific than second harmonic imaging [89-91]. Both IVUS contrast detection methods were evaluated in a tissue-mimicking phantom including channels perfused with a commercial ultrasound contrast agent.

MATERIALS AND METHODS

Tissue mimicking phantom for IVUS vasa vasorum imaging | To mimic a coronary artery cross section with intra-wall vascularization, we manufactured a tissue mimicking phantom [68] with five through cavities; a central lumen 3 mm in diameter and four side channels of diameters equal to 2 mm, 1 mm, 500 μm and 200 μm. Human VV vessel diameters, which range from a few hundred micrometers down to a single red blood cell dimension [82], were simulated in our phantom by the 200 μm channel. All side channels were situated at a distance of 500 μm from the central lumen border, and the total phantom diameter was equal to 2 cm (Fig. 1). The phantom material was made of 10% w/w polyvinyl alcohol gel mixed with 0.5% w/w silicon carbide particles less than 15 μm in size (SiC, K-800, MTN-Giethoorn) and 0.5% w/w silicon dioxide particles ranging 1–5 μm to account for scattering and attenuation. The mixture underwent three freeze thaw cycles to reach tissue mimicking mechanical properties (Hansen et al. 2010).

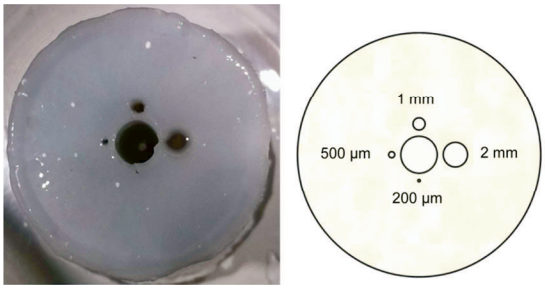

Figure 1. Channel phantom mimicking arterial wall vasculature. The 200 mm diameter vasa vasorum mimicking channel is visible below the central lumen. The phantom diameter is 2 cm.

IVUS imaging system overview | The IVUS imaging system used in this study was similar to the one described in Maresca et al. [44]. A mechanically rotated unfocused single element IVUS transducer (PMN-PT single-crystal, 0.5 x 0.5 mm^2, center frequency 34 MHz, -6 dB frequency bandwidth of 56% ranging 24–44 MHz) was mounted in a catheter assembly with an outer diameter of 0.9 mm [77]. The flat transducer had a natural focus distance of 2 mm and a lateral resolution of 270 μm at focus [44]. A schematic of the circuit is depicted in Figure 2. Interleaved sequences of excitations were transmitted using an arbitrary waveform generator (model WW2571A; Tabor Electronics, Tel Hanan, Israel) with angular steps of 1 degree. The received ultrasound radiofrequency data were amplified by 43 dB (Miteq AU1263), digitized at a sampling frequency of 350 MHz with a 12 bit dynamic range (DP310; Acqiris, Geneva, Switzerland), digitally filtered and scan converted. No power amplifier or filters were used in the circuit in order to minimize waveform distortion.

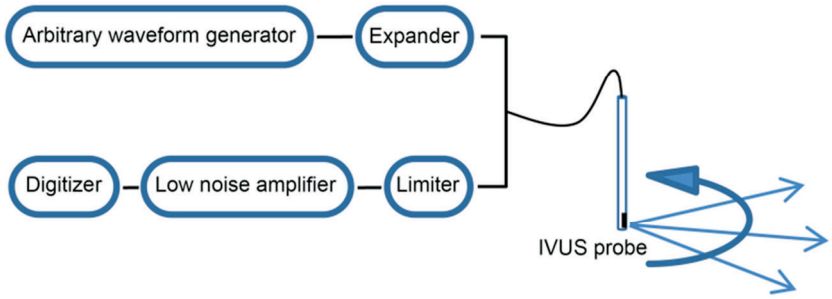

Figure 2. Overview of the intravascular ultrasound (IVUS) imaging system.

Contrast agent handling for IVUS | We used the commercial UCA Definity (Lantheus Medical Imaging, North Billerica, MA, USA). It essentially contains microbubbles with a diameter between 1.1 and 3.3 μm with 98% of the bubble population <10 μm according to the manufacturer's specifications. Micrometer-sized bubbles that resonate at IVUS frequency (20–50MHz) were selected by means of decantation as described by Goertz et al. [32]. A vial of the commercial UCA Definity was decanted for 1 h. 0.2 mL of UCA was extracted, diluted in 200 mL of degassed water (dilution ratio 1:1000, of the order of dilution ratios administered for human use; Giannoni et al. [93]) and stirred with a magnetic stirrer for 30 seconds. This protocol ensured an average resonance frequency of the prepared UCA close to 20 MHz and therefore suited for IVUS imaging. A tank containing the tissue mimicking phantom was filled with the UCA solution, ensuring that a uniform concentration of UCA was expected in the lumen and in the side channels. The UCA suspension remained static (no flow) during image acquisition.

IVUS pulse-inversion ultraharmonic sequence | The transmission of pairs of phase-inverted excitations, referred to as pulse inversion [37], is a powerful technique to selectively detect the nonlinear response of UCAs [94]. To test ultraharmonic IVUS imaging, we transmitted sequences of inverted Gaussian modulated sine bursts with a center frequency of 22 MHz, fractional bandwidth of 50%, duration of 0.2 μs and peak negative pressure of 500 kPa (Fig. 3a, 3b). The pressure level was chosen to limit tissue harmonics generation [71] and ensure a minimal destruction of the UCA. The harmonic content of received radiofrequency lines was extracted by summing consecutive inverted pulses and digital filtering from 30–50 MHz to extract the ultraharmonic and second harmonic components.

IVUS chirp reversal sequence | Chirp reversal [44, 75, 95] is a specific contrast detection method relying on the resonant behavior of microbubbles. The transient resonant response of a bubble close to resonance to up and down frequency sweeps differs, whereas the response conserves the waveform of the excitation in a non-resonant medium, such as tissue at low acoustic pressures. Novell at al. [75] reported that chirp reversal was most efficient for a transmitting frequency above the resonance frequency of the interrogated bubble. The IVUS chirp reversal imaging sequence was made of chirp-coded excitations centered at 35 MHz (20–50 MHz linear frequency sweep, duration of 0.42 μs, peak negative pressure of 300 kPa, Tukey windowed with a 90% taper ratio) as shown in Figure 4. The peak negative pressure was chosen to minimize artifacts generated by nonlinear propagation, visible at higher pressures [44]. Pairs of upsweep and downsweep chirps were subsequently transmitted at 1 degree angular position steps. The received ultrasound data were digitally filtered (20–50 MHz) and compressed by cross correlation with the chirp excitation signal (matched filtering) as reported by Maresca et al. [44]. Transmitted excitations do not have the same temporal length in both pulse sequences. Chirp excitations were designed (duration, bandwidth and envelope) to obtain, after compression, an axial resolution equal to that of the pulse inversion excitations.

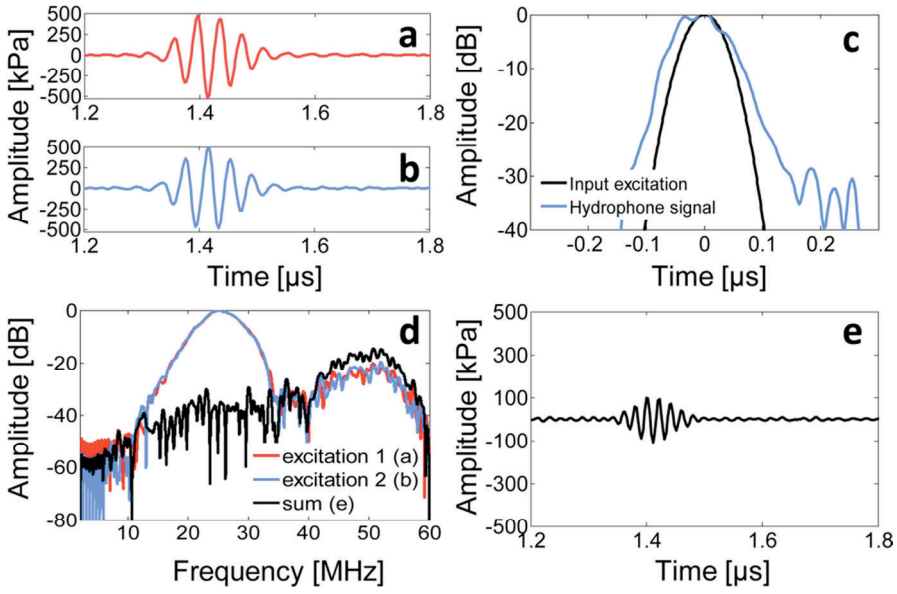

Figure 3. Needle hydrophone measurements. (a, b) Phase-inverted excitations of the ultraharmonic sequence. (c) Envelope of an excitation of the ultraharmonic sequence, (d) frequency spectra of the excitations of the ultraharmonic sequence and (e) residual signal after addition of the inverted excitations of the ultraharmonic sequence.

RESULTS

Hydrophone characterization of axial resolution and tissue cancellation | To characterize the imaging performance of both IVUS contrast imaging pulse sequences, the transmitted waveforms were recorded in water at the transducer focus using a calibrated hydrophone (75 μm polyvinylidene fluoride needle hydrophone; Precision Acoustics Ltd., Dorchester, Dorset, UK) and corrected for frequency dependent hydrophone sensitivity (Figs. 3a, 3b, 4a, 4b). The axial resolution (full width at half maximum) of the pulse inversion waveforms (ultraharmonic imaging) was 122 μm for the input excitation and 171 μm experimentally (Fig. 3c), computed with the average speed of sound in tissue (1540 m/s). The axial resolution of the compressed chirp signals (chirp reversal imaging) was 122 μm theoretically and 144 μm experimentally (Fig. 4c). The experimental waveforms of the ultraharmonic pulse inversion sequence overlapped accurately in the frequency domain (Fig. 3d). In the time domain, their summation gave a residual signal of relatively small amplitude (20% of the experimental waveform amplitude at focus) that corresponds to the second harmonic component generated by nonlinear propagation in water (Fig. 3e). The experimental chirp reversal waveforms (Fig. 4a, 4b) were not fully symmetrical in terms of envelope, and their frequency spectra did not overlap perfectly in the 40–50-MHz range (Fig. 4d) because of the transducer response. However, the compressed chirp signals overlapped in the time domain with a limited mismatch, and their subtraction gave a residual signal of small amplitude (16% of the compressed chirp amplitude; Fig. 4e). In practice, the residual signals in contrast modes are expected to be smaller in tissue than in water. Nonlinear propagation creates part of the residual signal because it distorts the waveform. The higher attenuation in tissue reduces nonlinearity compared to water.

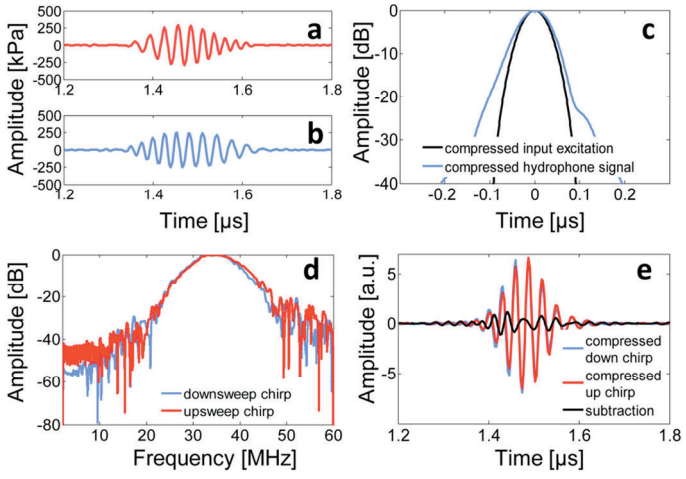

Figure 4.
Needle hydrophone measurements:(a, b) Upsweep and downsweep chirps of the chirp reversal sequence. (c) Compressed chirp envelope, (d) frequency spectra of the chirp excitations and (e) compressed excitations and their residue after subtraction.

Detection of tissue-mimicking phantom side channels | IVUS contrast imaging results are presented in Figure 5. B-mode images are displayed with a 40 dB dynamic range. For both B-mode and contrast mode images, the 0 dB level is defined by the maximum amplitude in the B-mode. For both contrast-imaging sequences, the three largest phantom side channels were resolved in the absence of UCA, whereas the smallest VV mimicking channel was not visible (Fig. 5a, 5d). After UCA injection, all channels had tissue level echogenicity, and were therefore undetectable with conventional B-mode imaging (Fig. 5b, 5e). In both contrast modes (Fig. 5c, 5f), the central channel and the four side channels were detected above residual tissue signal level. The smallest VV mimicking channel was at the edge of detection with the chirp reversal sequence, but well resolved with the ultraharmonic pulse inversion sequence. Contrast images (Fig. 5c, 5f) were further characterized in terms of contrast-to-noise ratio (CNR), measured as the ratio of the maximum intensity in a contrast-filled region of interest over the maximum noise intensity, and contrast-to-tissue ratio (CTR), defined as the ratio of the maximum contrast intensity over adjacent maximum residual tissue intensity at equal depth. Results per phantom channel were computed for three datasets and are presented in Figure 6. As expected from chirp processing, the CNR of chirp reversal imaging proved to be superior for all channels (up to 20 dB for the 2 mm channel), whereas the CTR proved to be superior for the three largest channels (up to 9.8 dB for the 2 mm channel) than in the pulse-inversion ultraharmonic sequence. The VV mimicking channel was detected more clearly in the ultraharmonic contrast image that featured a larger echogenic area corresponding to the 200 μm channel as well as a higher CTR (10.6 dB) compared with the chirp reversal image. Despite the lower peak negative pressure, residual tissue-to-noise ratio was 20% higher for chirp reversal imaging (Fig. 5c) than for ultraharmonic imaging (Fig. 5f). CTR is critical for the detection of sub-resolution targets, such as VV, which can be easily misinterpreted from a tissue residual signal. Our results indicate that ultraharmonic IVUS is more robust for VV detection. Subharmonic contrast imaging was also evaluated by transmitting a 0.35 μs, Gaussian-modulated sine-burst with a center frequency of 45 MHz and with a peak negative pressure of 560 kPa (maximum pressure output of our system at 45 MHz). The subharmonic component was extracted using pulse inversion (Goertz et al. 2006b). A maximum CTR value of 7 dB was found for the 2 mm channel.

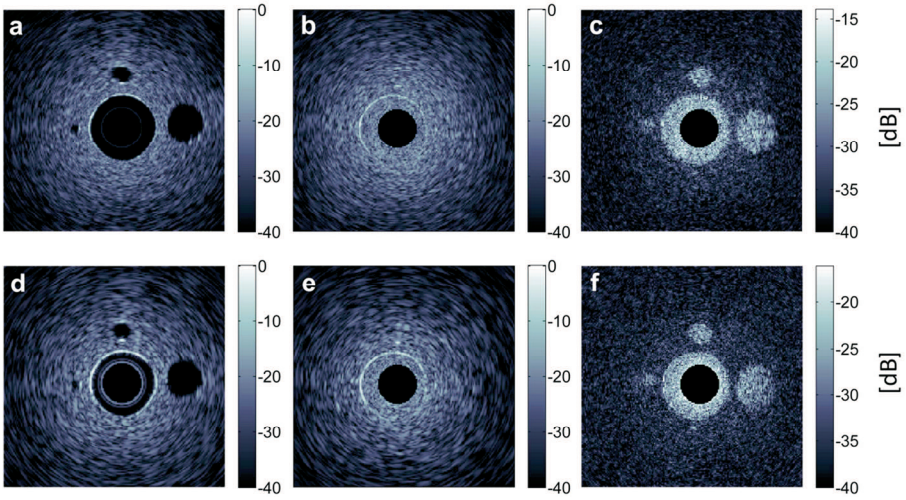

Figure 5. Images acquired in the tissue-mimicking phantom using the chirp reversal sequence and the pulse inversion sequence. (a) IVUS chirp image without contrast. (b) IVUS chirp image with contrast. (c) IVUS chirp reversal contrast image. (d) 22 MHz conventional IVUS image without contrast. (e) 22 MHz conventional IVUS image with contrast. (f) Ultraharmonic IVUS contrast image. Intensity scales in contrast

Ultraharmonic contrast IVUS | The analysis of the frequency content of the pulse inversion contrast image (Fig. 5f) revealed that most of the UCA signal came from the ultraharmonic frequency band rather than from the second harmonic band (Fig. 7b, 7c). This finding is understandable because the sensitivity of the transducer at the second harmonic frequency is low. The amplitude of the 200 μm channel was indeed 4.2 dB higher in the contrast image filtered in the ultraharmonic band (Fig. 7b) than in the image filtered in the second harmonic band (Fig. 7c). To illustrate the nonlinear components extracted by the pulse inversion sequence, we simulated the pressure backscattered by a single Definity bubble (diameter = 1 μm; viscosity $\varkappa_s = 4.2 \times 10^{-10}$; shell elasticity $\chi = 0.75$ N/m; low initial surface tension $\sigma[R_0] = 0.0015$ N/m) in response to the experimental pair of phase-inverted IVUS excitations [62]. Figure 7a presents the pulse inversion spectrum of the single bubble response. While the fundamental frequency peak is suppressed, the subharmonic, ultraharmonic and second harmonic components are observed. Knowing the transducer -6 dB frequency bandwidth (Fig. 7a), the transmitted pulse frequency was chosen to generate a UCA ultraharmonic response at the maximum transducer sensitivity (34 MHz). The simulation also indicated that at high frequency, the amplitude of the ultraharmonic response of a single UCA microbubble can be of the same order as the amplitude of the subharmonic response. Although the second harmonic component showed the highest peak in the simulated pulse-inversion spectrum, its frequency lay outside the transducer bandwidth of -6 dB. The second harmonic component therefore had a lower amplitude (Fig. 7c).

DISCUSSION

Ability to detect a vasa vasorum sized channel | Ultraharmonic IVUS contrast imaging enabled the detection of a 200 μm diameter channel invisible in conventional IVUS images, allowing for functional imaging of sub-resolution microvascular structures such as VV. The capacity of ultraharmonic IVUS contrast imaging to detect the smallest phantom channel proved to be superior to that of chirp reversal IVUS contrast imaging. This may be due to the higher susceptibility of chirp reversal to nonlinear propagation artifacts, to the effects of frequency dependent attenuation on chirp waveforms and to the transducer response. For all these reasons, chirp reversal IVUS is likely to be less robust than a pulse inversion sequence when it comes to imaging microvascular networks. We observed that the B-mode chirp image (Fig. 5a) provided a better spatial resolution than the B-mode image of the ultraharmonic pulse inversion sequence (Fig. 5d). Although the input excitations had a similar axial resolution (Figs. 3c, 4c), hydrophone measurements showed a superior axial resolution in chirp IVUS (144 vs. 171 μm). As the 22 MHz input excitation was outside the transducer bandwidth of -6 dB, its transmission resulted in an elongated waveform because of longer transducer ringdown. In addition, the lateral resolution in the B-mode chirp image (34 MHz center frequency) is finer than in the pulse-inversion B-mode image (22 MHz center frequency). Nonetheless the 200 μm channel was undetected in both B-mode images because its diameter was below the lateral resolution of the transducer, equal to 270 μm at the center frequency [44]. An adequate comparison between the contrast imaging methods we propose in this study, and subharmonic imaging, would require higher transmitting pressure to attain sufficient subharmonic generation. This higher pressure can be generated only if a power amplifier were to be included in the transmit circuit. Because short transmission pulses and minimal dead time after transmission are key in these experiments, which use short ranging depths and small targets, fast gating of such an amplifier is essential. We had no access to a suitable instrument, and as a result were not able to perform this experiment. For this reason, we cannot truly rank chirp reversal, ultraharmonic and subharmonic imaging in terms of contrast detection capability. The scarcity, cost and bulk of suitable power amplifiers, which have sufficient harmonic suppression, places subharmonic imaging at a disadvantage for practical implementation.

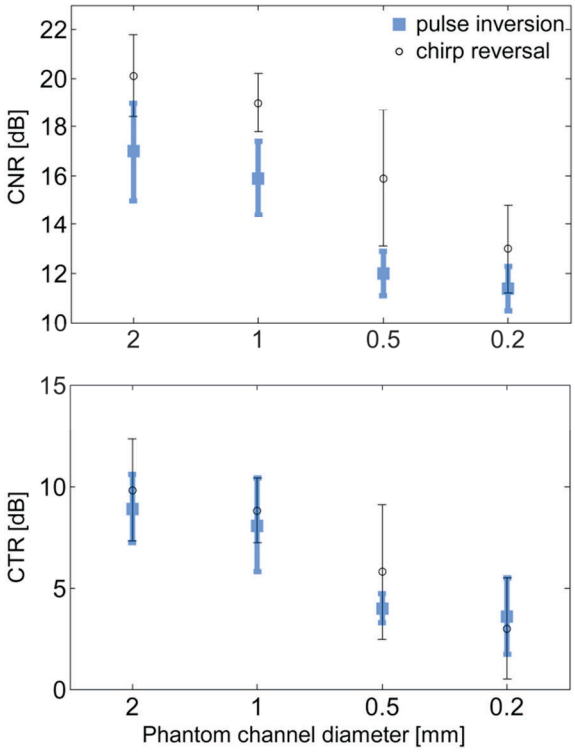

Figure 6. Contrast to tissue ratio (CTR) and contrast to noise ratio (CNR) per phantom channel of the two IVUS contrast imaging modes presented.

Future developments in harmonic contrast IVUS imaging | To achieve a higher B-mode resolution, a short pulse at the transducer center frequency could be transmitted in addition to the two pulses dedicated to ultraharmonic imaging. If broadband IVUS transducers become available in the future, new possibilities would emerge for IVUS contrast imaging. With a transducer bandwidth of 70% (frequency bandwidth at half maximum), a pulse inversion sequence would be able to detect the ultraharmonic and the second harmonic responses of contrast microbubbles. However, such an approach would suffer from the generation of a second harmonic component by tissue and artifacts owing to the distortion of transmitted waveforms because of nonlinear propagation in contrast agent [89, 91]. With a 100% transducer bandwidth, a contrast mode combining the subharmonic and the ultraharmonic signals could be implemented. Contrary to the second harmonic component, these signals are only produced by UCA microbubbles. A gain in CTR of 6 dB can be expected compared with ultraharmonic imaging only, because the backscattered pressures at the subharmonic and ultraharmonic frequencies can have similar amplitudes (Fig. 7a).

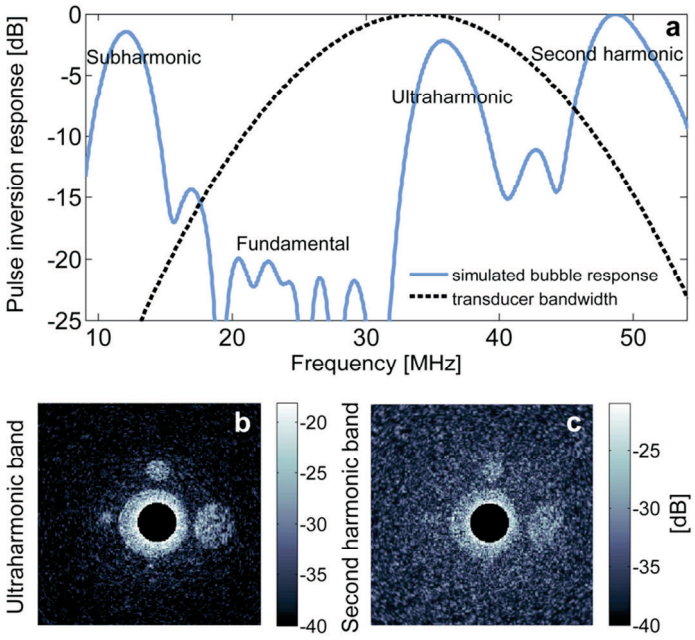

Figure 7. (a) Simulated pulse inversion backscattered pressure of a micrometer-sized Definifty bubble. (b) Pulse-inversion contrast image filtered in the ultraharmonic band (31–44 MHz) and (c) filtered in the second harmonic band (44–52 MHz).

CONCLUSION

Chirp reversal IVUS emerged from our experiments as a balanced two-pulse technique that performs well both in terms of B-mode imaging and contrast detection of targets within the system resolution, but could not detect the vasa vasorum sized channel. The ultraharmonic IVUS pulse sequence presented does not require any additional hardware implementation (contrary to chirp excitations) and could therefore be readily applied on existing commercial IVUS scanners in in vivo applications. Between the two methods investigated in this study, we recommend ultraharmonic imaging as the best method for IVUS imaging of vasa vasorum because it enabled the detection of a 200 μm channel.

Acknowledgements | Funding was provided by the Simon Stevin grant 2007 of the Dutch Technology Foundation (STW). The ultrasound contrast agent Definity was supplied by Lantheus Medical Imaging.

6.

Imaging Microvasculature with Contrast-Enhanced Ultraharmonic Ultrasound

Based on the manuscript by D. Maresca, I. Skachkov, G. Renaud, K. Jansen, G. van Soest, N. de Jong, A. F. W. van der Steen, **Imaging Microvasculature with Contrast-Enhanced Ultraharmonic Ultrasound**. *Submitted.*

ABSTRACT

Atherosclerotic plaque neovascularization was shown to be one of the strongest predictors of future cardiovascular events. Yet, the clinical tools for coronary wall microvasculature detection *in vivo* are lacking. Here we report an ultrasound pulse sequence capable of detecting microvasculature invisible in conventional intracoronary imaging. The method combines intravascular ultrasound with an ultrasound contrast agent, e.g. a suspension of microscopic vascular acoustic resonators that are small enough to penetrate the capillary bed after intravenous administration. The pulse sequence relies on brief chirp excitations to extract ultrasound contrast agent specific ultraharmonic echoes. We implemented the pulse sequence on an intravascular ultrasound probe and successfully imaged the microvasculature of a 6 days old chicken embryo respiratory organ. The feasibility of microvasculature imaging with intravascular ultrasound sets the stage for a translation of the method to studies of intraplaque neovascularization detection in humans.

INTRODUCTION

The progression of human coronary atherosclerosis is associated with increased arterial wall microvasculature density [28, 66]. This network of microvasculature, the vasa vasorum, originates from the adventitial layer of large blood vessels to supply the deeper media and intima layers with nutrients and oxygen [26]. In atherosclerotic arteries, erratic vasa vasorum neovascularization can occur (fig. S1), leading to intra-plaque hemorrhage and ultimately plaque rupture [3, 96]. It is hypothesized that atherosclerotic plaque neovascularization density could serve as surrogate marker of plaque vulnerability [3]. However, existing clinical tools are unable to detect coronary vasa vasorum *in vivo*. Intravascular ultrasound (IVUS) in combination with an ultrasound contrast agent has demonstrated potential for vasa vasorum imaging [31, 32] but fails to reach clinical practice to date due to IVUS transducer limitations in frequency bandwidth and sensitivity [97]. To overcome these limitations, we developed ultraharmonic IVUS imaging, a narrow frequency bandwidth contrast detection method able to visualize sub-resolution microvascular networks without the blood flow velocity limitations of Doppler ultrasound [98].

Ultrasound contrast agents are suspensions of high molecular weight gas microbubbles encapsulated by thin lipid shells [94]. Bubbles are typically designed to be of a size (1-10 μm) that passes through capillary beds and are acoustically active at diagnostic ultrasound frequencies. The primary advantages of using ultrasound contrast agents are the improvement of the signal strength from blood, which becomes bright in echographic images (a parallel can be drawn with bright blood pulse sequences in magnetic resonance imaging), and the detection of slow microvascular flow in the presence of tissue motion [99]. Contrast ultrasound imaging techniques rely upon the stimulation of resonant microbubble behaviours to generate and detect harmonic ultrasound contrast agents' backscattered signals [94] that differ from tissue backscattered signals. Current harmonic contrast ultrasound imaging methods are limited to second harmonic (echo at twice the transmit frequency) or subharmonic (echo at half the transmit frequency) imaging. However, second harmonic echoes are not ultrasound contrast agent specific, while the use of subharmonic echoes lowers image resolution [88]. Furthermore, detecting second or subharmonic echoes demands a transducer frequency bandwidth of 67% which exceeds clinical IVUS transducers specifications [97]. Several contrast echocardiography studies relied on second order ultraharmonics at 2.5 times the transmit frequency [100, 101]. But this strategy requires very wideband systems (86% frequency bandwidth) and sensitive detection of these low amplitude harmonics is further limited by the frequency-dependent ultrasound attenuation in cardiac tissue (0.5 dB/cm/MHz).

Our approach consisted in imaging contrast microbubbles using the first order ultraharmonics that arise at 1.5 times the transmit frequency [94]. These signals are specific to ultrasound contrast agents and their proximity to the transmit frequency makes their capture possible with a transducer frequency bandwidth

of 40% (Materials and Methods). Hence, ultraharmonic imaging allows for the emission and reception of ultrasound pulses within the sensitive frequency range of commercially available IVUS transducers. Furthermore, relying on contrast-specific ultraharmonic echoes prevents misclassifying tissue artefacts as microbubbles [89], as in the case of second harmonic imaging. For a given probe having a given bandwidth, it also provides an enhanced lateral image resolution compared to subharmonic imaging [88]. In practice, the ultrasound echoes backscattered by ultrasound contrast agents are dominated by signal at the transmit frequency. In order to isolate contrast agent ultraharmonics, we transmitted pairs of phase inverted chirp excitations, summed the backscattered echoes and filtered the residual signal in the ultraharmonic frequency range (see Material & Methods). This approach, known as pulse-inversion [37], suppresses transmit frequency signals while preserving most of harmonic signals.

RESULTS

Contrast agent ultraharmonic echoes locate microchannels below IVUS resolution | We first evaluated the ultraharmonic IVUS pulse-inversion sequence by simulating [62] the scattering response of a single contrast microbubble to a pair of phase inverted chirp excitations. Transmitted IVUS chirp excitations had a 23 to 29 MHz frequency sweep, corresponding to a center frequency f_0 equal to 26 MHz. The frequency response of the single microbubble after summing the pair phase-inverted backscattered echoes is reported (Fig. 1). The simulation result illustrates that the spectrum amplitude at the transmit frequency (f_0 = 26MHz) and its odd multiples (third harmonic at $3f_0$ = 78 MHz) are significantly suppressed whereas even harmonics (second harmonic at $2f_0$ = 52 MHz) and ultraharmonics ($1.5f_0$ = 39MHz, $2.5f_0$ = 65MHz) are successfully extracted. As expected, the simulation also shows that the first ultraharmonic ($1.5f_0$) has a higher amplitude than subsequent ultraharmonics ($2.5f_0$, $3.5f_0$). Note that ultrasound attenuation in cardiac tissue, not taken into account in the simulation (Fig. 1), further increases this amplitude difference since the first ultraharmonic is less attenuated that the 2nd ultraharmonic.

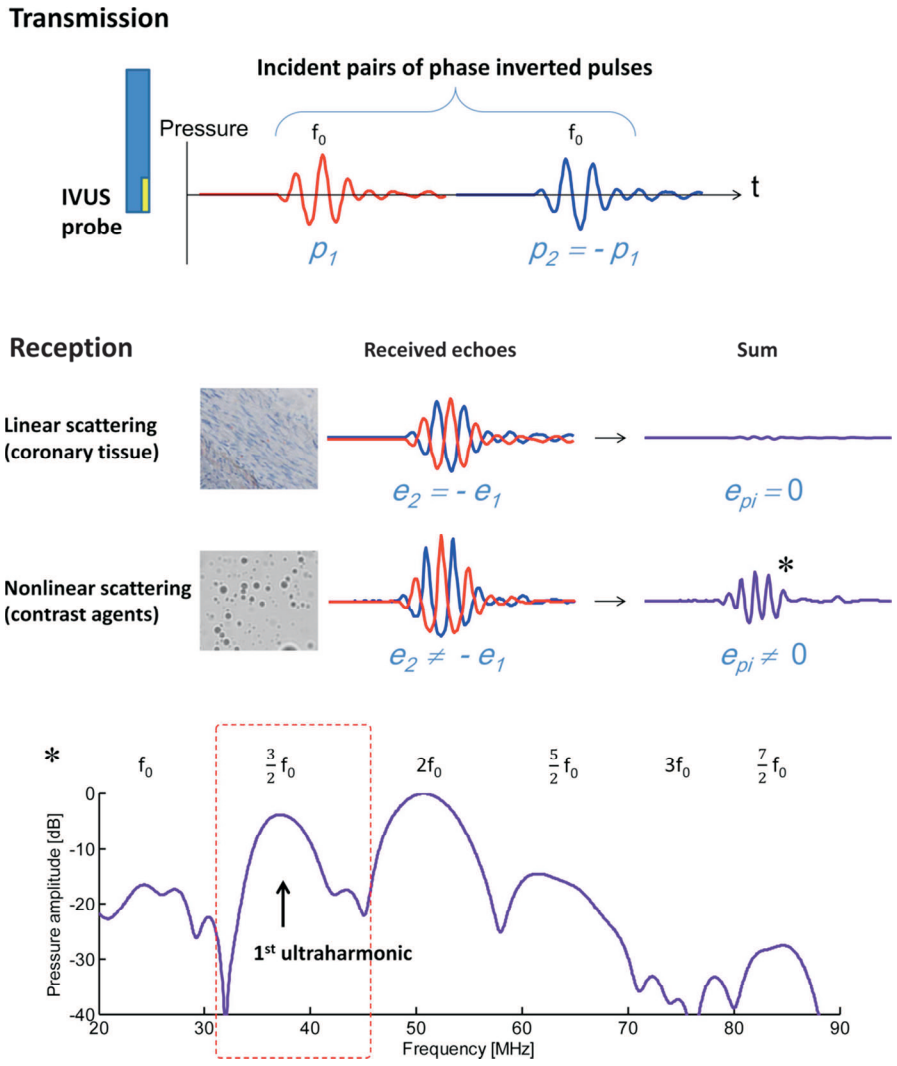

Figure 5. Principle of the intravascular ultrasound pulse sequence. Pairs of phase inverted pulses noted p_1 and p_2 are transmitted by the IVUS transducer (called a pulse-inversion sequence). Corresponding backscattered echoes e_1 and e_2 are received by the transducer. If the insonified medium is linear (biological tissue) echoes stay symmetric and their sum is zero. If the medium is nonlinear (ultrasound contrast agent) echoes are distorted and their sum leaves a residue. The residual frequency spectrum of a single contrast microbubble was simulated with the Marmottant model [62] (1.3 µm diameter that resonates at 26 MHz, viscosity $\kappa_s = 4.2.10^{-10}$, shell elasticity x = 0.75 N/m, initial surface tension σ(R0) = 0.006 N/m). A range of harmonics are visible at multiples of the transmit IVUS frequency (26 MHz), including the first ultraharmonic response at 39 MHz, whereas the transmit frequency peak is efficiently suppressed by the pulse inversion sequence. The waveforms utilized in the simulation are displayed in fig. S6.

Experimentally, we first investigated the performance of ultraharmonic contrast IVUS *in vitro* by imaging a custom coronary vasa vasorum phantom with our laboratory IVUS imaging system (Material and Methods, Fig. 2A). To ensure that phantom measurements are predictive of the performance of ultraharmonic IVUS in perivascular coronary tissue, we selected a tissue mimicking material [102] that realistically renders ultrasound properties in biological tissue (speed of sound, attenuation) at our frequency range (20-50MHz). Therefore, tissue cancellation levels observed in the phantom experiment with the pulse inversion sequence are good predictors of the *in vivo* situation. We first insonified the coronary artery vasa vasorum phantom with conventional 35 MHz IVUS pulses in the absence of ultrasound contrast agent. As anticipated, the lumen contour and the 500 μm side channels were detected while the 200 μm channels, smaller than IVUS lateral resolution [4], remained undetected (Fig. 2B). Next, we immersed the coronary vasa vasorum phantom in a static ultrasound contrast agent suspension, using a realistic *in vivo* dilution (10^6 microbubbles per mL). The acoustic pressure transmitted (of the order of 600 kPa at focus in tissue) is considered non-destructive for contrast microbubbles at IVUS frequency. This time, the phantom was insonified with the IVUS pulse sequence, consisting in pairs of chirp excitations with a center frequency of 26 MHz. As a result, the lumen and side channels echogenicity rose to tissue level, making the channels invisible in the conventional IVUS image (Fig. 2C). Application of the ultraharmonic signal processing revealed all side channels, including the 200 μm sub-resolution channels (Fig. 2D). We measured the intensity of the side channels in terms of contrast-to-tissue ratios. Values reached a maximum of 9.8 dB at a distance of 2.8 mm before decreasing to 2.9 dB at 3.8 mm (Fig. 2E), following conventional unfocused transducer beam characteristics [103]. Note that in the presence of a contrast filled lumen, which is a more attenuating medium than blood, the ultraharmonic ultrasound imaging method detected microchannels up to a distance of 4.3 mm from the transducer. This range is well adapted to the detection of intraplaque coronary neovascularture in humans. The results also demonstrate that it is possible to perform ultraharmonic ultrasound imaging at IVUS frequency using the native size distribution of a commercial ultrasound contrast agent. In light of these results, we subsequently performed an *in vivo* investigation of the ultraharmonic IVUS imaging.

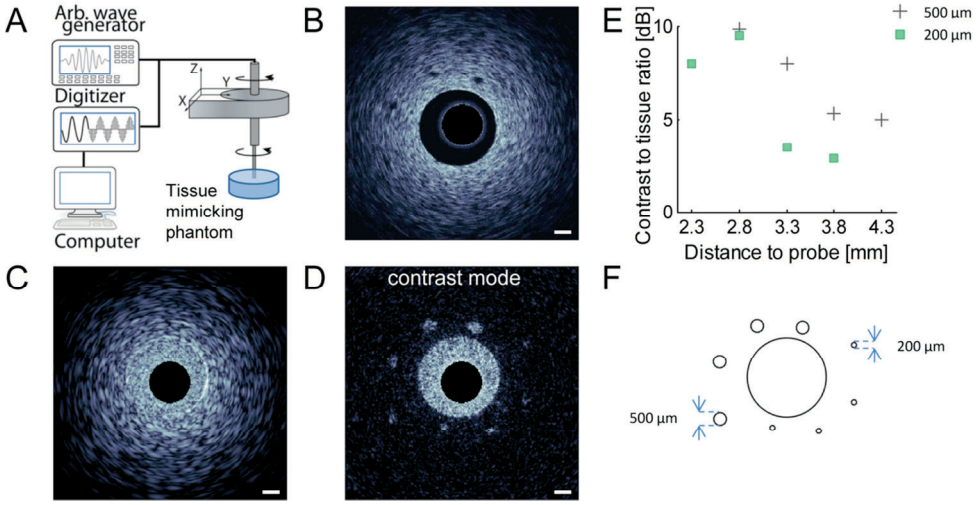

Figure 6. *In vitro* evaluation of ultraharmonic IVUS imaging. (A) Schematic setup depicting the IVUS probe actuated by the rotary stage, the arbitrary wave generator transmitting the pulse-sequence and the digitizer for data acquisition. (B) 35 MHz conventional IVUS image of the coronary vasa vasorum phantom; only the 500 µm side channels were detected. Scalebars in IVUS images represent 1 mm. (C) Conventional 26 MHz IVUS image in the presence of an ultrasound contrast agent. The lumen and side channels became echogenic and could not be distinguished from the phantom material. (D) Ultraharmonic IVUS image. The lumen and all the side channels filled with the ultrasound contrast agent were detected, including the 200 µm sub-resolution channels. On the contrary, tissue signals were suppressed below noise level. (E) Contrast to tissue ratio of the 500 µm and 200 µm channels. The contrast to tissue ratio reached a maximum at 2.8 mm. Note that the distances of the 500 µm and 200 µm channels to the probe are shifted because the IVUS probe was not at the center of the lumen. (F) Schematic cross section of the coronary vasa vasorum phantom channels. The lumen diameter is 4 mm.

Ultraharmonic IVUS imaging reveals an embryonic respiratory vascular plexus | We translated the experiment *in vivo* to establish the capacity of ultraharmonic IVUS to image intricate microvasculature of vasa vasorum dimension. We selected a chicken embryo model as it enabled the optical registration of the insonified vascular geometry, contrary to former intravascular *in vivo* studies [31, 32]. By day 6, chicken embryos have developed a respiratory and waste elimination organ called the allantois. This organ appears as an extra-embryonic hollow sphere delineated by a thin membrane. The allantois membrane itself is webbed with a dense network of microvessels exhibiting cross sections (diameters < 200 µm) of the order of human atherosclerotic plaque vasa vasorum [82]. We positioned the IVUS probe next to the allantois membrane for insonification (fig. S2, Fig. 3B). We first acquired a 35 MHz conventional IVUS image as well as an ultraharmonic IVUS image of the allantois membrane before administration of the ultrasound contrast agent (Fig. 3A). The allantoic membrane appears in the bottom left quadrant of the conventional IVUS image. Due to the membrane intrinsic echogenicity, the dense allantois microvasculature is not resolved in the image. The echogenic structures on the right hand

side of the conventional IVUS image correspond to the yolk. In the ultraharmonic image, the echogenicity of the allantois membrane and the yolk is suppressed to noise level by the pulse inversion sequence. Next, a 4 μL bolus of ultrasound contrast agent was administered in the vitelline vein of the chicken embryo using a capillary glass injection needle. We acquired a set of conventional and ultraharmonic IVUS images of the allantois membrane at the same location with two minutes intervals (Fig. 3A). The spread of the ultrasound contrast agent though the allantois microvasculature was clearly visible in the set of ultraharmonic images, indicating that hemodynamics can be tracked. Note that an enhancement of the microvessels infused with contrast is also visible in the conventional IVUS images. By subtracting the pulse-inversion frequency spectra of the allantois membrane before and after contrast administration, we observed experimentally the appearance of an ultraharmonic frequency peak induced by the ultrasound contrast agent generation in response to the pulse-inversion sequence (Fig. 3C).

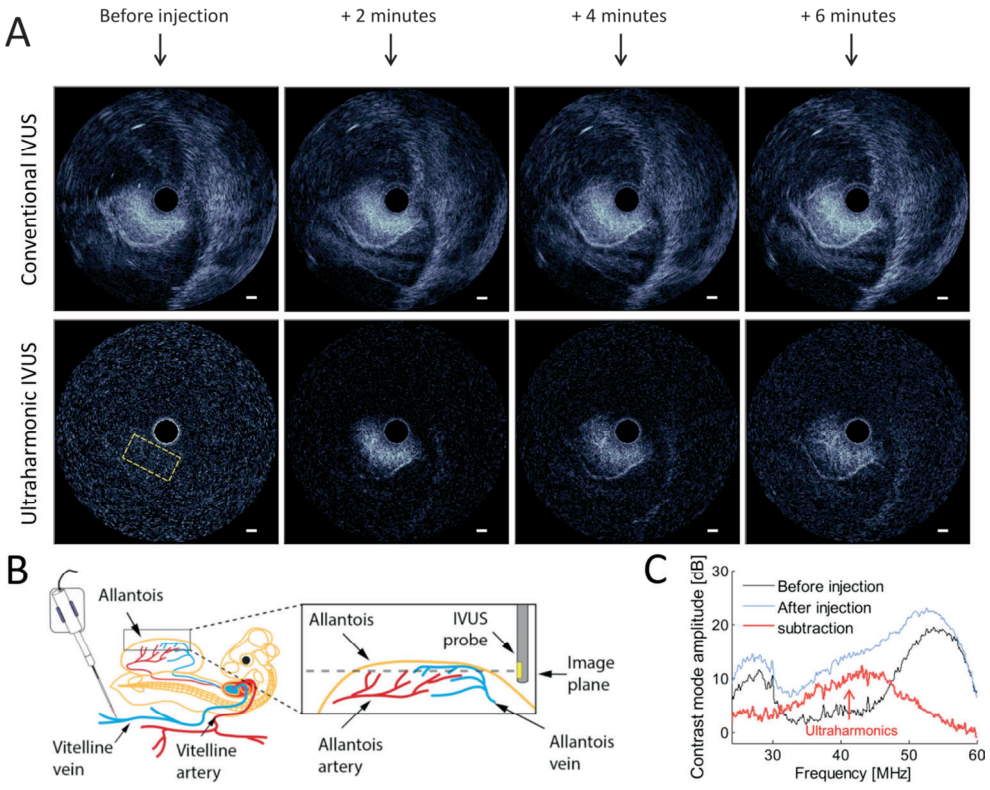

Figure 7. *In vivo* evaluation of ultraharmonic IVUS imaging. (A) Conventional 35 MHz IVUS and co-registered ultraharmonic IVUS imaging of the ultrasound contrast agent spreading in the allantois membrane of a 6 days old chicken embryo. Before injection, the allantois membrane appears echogenic in conventional IVUS but its microvasculature is not resolved. In the corresponding ultraharmonic IVUS image,

intrinsic tissue echogenicity is suppressed to noise level and the image appears black in the absence of contrast. After ultrasound contrast agent administration, ultraharmonics reveal the membrane perfusion over time. Microvascular structures clearly emerge after 6 minutes. Note that the conventional IVUS images are also enhanced but one cannot disentangle microvessel echogenicity from the intrinsic membrane echogenicity. Scalebars in IVUS images represent 1mm. (B) Schematic of the setup. A bolus of contrast is injected using a capillary glass needle. The IVUS probe is positioned perpendicular to the allantois membrane for insonification. (C) *In vivo* pulse-inversion frequency spectra before (black line) and after (blue line) contrast injection. Their subtraction (red line) reveals the ultraharmonic intensity backscattered by the ultrasound contrast agent. Frequency spectra were computed in the yellow outline depicted in Fig (3A).

Complementary to these in-plane contrast dynamic observations, we performed an in-depth scan of the allantois membrane. Conventional IVUS images at 35 MHz and ultraharmonic IVUS images were acquired at five equidistant positions in depth, covering in total a distance of 800 μm (Fig. 4A). Microvessels infused with contrast appear in the ultraharmonic IVUS images, as seen at the 0 mm and -0.2 mm positions (Fig. 4A). We computed a mean intensity projection of the five planes imaged with both the conventional and ultraharmonic IVUS (Fig. 4B). In the conventional IVUS image, the presence of microvessels can be suspected thanks to the enhanced echogenicity induced by the ultrasound contrast agent. However, based on echogenicity levels alone, it is not possible to disentangle the contrast-enhanced microvessels from the intrinsic echogenicity of the allantoic membrane. On the contrary, as the ultraharmonic IVUS image displays only the microvasculature filled with contrast agents, the allantois vascular plexus appears with a superior contrast. Quantitatively, the contrast to tissue ratio between a microvessel and the adjacent membrane was up to doubled (12.5dB in ultraharmonic IVUS image as opposed to 6 dB in the conventional IVUS image). For reference, a photograph of the allantois microvasculature insonified with the IVUS probe was taken and corroborated the ultraharmonic ultrasound result with a strong agreement (Fig. 4C). Note that the photograph also displays deeper vessels that were outside of the volume insonified with IVUS.

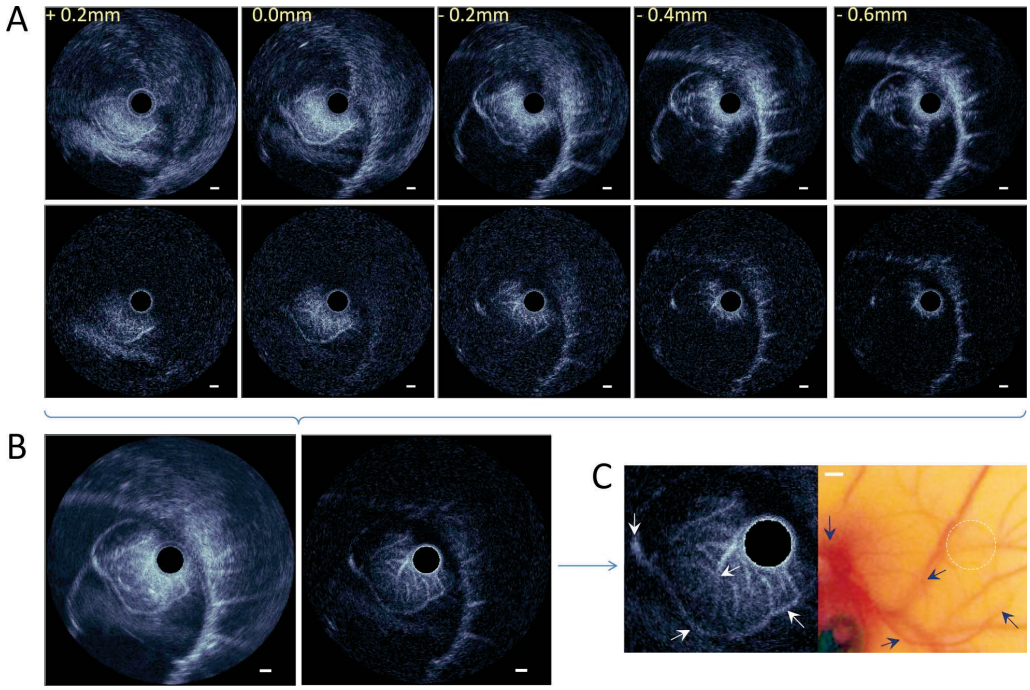

Figure 8. *In vivo* ultraharmonic IVUS scan across the allantois membrane microvasculature. (A) Conventional and ultraharmonic IVUS imaging at 5 different depths, equally spaced by 200 microns. Positions in mm are labeled yellow. (B) Corresponding mean intensity projections. The ultraharmonic IVUS image reveals the allantois microvasculature. (C) Zoom in the membrane microvasculature imaged with ultraharmonic IVUS and comparison to a photograph of same the region of interest. Arrows indicate corresponding vessels in the two images. Scalebars in IVUS images represent 1 mm.

This final result demonstrates the capacity of ultraharmonic IVUS to image a dense network of vasa vasorum sized vessels that would have been invisible in the absence of an ultrasound contrast agent (as in the conventional IVUS image before contrast injection in Fig. 3A).

DISCUSSION

Intraplaque vasa vasorum density was shown to be one of the strongest predictors of atherosclerotic plaques at risk that require intervention [3]. Yet, there are no clinical tools at present for coronary vasa vasorum detection *in vivo*. Our results demonstrate that the implementation of an ultrasound contrast agent detection pulse sequence enhances the physiological contrast of IVUS by enabling the detection of intricate vasa vasorum sized targets. Our strategy consisted in sensing contrast agent specific echoes at 1.5 times the transmit frequency, referred to as ultraharmonics. The *in vivo* echolocation of ultraharmonics with an IVUS probe revealed microvasculature infused with ultrasound contrast agents (Fig. 3 and Fig.

4). The limited frequency bandwidth requirement of ultraharmonic ultrasound imaging made its implementation on a conventional IVUS transducer possible, contrary to other existing harmonic methods. We also show that one can augment the ultraharmonic response of an ultrasound contrast agent by relying on chirp excitations rather than conventional imaging pulses (fig. S6).

To date, ultraharmonic ultrasound imaging has received little attention in the field of medical ultrasound, probably because the amplitude of ultraharmonics is usually lower than the amplitude of subharmonics. Yet, the ability to transmit and receive ultrasound pulses within the bandwidth of commercially available transducers is a major advantage for imaging as it improves sensitivity [97] (Materials and Methods). We also report in the phantom experiment that despite its high frequency range, ultraharmonic IVUS could be performed without manipulating the size distribution of a commercial ultrasound contrast agent. Finally, contrary to ultrasound Doppler techniques for blood flow imaging, contrast-enhanced IVUS is not impaired tissue motion [99]. In light of these results, the next step will consist in performing intracoronary ultraharmonic IVUS imaging in a porcine model of atherosclerosis. A limitation of the method is that, despite its enhanced microvasculature detection capabilities compared to conventional IVUS, image resolution itself is not improved. A subresolution microvessel filled with contrast will still appear as big as the imaging system's point spread function. This can be observed in Figure 4C. Accurate volumetric quantification of microvasculature relies on imaging resolution and remains a future target. Meanwhile, ultraharmonic IVUS fulfills its primary role of providing a metric of microvascular density in the coronary artery wall by successfully detecting small blood vessels.

The dose of ultrasound contrast agent injected in the phantom experiment was in line with current medical guidelines. In the embryo case it was one order of magnitude higher (10^7 bubbles per mL). Guidelines must be defined for contrast IVUS investigations in larger animal models of atherosclerosis and eventually in humans. From the point of view of imaging, it is critical that enough ultrasound contrast agents reach the vasa vasorum. As the vasa vasorum is mostly perfused from the outside-in, through the external venous network, rather than from the artery lumen [26], bolus injections of contrast will need to be performed upstream from the site of interest. Studies need to be conducted to establish optimal ultrasound contrast guidelines for contrast IVUS investigations of coronary arteries. Note that we do not anticipate motion artifacts in ultraharmonic IVUS images. 20 μs are required to transmit and receive a pair of phase inverted excitations in order to scan a depth of 8 mm. Lateral motion of the artery wall reaches peak velocity of a few cm/s. The effect of this motion within 20 μs is negligible.

Analogous to the development of MRI blood detection sequences, IVUS will widen its scope by adopting blood detection pulse sequences like ultraharmonic ultrasound imaging. Ultraharmonic IVUS could not only help identifying vulnerable plaques requiring intervention but also be play a role in the follow-up of cardiac patients. The resurgence of atherosclerosis at stented sites is a growing concern in interventional cardiology and became a target for novel intravascular imaging techniques [104]. Here again, the vasa

vasorum could be a valuable early risk predictor. Beyond the scope of IVUS, ultraharmonic ultrasound imaging can be implemented on any conventional ultrasound scanner to study inflammatory processes of clinical importance, such as atherosclerosis, rheumatoid arthritis or cancer development.

MATERIALS AND METHODS

Frequency bandwidth of harmonic contrast ultrasound imaging methods | The frequency bandwidth *BW* required for harmonic contrast ultrasound imaging is defined as the difference between the transmit ultrasound pulse frequency f_T and its harmonic echo frequency f_H over the center frequency $f_c = (f_T + f_H)/2$,

$$BW = \frac{|f_T - f_H|}{f_C} = \frac{2|f_T - f_H|}{f_T + f_H}$$

For second harmonic $(f_H=2f_T)$ and subharmonic imaging $(f_H=f_T/2)$, the frequency bandwidth requirement is $BW=2/3$ or 67%. For ultraharmonic imaging $(f_H=3f_T/2)$, the frequency bandwidth requirement is $BW=2/5$ or 40%. The feasibility of a given harmonic contrast ultrasound imaging method depends on the frequency bandwidth of the ultrasound imaging probe utilized.

Laboratory intravascular ultrasound imaging system | We conducted this study with a miniaturized unfocused IVUS transducer [77] (34 MHz center frequency, 56% frequency bandwidth) assembled into a side-looking IVUS probe and actuated with a rotary stage (Steinmeyer DT105). The transmission circuit of the IVUS imaging system comprised an arbitrary waveform generator (Tabor Electronics WW2571A), a custom-made expander and the IVUS probe. The receive circuit consisted of a custom-made limiter, a 43 dB low noise amplifier (Miteq AU1263) and a 12 bit digitizer (Acqiris DP310) (fig. S3). The imaging system functioned as follows: short ultrasound pulses were coded and transmitted as 16V peak-peak electric signals by the arbitrary waveform generator. The expander stopped low voltage noise while letting the pulses go to the transducer. The transducer converted electric pulses into ultrasonic pressure pulses that propagated in the medium of interest. Ultrasound echoes backscattered in the medium hit the transducer surface back where they were continuously converted into an electric radiofrequency (RF) signal. The limiter let the low amplitude RF signal go to the low noise amplifier, while blocking the 16V pulses transmitted by the waveform generator. After amplification, the received RF signals were digitized and saved in a computer. The pulse/delay generator synchronized all instruments. We performed cross-sectional scans by rotating the IVUS probe in 1° steps using a motorized rotary stage. Each IVUS image consisted of 360 evenly spaced pulse-echo radiofrequency lines digitized at a sampling frequency of 350 MHz. Conventional IVUS imaging (Fig. 2b) was achieved by

transmitting 35 MHz 60% bandwidth Gaussian envelope sine wave pulses. These full-band pulses transmitted at the transducer center frequency provide the highest resolution attainable with our IVUS system (axial resolution = 106 μm, lateral resolution = 272 μm). They were used to assess the micro channels detection capabilities of conventional IVUS imaging.

Ultraharmonic intravascular ultrasound pulse sequence | The ultraharmonic pulse-inversion sequence investigated *in vitro* and *in vivo* consisted of 3 pairs of phase inverted [37] chirp excitations (23 to 29 MHz linear frequency sweep, 0.3 μs duration, 880 kPa peak negative pressure at focus in water, Tukey windowed with a 100% taper ratio) transmitted at each angular step. We extracted the ultraharmonic content of the digitized radiofrequency lines by summing the echoes received in response to the pairs of inverted excitations and digitally filtering the summed radiofrequency data from 33 MHz to 47 MHz. Frequency values were selected to operate in the most sensitive region of the IVUS transducer bandwidth (fig. S4). Chirp excitations proved to enhance the ultraharmonic response of microbubble contrast agents by 2 dB compared to sine-bursts of identical center frequency, envelope and peak negative pressure (fig. S5). The simulation of the pulse-inversion response of a single contrast agent [62] supported this observation (fig. S6).

Coronary vasa vasorum phantom | The agar-based tissue mimicking material was characterized in the 10-47 MHz frequency range [102], covering our IVUS application. This ensured acoustic properties (speed of sound and attenuation) similar to those of human biological tissue. A schematic cross section of the phantom geometry is provided (Fig. 2F).

Chicken embryo model | A chicken embryo model was used for *in vivo* validation of the ultraharmonic ultrasound method. By day 6, chicken embryos have developed a respiratory and waste elimination organ called the allantois. This organ appears as an extra-embryonic hollow sphere delineated by a thin membrane. The allantois membrane itself is webbed with a dense network of microvessels exhibiting cross sections (diameters < 200 μm) of the order of human atherosclerotic plaque vasa vasorum [82]. Fertilized White Leghorn chicken eggs (Gallus gallus domesticus) were purchased from a local supplier (Drost BV). After 6 days of incubation at 37°C in a humidified incubator (Thermo Scientific) corresponding to stage HH27-29 according to the Hamburger and Hamilton criteria [105], the embryos were taken out of the eggshell and placed into the experimental setup (fig. S2). The optical reference measurements of the allantoic microvasculature imaged with IVUS were calibrated with a millimetric scale. Microvessel cross sections were measured in terms of pixel lengths using the ImageJ software and converted into metric units thereafter.

Ultrasound contrast agent handling | We used the commercial ultrasound contrast agent Definity™ (Lantheus Medical Imaging). This contrast agent contains mostly microbubbles of diameters ranging from 1.1 and 3.3 μm, with 98% of the bubble population below 10 μm. Since a 1 μm diameter single Definity™ bubble resonates at 25 MHz [40], it is the micron to submicron sized bubbles that contribute mostly to the harmonic signal at IVUS frequencies. In the phantom experiment, we activated the ultrasound contrast agent according to manufacturer's recommendations (45 seconds controlled shaking) and diluted it in degassed water with a dilution ratio of 1:1000, which of the order of dilutions administered in human use [106]. Subsequently, the phantom was immersed in a tank containing the prepared contrast agent solution.

In the *in vivo* experiment, we first performed a 10 minutes decantation of the contrast agent Definity™ after activation and subsequently extracted the bottom 0.2 mL to preferentially retain small contrast microbubbles active at our frequency range [97]. We administered a 4 ± 1 μL undiluted bolus of the ultrasound contrast agent in one of the vitelline veins of the chicken embryo using a home-made capillary glass needle and a commercial injection system (VisualSonics). This *in vivo* dose was shown to work in a previous chicken embryo study [107]. Due to the addition of the decantation step, however, the volumetric concentration of contrast microbubbles that we administered *in vivo* was lower [40].

Acknowledgments | We thank K. Shung and Q. Zhou (University of Southern California) for providing the IVUS transducer. This research was supported by the Dutch Technology Foundation STW (2007 Simon Stevin Meester grant).

SUPPLEMENTARY MATERIALS

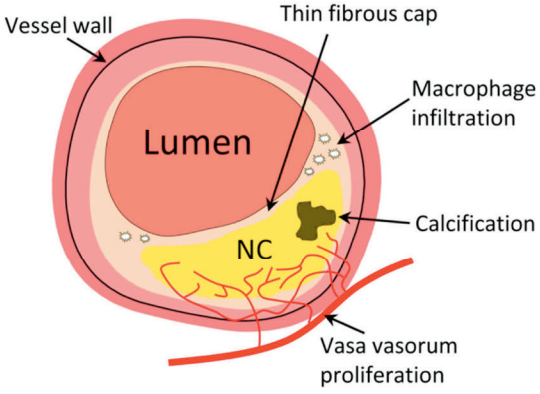

Supplementary Figure 1. Schematic cross section of a vulnerable atherosclerotic plaque, illustrating an outside-in proliferation of the vasa vasorum into the atherosclerotic lesion. Other makers of atherosclerotic plaque vulnerability are represented e.g. large necrotic core, thin fibrous cap, calcification and macrophage infiltration.

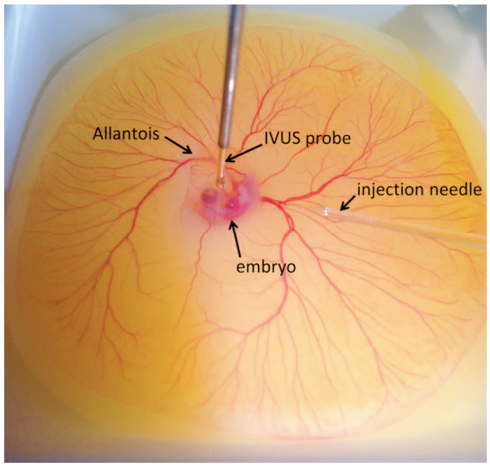

Supplementary Figure 2. Photograph of the 6 days old chicken embryo during ultraharmonic contrast IVUS scanning. The IVUS probe was positioned next to the allantois membrane, which developed above the embryo. The bolus of ultrasound contrast agent was administered using an injection needle via the vitelline veins, upstream from the heart.

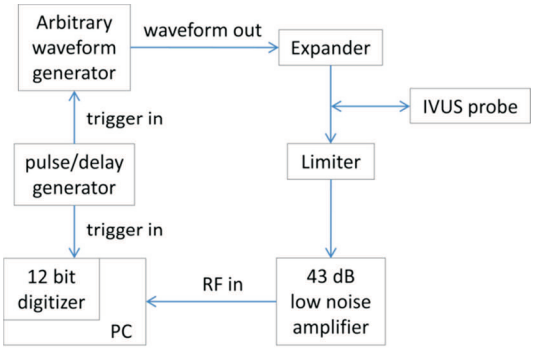

Supplementary Figure 3. Configuration of the laboratory intravascular ultrasound electronic circuit.

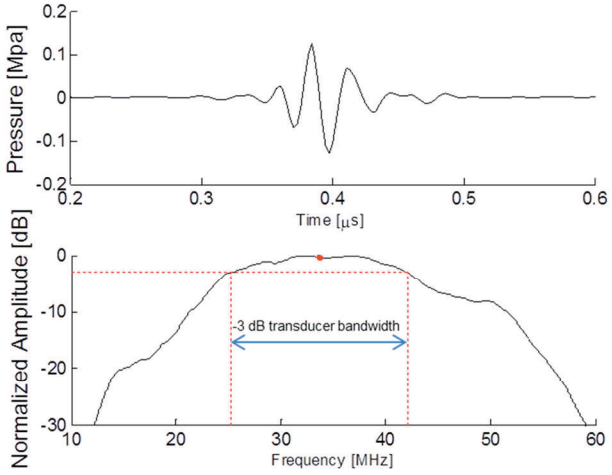

Supplementary Figure 4. Characterization of the IVUS transducer with a needle hydrophone (Precision acoustics). (Top) Time impulse response recorded at the natural focus of the transducer (2 mm). (Bottom) Frequency spectrum of the impulse response. The measured center frequency (red dot) and bandwidth (dotted lines) were in close agreement with the documented values (center frequency of 34 MHz, frequency bandwidth <60%).

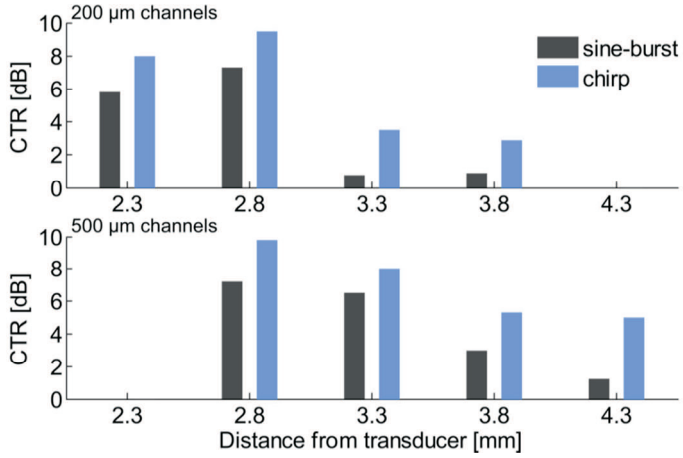

Supplementary Figure 5. Comparison of the contrast to tissue ratio (CTR) per phantom microchannel (Fig. 2) of the ultrasound contrast agent in response to the sine-burst and chirp ultraharmonic pulse-inversion sequence. The CTR performance of the chirps was superior at every depth.

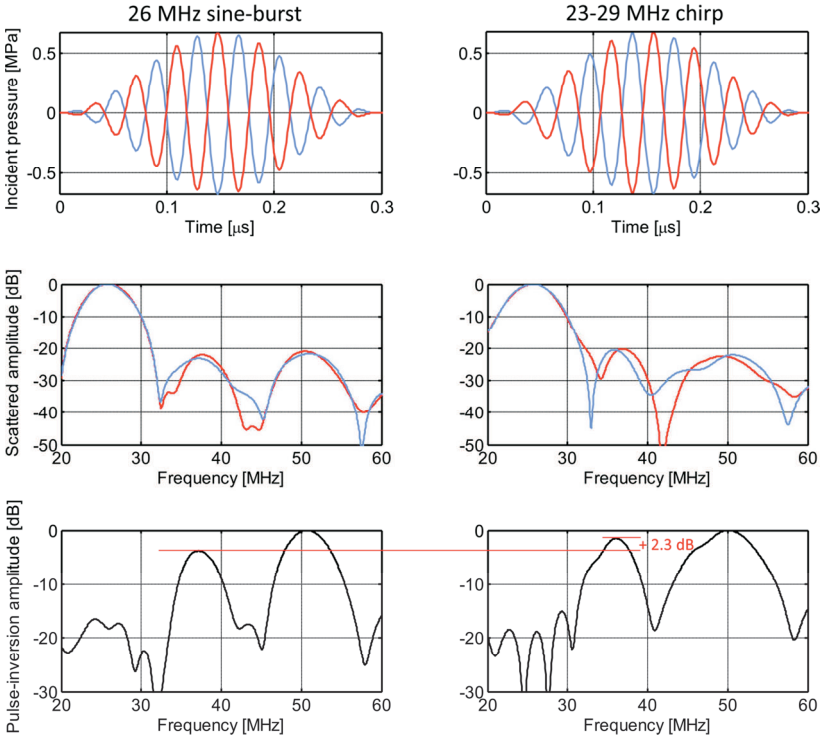

Supplementary Figure 6. The response of a single Definity™ contrast microbubble to the sine-burst ultraharmonic pulse-inversion sequence (Left column) and chirp ultraharmonic pulse-inversion sequence (Right column) was simulated using the Marmottant model (*17*) (diameter 1.3 µm, viscosity κ_s = 4.2.10^{-10}, shell elasticity x = 0.75 N/m, initial surface tension σ(R0) = 0.006 N/m). The transmitted phase inverted waveforms are plotted in red and blue (Top row). The frequency spectra of the waveforms scattered by a single bubble were modeled and are displayed in red and blue (Middle row). The scattered pulse-inversion spectra are plotted in black (Bottom row). The model predicted a 2.3 dB increase of the ultraharmonic amplitude with the use of chirps compared to sine-bursts.

7.

Lessons learned through a Sociological Study of Intravascular Ultrasound Innovation

Based on the manuscript by D. Maresca, S. Adams, B. Maresca, A. F. W van der Steen, **Lessons learned through a Sociological Study of IVUS Innovation**. *Submitted*

INTRODUCTION

Tremendous advances occurred during the last 40 years in the field of medical imaging of the heart and the coronary vasculature, triggered by the increasing need to reduce acute myocardial infarctions. The intravascular imaging route led to the development of X-ray angiography in the 1960's, balloon angioplasty and related techniques in the late 1970's and early 1980's. Meanwhile, in the early 1970's, academic research programs focused on developing two-dimensional real-time ultrasound imaging of the heart, transferring in particular underwater acoustics knowledge to medicine. This noninvasive route let to echocardiography, an imaging modality acclaimed for its radiation free nature but lacking the resolution to image the coronary vasculature.

The need for a technique able to provide high resolution images of diseased coronary artery wall structures, referred to as vulnerable plaques [6, 7] and primarily responsible for myocardial infarctions, arose in the early 1990's when false-negative coronary angiography cases became evident [13]. Intravascular ultrasound (IVUS) is a catheter-based echocardiography modality that was patented in 1972 [16] and further developed to investigate the status of the coronary artery wall. IVUS catheters are side looking devices that generate circular cross sectional images of the arterial wall, perpendicular to the longitudinal artery axis. The tip of an IVUS catheter incorporates either a single piezoelectric transducer

(40 to 60 MHz frequency range) or a circular array of transducers (20 MHz). Single transducer IVUS images are acquired by mechanically rotating the transducer over 360 degrees, while in circular array IVUS the ultrasound beam is steered electronically. The resolution of IVUS images is of the order of 100 μm in the axial direction, 300 μm in the lateral direction [44], and IVUS imaging depth typically ranges from 5 to 10 mm. IVUS technology has played an important role in the standardization of balloon angioplasty and stent treatments. Before intervention, IVUS can provide the artery lumen diameter, the plaque morphology and burden [18] thanks to the delineation of the external elastic membrane, and can be used to select optimal stent dimensions. Post intervention, IVUS is also useful to control stent apposition and possible complications. In addition, IVUS technology proved to be very useful in cardiovascular research. Since plaque progression and regression can be accurately measured with IVUS, the efficacy of new cardiovascular therapies on plaque volume can be quantified. IVUS also serves as gold standard for the evaluation of new intravascular modalities. Next to the estimation of plaque burden, the most valued IVUS function is calcium detection. Yet, to predict the risk for future acute cardiovascular events, the knowledge of plaque composition, which is not provided by conventional IVUS, is critical [20]. To that end, several IVUS signal processing techniques have been developed to augment IVUS capabilities in detecting and characterizing coronary artery plaques at risk.

Looking back, the realization of IVUS is undoubtedly a technical success. Twenty years after its introduction in the clinic in the early 1990's, IVUS technology continues to bring scientific insight into the pathophysiology of the coronary artery disease and helps guiding percutaneous coronary interventions. To date, noninvasive imaging techniques capable of identifying coronary artery wall lesions comprise magnetic resonance imaging (MRI) and multi-slice computed tomography (MSCT), but their resolution remains inferior to in situ catheter techniques. Minimally invasive techniques include coronary angiography, angioscopy, IVUS, intravascular optical coherence tomography (OCT), the combination of near infrared reflectance spectroscopy (NIRS) with IVUS and fractional flow reserve (FFR). OCT in particular has emerged as a rival for IVUS by generating more superficial but higher resolution images of the arterial wall.

Since its introduction in the clinic, however, IVUS innovation appears relatively limited, especially in terms of image quality. Significant academic innovations such as IVUS flow [22], IVUS palpography [24] or harmonic IVUS [108] were not transferred to market by industry. Furthermore, IVUS remains a niche technology, whose clinical practice did not vastly expand nor disappear. Looking at IVUS reimbursement worldwide, which varies considerably, gives insight in how IVUS is accepted. Japan, for example, reimburses IVUS separately, even for a diagnostic use, whereas in the United States, IVUS is not separately reimbursed but specific procedure codes do leave enough room for IVUS utilization where

necessary. In the rest of the world, there is no separate reimbursement for IVUS. Market penetration follows accordingly.

In this paper, we explored the current adoption and the future perspective for IVUS technology in light of sociology of innovation. By mapping IVUS controversies conveyed by international experts in the field together with the dynamics of their professional interaction, we sharpen our understanding of the IVUS status quo.

METHODS

To outline the dynamics of the actor-network [109] that generates IVUS innovations and uses IVUS technologies, we conducted a questionnaire-based survey [110] of biomedical experts with experience in the technology and practice of IVUS. To that end, we selected a deliberative sample of respondents: a representative group of 49 experts dealing with the question of IVUS innovation or adjacent fields. Potential respondents were identified through publications in the field and confirmed through an expert check (Professor van der Steen, head of the Biomedical Engineering Department of the Thorax Centre, Erasmus University Medical Center, the Netherlands). Identified actors comprised interventional cardiologists, academic and corporate engineers, corporate leaders and public and private funders.

Survey design | We developed a questionnaire on IVUS innovation and refined it through face-to-face interviews with three actors. After revision, the questionnaire was issued to all other actors (the final questionnaire is annexed to the present manuscript). The questionnaire started with two open questions about coronary atherosclerosis diagnostic in humans: *"What is the best method available to diagnose human coronary atherosclerosis?"*, and *"What would be an ideal technique to diagnose coronary arteries?"*. The first question permitted to review the coronary diagnostic tools that are currently appraised. The second question aimed at highlighting the limitations of existing diagnostic tools and identifying future diagnostic solutions with strong potential in the respondents' opinion. The questionnaire followed with questions centered on IVUS. To characterize the homogeneity of the respondents, we asked them to rate (from 0 - not so much, to 10 - extensive) their technical, clinical and market knowledge representation of IVUS. We collected their opinions on the advantages and drawbacks of IVUS. Next came two central questions: the room IVUS technology has left for improvement (to be rated from 0 - no room, to 10 - lots of room), and the likelihood of the existence of IVUS 20 years from now (to be rated from 0 – uncertain, to 10 - certain). These questions were inserted to quantify the future perspective of IVUS technology in the respondents' opinion. Next, we asked what the reimbursement procedure was for new medical devices in the respondent's country of residence before to specifically address the status of IVUS

reimbursement. Then, we asked what were the prevailing factors that could explain the continuous but limited clinical utilization of IVUS in the respondents' opinion. Interventional cardiologists were specifically asked how IVUS helps them complete the regular tasks of their job. These questions were inserted to collect material explaining current IVUS adoption. The last part was made of questions on additional factors likely to impact IVUS innovation (e.g. educational efforts in IVUS, role of patents, and competition between actors in the IVUS market). Finally, we provided room for further comments related to IVUS technology that the respondents might want to share.

Network analysis | In the second part of the questionnaire, we asked the respondents to indicate the frequency and nature of their interaction with other identified actors. We analyzed the level of interaction among our deliberative sample of respondents using the social network analysis software UCINET (Harvard University, Boston, USA) [111]. A clique analysis was performed, assembling groups of four members or more who declared symmetric interactions [112]. Subsequently, we proceeded to a hierarchical cluster analysis of the respondents' adjacency in the network: an algorithm ordered the respondents hierarchically based on their level of similarity (amount of clique memberships shared by pairs of actors) and their proximity in the network. The result was displayed as a hierarchical clustering tree diagram using UCINET (see Figure 1). Having registered the bonds between actors, which informs on the professional network architecture, as well as the respondents' opinions on IVUS technology, we could map IVUS controversies and discuss their implications for the future of IVUS in light of the hierarchized network architecture. It is important to realize that the individuals who contributed to this study represent only a part of a greater professional network, which is a limitation of this study. However, we postulate that the group of respondents that was surveyed is representative of the hierarchies and opinions present in the IVUS community.

Description of the respondents | With the initial list of potential respondents, 38 international institutions were represented (20 American, 9 Dutch, 3 Canadian, 2 Japanese, 2 French, 1 German, and 1 South Korean). The list comprised the following types of respondents:

- Fifteen corporate leaders, encompassing existing IVUS companies (Boston Scientific, Volcano, Terumo, Infraredx, Silicon Valley Medical Instruments and Colibri Technologies), a company fostering competing intravascular technologies, two general medical ultrasound companies, and a clinical research organization with experience in interventional cardiology. The response rate among corporate leaders was 40% (6/15).
- Fourteen cardiologists conducting clinical research involving IVUS or practicing IVUS-guided percutaneous coronary interventions (PCI). The group identified comprised key opinion leaders as well as international cardiologists in activity performing IVUS related research. The response rate was 57% (8/14).

- Ten engineers involved with IVUS innovation or related fields. This included two academic engineers who filed constitutive IVUS inventions, four academic engineers currently in activity as well as four corporate engineers. The response rate was 70% (7/10).
- Ten funders involved with IVUS innovation or related fields. Six were public funders and four private funders. Public funders represented public research organizations, public technology foundations. Private funders encompassed private technology foundations and investment firms. The response rate was 20% (2/10).

Of the initial 49 actors, 23 (47%) returned a completed questionnaire. We analyzed the responses by first reassigning them into pertinent categories. Among cardiologists (8), a distinction was made between opinion-leading cardiologists (3) and principal academic cardiologists (5), based on internal knowledge of the field of IVUS and top authors tracking on a biomedical experts platform. Among corporate leaders, a distinction was made between IVUS companies (4) and related field companies (2). Public and Private funders were merged in a single group because of the limited contributions (2). Finally, engineers were divided into academic (5) or corporate engineers (2).

For figure and citation purposes, we labeled IVUS corporate leaders as *IVUS Corp Leader*, corporate leaders in adjacent fields as *Adj Corp Leader*, opinion leading cardiologists as *Lead Cardiol*, principal academic cardiologists as *Acad Cardiol*, academic engineers as *Acad Eng*, corporate engineers as *Corp Eng* and funders as *Funder*.

RESULTS

Auto-characterization of the respondents | Overall, respondents demonstrated a homogeneously high technical knowledge (total average of 8.1) and clinical knowledge (total average of 7.6) of IVUS, indicating that we successfully surveyed actors involved at the technical and medical interface of IVUS. The technical knowledge was well aligned among all categories of actors. Engineers reported a deficit in clinical knowledge (average of 6.0), below cardiologists and corporate leaders, indicating that they do not perceive themselves as medical specialists. Market knowledge of the respondents appeared to be more widespread (total average of 7.0), above average for opinion-leading cardiologists and corporate leaders and below average for principal academic cardiologists. The actors' knowledge representation of IVUS reimbursement policies worldwide was the lowest (total average of 5.0). IVUS corporate leaders and corporate leaders of related fields were above average while corporate engineers and funders were below. Cardiologists and academic engineers were on average. Corporate leaders naturally appeared to be more focused than the rest on the non-technical factors that governing the development of medical technologies.

Historical context of IVUS introduction | Twenty years elapsed between the registration of the first IVUS patent in 1972 [16] and its transfer to clinical research in the early 1990's [113], when the technology caught the attention of interventional cardiologists willing to visualize coronary artery lesions. This was clear, for example, in this response from a historical European actor:
"As the big worry for cardiac echography was to see through the ribs, the idea of a phased array catheter was suggested. But in the meantime, the external linear array proved to be successful. People could see the heart and babies. Since the noninvasive approach worked, people forgot about the phased array catheter until 1992, when the need for a high resolution technique able to characterize coronary artery lesions emerged." *(Acad Eng)*

The introduction of IVUS as a high tech medical device followed a classical path. It first started as an academic engineering project aiming at developing intracardiac echocardiography in real time. IVUS technology eventually found light as a high resolution tool to characterize coronary artery lesions, as a result of the academic collaboration of cardiologists and engineers. This was clear, for example, in this response about the advantages of IVUS from Canada:
"It [IVUS] has good penetration through blood and soft tissue, enabling estimation of vessel dimension, vessel remodeling, and plaque burden with high sensitivity and specificity in identifying coronary calcifications". *(Acad Eng)*

The second phase of IVUS introduction was its assimilation by industry. Historically, the industrial development and aim given to IVUS was largely shaped by Boston Scientific (BSC). This is evident, for example, in this response from the US:
"In the first 10 years, Mansfield/BSC and CVIS were alone; then BSC bought CVIS and merged their platform." *(IVUS Corp Leader)*

As Boston scientific is primarily a stent manufacturer, IVUS holds an adjacent technology position within the company portfolio. IVUS was positioned as a percutaneous coronary intervention (PCI) guidance tool, allowing for peri-interventional planning and assessment of complications. This role is clear, for example, in the response of an interventional cardiologist who explains how IVUS helps him complete the regular tasks of his job:
"IVUS-guided PCI:
1. PRE: Plaque assessment, luminal diameters, stent length sizing.
2. INTRA: Stent apposition, re-entry in dissected planes, ante/retrograde chronic total occlusion (CTO).
3. POST: thrombus, edge prolapse, dissection, etc." *(Lead Cardiol)*

This tells us that the use of IVUS evolved from a research diagnostic tool to a PCI intervention guidance tool. It raises the question of the role for intracoronary imaging technologies. To date, IVUS technology is perceived as well aligned within the product portfolio of IVUS companies. This was reported in this response from the US:

"All companies try to create a coronary artery imaging platform. For Boston Scientific and Terumo, IVUS is an adjacent market. For Volcano, Infraredx, it is a central market." *(Funder)*

The third stage of the introduction of IVUS is its reimbursement via public health policy. Overall, the reimbursement process for a new medical device consists in the following: evidence-based medicine must prove benefits in using the technology. Subsequently, randomized clinical trials are to be conducted to determine whether the technology leads to an improved effectiveness in terms of patient outcome as well as a superior cost-effectiveness than the standard of care. The reality of IVUS reimbursement appears contrasted. In the US, the situation was reported as follows:

"There is no separate reimbursement for IVUS and it must be bundled into the existing Diagnosis-related group (DRG) for the specific coronary intervention. A separate set of cost-effectiveness and clinical utility data would be required to create stand-alone IVUS reimbursement" *(IVUS Corp Leader)*

This indicates that IVUS only partially fulfills the usual requirements for the reimbursement of a new device. Most notably, it appears that the technology has failed to demonstrate clinical utility. However, a clear dissymmetry in the reimbursement of IVUS worldwide is observed by several respondents. This was clear, for example, in these responses from the US and from Japan:

"Separate reimbursement exists in Japan, where IVUS penetration is widely viewed as the deepest in any part of the world. This is not circumstantial. The second highest major market penetration is in the US, where it is not reimbursed separately but in which specific procedure codes do leave enough room for IVUS utilization where necessary. The lowest penetration exists in EU and Asia/Latin America markets where per-procedure economics are tightest and no separate reimbursement exists. Thus, while there is undoubtedly strong clinical belief in the utility of IVUS, there is an undeniable correlation between where that clinical belief manifests and where the economic policies are most accommodating." *(IVUS Corp Leader)*

Japan's separate reimbursement of IVUS is unique worldwide and seems to be the result of a specific society willingness to integrate high-quality, high-tech care in interventional cardiology. Yet, the status of IVUS reimbursement is a strong indicator of a contrasted acceptance of the technology and reveals that IVUS must be engaged into a set of controversies.

Open debates surrounding IVUS technology | IVUS adoption is scarce outside of academia. By reviewing the contributors' answers, we identified six 'controversies' revolving around IVUS technology; a controversy being defined as a debate surrounding a technique that has not yet been determined [114]. The controversies identified are reported in Table 1.

Table 1. Classification of the IVUS controversies conveyed by the respondents

Controversy	Positive responses	Negative responses
Invasiveness of IVUS	"Minimally invasive" "The technique is invasive but I am an interventional cardiologist. IVUS takes 30 seconds."	"IVUS is very invasive to find the site of interest" "A major disadvantage is that IVUS is invasive"
Resolution of IVUS	"High resolution and similarity to pathology" "It has good penetration through blood and soft tissue, enabling estimation of vessel dimension, vessel remodeling, and plaque burden with high sensitivity and specificity in identifying coronary calcifications"	"Unacceptably poor resolution" "resolution is not enough for some particular purpose (TCFA)"
Usefulness of IVUS as diagnostic tool	"In order to understand the local problem, a catheter is the best" "Large investigation range in combination with pull-back" "Relatively quick, you can see obstruction, size shape of the lesion (morphology)" " Well validated quantitative measurements, many related outcome evidence by IVUS measurements (example, minimum stent area to predict future revascularization), easy to learn/use" "Resolves ambiguous anatomy on angiogram, especially at left main"	"Intra-coronary imaging is too invasive and too late to use" "most information not needed in daily practice unless complication" "Lack of clarity of the images (I think I know what I'm looking at but not entirely sure) and the difficulty of acquiring those images" "A catheter does not provide a complete view of the vascular tree"
Usefulness of IVUS as PCI guidance tool	"Inadequacy of angiography to guide clinical decision making in complex anatomy" "Clinical trials have shown that the use of IVUS is reasonable during PCI for several indications. The medical literature continues to demonstrate limitation of angiographic-only guidance for PCI"	"Clinical impact on decision making is limited" "There is no large clinical trial to show the benefit of using IVUS" "absence of evidence based medicine guidelines/Competition with FFR&OCT"
Impact of IVUS reimbursement on IVUS innovation	"Separate reimbursement exists in Japan, where IVUS penetration is widely viewed as the deepest in any part of the world. This is not circumstantial. "	"Reimbursable for appropriate use" "I think the biggest limit is the lack of investment in academic research" "It affects the clinical use. Institutions like the Thoraxcenter simply supply the difference, but in peripheral hospitals the clinical use is affected. The IVUS innovation is an academic/industrial process and is financed by other means"
Educational efforts in IVUS	"A focused educational program is needed for realizing the potential of this technique"	"Today it's a niche technology , teaching efforts questionable given poor penetration"

- The first controversy concerns the invasive nature of IVUS. It opposes actors that perceive invasiveness as a limitation, e.g. by preventing the screening of asymptomatic patients, to actors who relativize the minimal invasiveness of IVUS in light of the interventional nature of their job.
- The second controversy identified concerns the resolution of IVUS. It opposes actors who perceive IVUS resolution as insufficient to detect important features of atherosclerotic plaques (e.g. thrombi, thin cap fibroatheroma, plaque composition) and/or consider IVUS images as difficult to interpret, to actors who praise the sufficient clarity of IVUS whose resolution provides well validated quantitative measurements of atherosclerotic plaques (e.g. size and shape of coronary lesions, residual lumen, calcium detection, clear images of stent struts).
- The third controversy concerns the practicability of IVUS as a diagnostic tool. It opposes actors who consider that IVUS is an expensive and late diagnostic solution (restricted to patients who already need an intervention) which is tedious to analyse, to actors who praise the local knowledge of the plaque provided by IVUS and therefore its prognostic value, as well as the fact that IVUS is relatively quick to use.
- The fourth controversy concerns the utility of IVUS as a percutaneous coronary intervention (PCI) tool. It opposes actors considering that IVUS has a limited impact on clinical decision making and failed to prove clinical benefits in terms of PCI treatment outcome, to actors who consider that IVUS improves safety overall by resolving ambiguous anatomy on angiograms (for example at the left main coronary artery), permitting an adequate selection of stent landing zones and stent size, and allowing for the evaluation of post-intervention complications.
- The fifth controversy concerns the impact of IVUS reimbursement on IVUS utilization worldwide. It opposes actors who consider that IVUS current reimbursement leaves enough room for an appropriate and that expansion is primarily limited by the lack of demonstrated IVUS benefits, to actors who consider that a separate reimbursement of IVUS, even for diagnostic use, would favour its development as observed in Japan.

The sixth controversy concerned the means invested in the formation of IVUS experts. In light of the absence of clearly demonstrated clinical benefits in using IVUS, some actors consider that enough educational efforts are consented (live cases at conferences, publications, experts visits), while others consider that because IVUS technology is not exploited at its full potential, a global educational efforts is required (e.g. exposure of cardiologists in training, creation of a certification program, online consulting systems).

It is interesting to notice that only one of the six controversies identified - the ongoing debate on IVUS resolution - was intrinsic to the technology itself. All others appeared as adjacent debates surrounding IVUS practice and questioning aspects of interventional cardiology practice in general. Nonetheless, the amount of controversies identified is not negligible and raises the question of the future of IVUS,

especially since the field of intracoronary imaging has become more competitive with the introduction of OCT. In particular, the role of intravascular imaging seems to be questioned: is the goal to mimicking histology, to perform prognostic imaging and/or to provide procedure guidance?

Mapping IVUS controversies | In order to analyze controversies as a function of the network architecture, we generated a hierarchized representation of respondents based on their centrality in the network and projected their opinion in the tree diagram obtained (Methods section). In Figure 1, we projected the actors' answers mentioning resolution in response to the question of the disadvantages of IVUS. By doing so, we map the controversy of IVUS resolution that was identified earlier as the only one intrinsic to the technology of IVUS. It appeared that the six most central actors in the network perceive IVUS resolution as insufficient. Interestingly, the figure reveals that none of the historic actors (marked with a star in the figure) cited resolution as a disadvantage of IVUS. Historically, they introduced IVUS as a high resolution technique, filling a void in interventional cardiology. In fact, Figure 1 displays the evolution of the debate on resolution. We know that IVUS image quality is the same since its introduction. Still it changed from high to low at the advent of OCT. A clear change in understanding of what "high resolution" means is observed, independent from the developmental path of IVUS technology: it indicates a mutual shaping between technology and society.

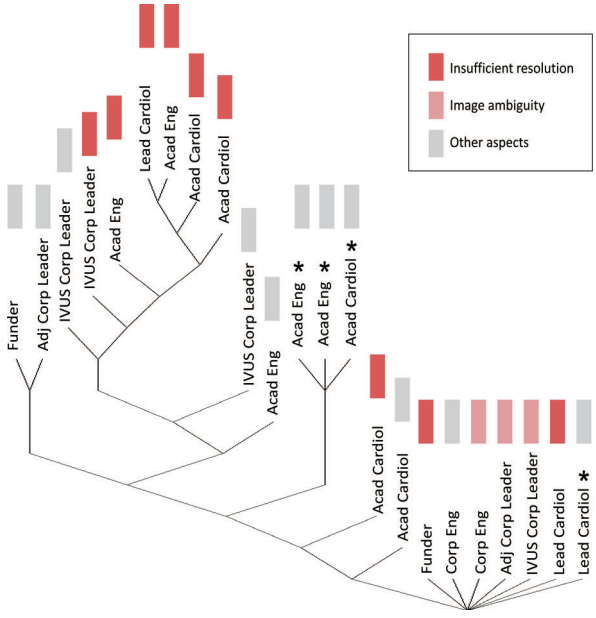

Figure 1. Resolution as limitation projected on hierarchical clique membership graph. Early actors are indicated with a star. Actors that were the least central in the network, who declared a limited level of interaction with other members, appear at the bottom of the diagram. The diagram can be subdivided as follows: a base of peripheral actors that are the least central in the network, a middle group, including early

IVUS actors, with an intermediate centrality level, and finally the leading group of the network gathering the most central actors.

Future perspective for IVUS technology | When looking at the distribution of the answers of the respondents to the two central questions (the room for improvement left for IVUS technology and the perspective of existence in 20 years), we observed a singular double peaked distribution (Figure 2).

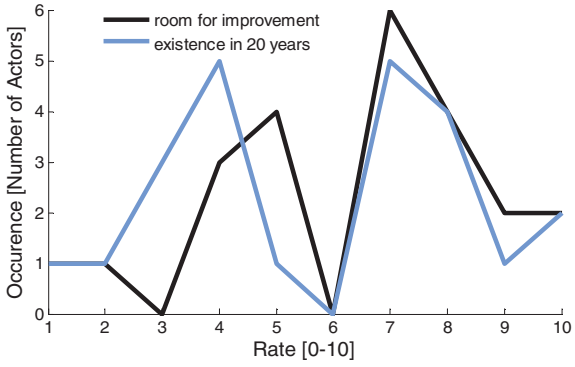

Figure 2. Distribution of answers of the respondents to the questions on IVUS perspective.

This result clearly indicates that two populations coexist in the IVUS network surveyed, one optimistic and one pessimistic about the technology perspective. We rearranged the responses into two categories, the positive opinions (values above 6) and the negative opinions (values below 6). Academic engineers were the most optimistic when rating the room for improvement that IVUS technology has (average of 7.8), which is natural considering that they are professionally invested in IVUS innovation. Principal academic cardiologists were optimistic as well (7.3) followed by IVUS corporate leaders (6.8). On the contrary, corporate engineers appeared pessimistic (4.5) while other corporate leaders were the most pessimistic (1.5). Logically, it appears that the judgment on the room for improvement of IVUS is directly dependent on the degree of investment the actors have in IVUS: engineers and corporate leaders involved with other intravascular technologies were negative on the innovation potential of IVUS. Results were projected on the tree diagram in Figure 3, showing that historic actors emerge as the principal subgroup sharing a positive opinion about the room for innovation left in IVUS. Central actors, who are currently professional active, conveyed a rather negative opinion.

Concerning the existence of IVUS in 20 years, the optimistic group gathered principal academic cardiologists (7.1), academic engineers (6.6) and IVUS corporate leaders (6.5). The pessimistic group was made of the opinion-leading cardiologists (4.3), other corporate leaders (4.0) and funders (3.3). Engineers and IVUS corporate leaders were convinced of the future of the technology. Conversely, opinion-leading cardiologists and funders were skeptical about the future of IVUS. Again, historic actors shared an

optimistic vision of the future of IVUS as for the previous question. Central actors in the network appeared more balanced. Actors with a low centrality (potentially less tied to IVUS) were rather pessimistic.

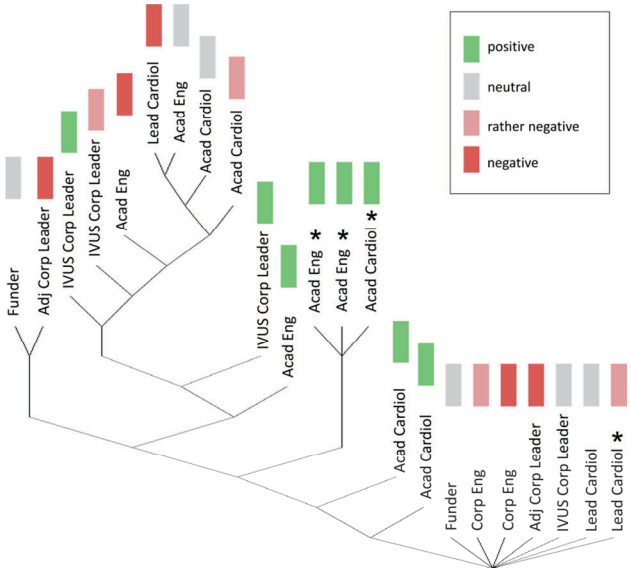

Figure 3. Room for innovation in IVUS as perceived by the respondents. Early actors are indicated with a star. Least central actors in the network appear at the bottom of the diagram and most central actors at the top.

When the answers to both questions are coupled, it appears that academic engineers, principal academic cardiologists and IVUS corporate leaders share a globally optimistic view, whereas opinion-leading cardiologists, other corporate leaders and funders shared a globally pessimistic view. Therefore, a major conclusion is that opinion-leading cardiologists and funders, who orientate innovation due to their position, disclosed a pessimistic opinion of the existence of IVUS technology 20 years from now. Their regard on the future of the technology was clearly exposed, for example, in this response from the US:

"In my opinion, the use of IVUS only makes sense as part of conventional angioplasty. If it were incorporated as part of the procedure, then there would not be a need for a second invasive procedure. However, the fact that IVUS is invasive may limit its capability for growth, especially if non-invasive MRI and CT coronary diagnostic imaging capabilities reach the point that they become more attractive, competitive diagnostic procedures. This may be possible in the near future, and might decrease the need for invasive diagnostic procedures like IVUS.

A more important consideration would be the results of comparative effectiveness studies of IVUS, compared to conventional angioplasty. If it could be proved that IVUS increased longevity or decreased complications, this would contribute toward making this procedure more attractive to practitioners" *(Funder)*

DISCUSSION

This study demonstrates that the development and positioning of IVUS, in the high-tech environment of interventional cardiology adjunctive devices, is shaped by co-developing controversies surrounding the technology. We questioned why IVUS neither expanded nor disappeared since its introduction 40 years ago. The capacity of IVUS to estimate total coronary plaque burden was almost unanimously reported by the respondents and appears as the principal advantage of IVUS. Plaque burden can only be measured *in vivo* with IVUS [115] and was shown to be a predictor of major adverse cardiovascular events [18]. For this reason, the technology is praised in cardiovascular research since it allows for longitudinal studies of atherosclerosis progression. IVUS can also rely on an extensive publication database that makes it the standard technology to compare when new intravascular imaging technologies. We can therefore assume that it is the utilization of IVUS in cardiovascular research that kept the technology alive in academic medical centers. On the other hand, the fact that IVUS failed in demonstrating clear benefits in terms of patient outcomes appears as the strongest factor that prevents its expansion - outside Japan at least. The case of Japan is illustrative of the mutual shaping between science, technology and society. This was clear, for example, in this response from the US:
"In IVUS the forerunner is certainly Japan with a stricter regulatory process, however combined with a higher willingness to use new technologies to improve patient safety and care." *(Corp Eng)*

IVUS adoption in Japan can only be explained by distinct society views in healthcare. This observation illustrates that IVUS technological advancements result from a mutual shaping between science and society rather than from undisputed scientific facts only. Several other lessons, relevant for both the future of IVUS and the introduction of new intracoronary imaging techniques, can be learned from this sociological study of IVUS innovation.

First, we observed that the only controversy intrinsic to IVUS technology itself was the debate on IVUS resolution. Looking at the hierarchical architecture of the IVUS actor-network surveyed is important to evaluate the implications of this debate on resolution. The tree diagram (Figure 1) can be subdivided in three groups: a base of peripheral actors that are the least central in the network, a middle group of early IVUS actors with an intermediate centrality level and finally, the leading group of the network gathering the most central actors. Actors at the top of the diagram are likely to be in close collaboration and/or competition with each other and to be the most deeply involved with IVUS or adjacent technologies. Furthermore, their point of view is dominant because of their central position in the network. But they

are also likely to have the highest interest in promoting a given imaging modality. Since the six most central actors in this survey are all indicating that IVUS resolution is insufficient, we can assume that the future of IVUS technology will depend from its capacity to improve on that front. Interestingly, we observed that the middle group of early actors who were involved with the introduction of IVUS pointed at other IVUS limitations than resolution. Certainly because, from their perspective, IVUS filled a void in the interventional cardiology space and entered as a high resolution modality. On the contrary, peripheral actors is likely to be involved to a lesser extent with IVUS and judges potentially a more objectively the advantages and disadvantages of IVUS technology. More than resolution, it is the ambiguity of IVUS images that they incriminate, telling us that understanding IVUS images requires expertise. Whether a higher resolution will solve image interpretation issues is not clear: despite its microscopic resolution, OCT is still in a phase of standardization, proven benefits are yet to be demonstrated and as for any modality the technology is not exempt of artifacts affecting image interpretation. This raises the issue of the training of experienced IVUS users. Several respondents stressed the need for focused educational programs in order to fully realize the potential of intracoronary imaging techniques, independent from their resolution. Several actors criticized the lack of exposure of medical doctors to these techniques at resident stage. Educational efforts in IVUS were considered as "hobbyist" by an early European practitioner. Such efforts were questioned by others given the poor penetration of IVUS.

Second, most central actors in the network had a skeptical perception of the potential for innovation that IVUS technology has left (Figure 3). This can be understood from a historical perspective: the field of IVUS faced a relative lack of IVUS innovation in the past 20 year. 40 MHz IVUS was reported as early as 1991 in scientific literature [116] and remains the standard product of major IVUS companies today. Image quality in IVUS did not experience any breakthrough in 20 years. Several respondents criticized the lack of competition in the IVUS market that stifles innovation, and call for new start-ups to re-energize clinical translation. Patents are considered to play minor role to date as they mostly expired. In some cases though, IVUS companies happened to sit on innovation therefore limiting the dissemination of new technological developments [e.g. palpography]. Despite this overall negative judgment, academic engineers as group appeared to be clearly positive about the potential left for IVUS innovation (Figure 2). Novel technological solutions can be envisioned at an academic level, in particular to improve IVUS resolution. For example, it is well known that the axial resolution in ultrasound imaging can be enhanced by shifting to higher frequencies. This applies to IVUS as well and is being pursued academically and industrially. However, since the laws of Physics impose a tradeoff between ultrasound frequency and ultrasound attenuation, high frequency IVUS is achieved at the cost of imaging depth. Because the added value of IVUS comes from its imaging depth, that enables total plaque burden assessment, the room to improve axial resolution is limited. Yet, a significant enhancement in IVUS image quality could be

achieved by improving IVUS lateral resolution [117], which is currently three times worth than axial resolution [44]. When characterizing themselves, engineers declared a deficit in clinical knowledge of IVUS compared to other groups, whereas technical knowledge was homogeneously high among actors. A more extensive education of engineers to the reality of clinical procedures and catheter laboratory workflow might prove to be critical to for the successful introduction of future intracoronary imaging modalities. Complementarily, educating interventional cardiologists further in the physics of intravascular imaging could improve patient treatment, by helping them to recognize image artifacts to secure their diagnostic. Maximizing the IVUS knowledge overlap of interventional cardiologists, biomedical engineers, industry leaders and investors would accelerate technological developments.

Third, as five of the six controversies that were identified are external to IVUS technology, we can hypothesize that decision making at the industrial, financial and regulatory levels will orientate predominantly future innovations in intracoronary imaging. As reported earlier, a major conclusion is that opinion-leading cardiologists and funders, who orientate innovation to a large extent, disclosed a pessimistic opinion of the existence of IVUS technology 20 years from now. In general, minimally invasive imaging modalities are logically not perceived as adequate for the early screening of coronary atherosclerosis in asymptomatic patients. First, because the information they provide is local (as opposed to a full view of the coronary anatomy e.g. angiography/MRI/CT) and second because of their invasive character. Therefore, wide adoption of intravascular imaging will depend on potential added benefits for cardiac patients requiring intervention - to be proven through clinical trials. If a medical consensus advocates the identification of flow limiting lesions, then FFR and angiography are sufficient. If medical guidelines state that the assessment of plaque vulnerability is critical, then intravascular imaging techniques will play a role as diagnostic tools. A range of signal processing techniques of IVUS radiofrequency data, namely e.g. IVUS flow, IVUS palpography or contrast-enhanced IVUS, can augment IVUS capacity to characterize plaque vulnerability. Those modalities do not require extra hardware and can therefore be achieved at no extra cost. In the case of OCT, recent developments as tissue characterization might become useful [118]. Intravascular photoacoustics holds promises for depth resolved coronary wall lipid detection [119, 120]. In any case, next generation IVUS as well as new intravascular technologies will compete with OCT in terms of image quality and guidance of stent apposition, and with the combination of FFR and angiography in terms of clinical decision making [121].

If the future of IVUS as a stand-alone modality appears uncertain, the technology appeal could be renewed by improving lateral resolution and through combination with one or several other imaging modalities. To date, IVUS remains the only clinical tool capable of imaging plaque burden *in vivo*. Combination devices were suggested by several respondents as potential solutions to establish coronary

plaque vulnerability. For example, the combination of IVUS and OCT would provide OCT resolution and IVUS penetration simultaneously. The approach is appealing from an engineering or cardiovascular research perspective, but may not be cost effective in routine practice. Catheters are currently expensive and sparsely reimbursed disposables. Miniaturization and integration issues tend to increase costs. The development of intravascular imaging modalities like intravascular photoacoustics that couples light and sound may be an alternative: on top of photoacoustic images, a photoacoustic probe is also capable of generating IVUS images by design. In any case, the transfer of intravascular technologies in routine clinical practice and their reimbursement will be conditioned by a demonstration of clear clinical benefits and cost effectiveness, but also a higher willingness of care practioners to get experience in intravascular imaging in order to improve patient safety. Unless of course, in the advent of preventive medicine, percutaneous coronary intervention practice decreases drastically.

Acknowledgements | We warmly thank all the respondents for their time and answers. Their contribution made this study possible. We also thank the Dutch Technology Foundation STW for funding.

8.

Overview and Perspectives

STATE OF THE ART IN IVUS

Intravascular ultrasound (IVUS) celebrated recently its 40 years of existence, as the first patent related to the technology was filed in 1972. IVUS consists in a miniaturized echography unit mounted at the tip of a catheter. It was developed to provide high resolution images of coronary artery wall structures from the inside. A side looking piezoelectric transducer with a typical frequency of 40 MHz is mechanically rotated to acquire cross sectional images of the arterial wall, perpendicular to the catheter axis. IVUS generates circular grayscale images displaying the envelope of ultrasound pulse/echo radiofrequency data, with a resolution of the order of 100 microns along the depth axis (axial resolution) and 300 microns in the radial direction (lateral resolution).

Several innovations are currently pursued to enhance IVUS image quality further and consequently foster IVUS prognostic value. High frequency IVUS (SVMII, Freemantle, CA, USA) relies upon broadband high frequency transducers to offer a finer axial resolution. Next to conventional 40MHz IVUS images, the system can generate co-registered 60 MHz IVUS images featuring an axial resolution below 60 microns. The enhanced resolution will help detecting thin cap fibroatheromas, an established marker of atherosclerotic plaque vulnerability, as well as stent struts malapposition. In addition, conventional 40 MHz IVUS images provide deeper structural information of the arterial wall, such as the total atherosclerotic plaque burden. At an academic level, Chandrana *et al* [117] demonstrated the feasibility of second-harmonic IVUS with broadband focused IVUS transducers. Interestingly, this solution was foreseen by Martijn Frijlink in the concluding remarks of his PhD thesis [122] and could drastically enhance IVUS image quality by improving lateral resolution, currently three times worth than

IVUS axial resolution [44]. High resolution focused intravascular ultrasound catheters may be commercialized in the near future. Finally, IVUS detection capabilities can be augmented when combined with an ultrasound contrast agent. Ultraharmonic IVUS, a method introduced in this thesis, is capable of detecting a microvascular network below the limit of conventional IVUS. Ultraharmonic IVUS imaging has a role to play in the *in vivo* detection of intraplaque vasa vasorum, one of the most robust predictors of plaque vulnerability [3].

IVUS technology has also been increasingly combined with optics in the past few years. The association of near-infrared spectroscopy and IVUS (Infraredx, Burlington, MA, USA) aims at augmenting the morphological information provided by IVUS with local information on the arterial lipid content. Such a multimodal approach could tremendously improve the detection of lipid-rich plaques that are recognized by interventional cardiologists as prone to rupture.

IVUS has also been combined with optical coherence tomography (OCT) [123] to take advantage of the wide imaging range of IVUS and the ultrahigh resolution of OCT that allows for the clearer detection of thin cap fibroatheromas, macrophages and stent struts. Moreover, the fact that OCT requires flushing of the arterial lumen will enhance IVUS image quality as well by reducing ultrasound attenuation. A third approach combining light and sound is intravascular photoacoustics or IVPA [119]. Contrary to near infrared spectroscopy, IVPA can generate depth-resolved cross sectional maps of the arterial wall lipid content. As the method relies on the coupling of a laser and an IVUS transducer, IVPA can also generate IVUS images of the arterial wall morphology at no cost.

CONTRIBUTION OF THIS THESIS TO THE FIELD OF IVUS

To date, the size distribution of an ultrasound contrast agent after administration *in vivo* is largely unknown. Organs such as the lungs filter large contrast microbubbles while recent evidence indicates renal retention of ultrasound contrast agents as well. In consequence, the size distribution of a contrast agent is likely to be altered at each re-circulation. Insights in the dynamics of contrast agent size distributions *in vivo* could help tailoring ultrasound contrast agents dedicated to specific ultrasound examinations. In the second chapter of this thesis, we show that it is possible to estimate with a single transducer the size distribution of an ultrasound contrast agent by insonifying individual contrast microbubbles at IVUS frequency (25 MHz). In practice, we report that bubble size is derived from three parameters: the distance between a single bubble and the transducer, the incident pressure impinging on the bubble and the pressure backscattered on the transducer surface. *In vivo* feasibility might become possible thanks to recent developments in ultrafast ultrasound imaging. By calibrating both in transmit and receive the acoustic field of a 3D ultrasound probe and subsequently recording individual

microbubble scattering events *in vivo*, one may estimate the size distribution of an ultrasound contrast agent in a given organ.

In the third chapter, we show that a contrast-enhanced IVUS pullback can be used to reconstruct a microvascular structure invisible in conventional IVUS. Another goal of this study was to evaluate the accuracy of contrast IVUS reconstructions of microchannel diameters. We report that for channel diameters within IVUS axial resolution but below lateral resolution, channel diameter reconstructions were accurate, while for channel diameters inferior to both IVUS axial and lateral resolution, channel diameters detected with contrast IVUS were overestimated. Contrast IVUS is capable of detecting and reconstructing a simple microvascular structure but somewhat logically, contrast IVUS resolution cannot be enhanced beyond the transducer point spread function. A limitation of this study was that the absence of a sensitive IVUS contrast detection mode. As a consequence, we used a high dose of ultrasound contrast agent and the 3D reconstruction relied upon an arbitrary threshold level to disentangle contrast agent signals from tissue signals.

In the fourth chapter, we report the use of engineered transmission pulses in the field of IVUS. We show that short frequency-swept sine excitations, or chirps, can enhance the penetration depth of IVUS imaging while preserving the same acoustic pressure level than conventional IVUS pulses. Ultrasound chirp imaging could facilitate the study of large coronary arteries and improve side branches visualization. In addition, the use of chirps in IVUS allowed for the implementation of a contrast detection technique named chirp reversal, which is adapted to the current bandwidth limitations of commercial IVUS transducers. When excited with time reversed chirps, the transient resonant response of contrast agents generates dissymmetric echoes. On the contrary, biological tissue generates symmetric time reversed echoes. This phenomenon enabled the selective detection of ultrasound contrast agents with IVUS. This study is the first report of the feasibility of chirp reversal contrast imaging at high frequency. The implementation of chirps in IVUS imaging also revealed limitations specific to this technology. In IVUS, the transducer can be in direct contact with diseased arterial wall structures that require most attention. The temporal window for chirp transmission is therefore limited because a transducer cannot record echoes when it is active. As a consequence, the time - frequency bandwidth product of IVUS chirps transmitted is limited, which directly correlates to gain in penetration and resolution. A solution to this problem could be to move back to an IVUS catheter design where the transducer is positioned along the catheter axis inside the shaft, and the ultrasound beam deflected with a rotating mirror. This solution artificially elongates the acoustic path between the transducer and arterial wall, granting more time for the transmission of longer ultrasound pulses.

In the fifth chapter, we introduce ultraharmonic IVUS and compare its performance to chirp reversal IVUS for the detection of vasa vasorum sized channels. Both methods have limited bandwidth requirements and were successfully implemented on an IVUS probe with a conventional frequency bandwidth (<60%). In the case of ultraharmonic IVUS, the use of a pulse inversion sequence was necessary to extract ultraharmonic content that is overshadowed by transmit frequency energy otherwise. The two pulse sequences dedicated to the detection of ultrasound contrast agents are complying with current IVUS systems limitations and should therefore facilitate the translation of contrast IVUS imaging to clinical practice. If broader IVUS transducers bandwidths become available, one could think of a contrast mode relying on both subharmonics and ultraharmonics of ultrasound contrast agents. The contrast mode sensitivity could increase by up to 6 dB. However, coded excitations transmitted for contrast detection do not provide the highest resolution B-mode resolution. IVUS should therefore be operated in pulse sequences comprising at least one pulse at the transducer center frequency for high resolution imaging of tissue together with one or several pairs of engineered pulses dedicated to contrast detection. This way IVUS will display co-registered morphological and vascular information on the arterial wall. Operating at higher frame IVUS rates is not a technical challenge.

In the sixth chapter, we report the first *in vivo* ultraharmonic IVUS image of an intricate microvascular network, clearing way towards the translation of the method to coronary vasa vasorum detection in humans. Ultraharmonic IVUS imaging revealed vascular targets below the resolution limit of IVUS, without facing blood flow limitations as in ultrasound Doppler imaging. The method is ready for implementation on a clinical IVUS platform and should be tested in a coronary atherosclerosis animal model. As marketed ultrasound contrast agents differ in terms of nonlinear properties [124], testing several agents in combination with an ultraharmonic IVUS sequence might be valuable in order to establish optimal examination guidelines. Studies should also be undertaken to determine the correlation between vasa vasorum density and the advancement of coronary atherosclerosis. Ultraharmonic IVUS has a role to play in vascular biology studies of atherosclerosis and early diagnostic of coronary plaques at risk. Furthermore, it could also be a valuable tool for the longitudinal monitoring of neoangiogenesis on stented sites.

LESSONS LEARNED THROUGH A SOCIOLOGICAL STUDY OF IVUS INNOVATION

In the last chapter of this thesis, we discussed the perspective of IVUS technology in light of sociology of innovation. We conducted the survey of an international group of IVUS experts and collected their opinions on IVUS innovation. Their answers were analyzed in the scope of sociology of innovation. An important finding was that central actors in the network cast a rather negative judgment of the innovation potential remaining for IVUS technology and specifically pointed at IVUS resolution. Understanding what "high resolution" means in intravascular imaging was redefined with the introduction of OCT. One can conclude that the future of IVUS will depend on its capacity to demonstrate substantial improvements in image quality. IVUS development may come from multimodality devices that can rely on IVUS imaging depth to characterize total plaque burden as well as from another modality for the detection of plaque components associated with high risk of plaque rupture. In any case, competition in the field of adjunctive devices for percutaneous coronary interventions has become fiercer for IVUS, which failed to demonstrate to date added clinical benefits in terms of patient treatment outcome.

In the meantime, a focused collaborative effort between cardiologists, engineers and industrial partners is desired in order to realize the full potential of IVUS in the clinic. IVUS has survived to date as a niche technology in a few academic medical centers and is mostly praised for clinical research, rather than routine clinical practice.

Beyond the situation of IVUS, it is the role of intravascular imaging of the coronary arteries which is questioned here. Resolution is important but intravascular imaging is not aiming at replacing histology. The goal of intravascular imaging is twofold: to position itself as a prognostic tool for cardiac patients at risk who already require a percutaneous coronary intervention (PCI), as well as a PCI-guidance tool to reduce stent failure and monitor complications.

POTENTIAL INNOVATIONS IN IVUS IMAGING

Improving resolution appears necessary to leverage IVUS adoption and bridge a part of the gap with OCT. But this should be preferably achieved without losing imaging depth as it is the primary strength of IVUS. Embettering IVUS lateral resolution seems to be the most relevant option. IVUS lateral resolution is currently three times worse than axial resolution. Generating IVUS images with similar axial and lateral resolution would drastically improve image quality. Some technical solutions already exist, such as annular transducer arrays [125]. Second harmonic tissue imaging could be additionally implemented on such arrays to enhance image quality further.
In addition, IVUS would gain in relying on pulse sequences to display complementary co-registered imaging modalities. One could think of combining the following pulses in a single sequence:

- Short IVUS pulses at the transducer center frequency to generate high-resolution morphological IVUS image of reference.

- IVUS chirps with an optimized time-bandwidth product to visualize the total plaque burden in large vessels and/or investigate side branches deeper.

- Lower frequency pulses for second harmonic tissue imaging, in order to improve lateral resolution and reduce stent reverberation artifacts.

- Pairs of pulses dedicated to contrast-enhanced ultraharmonic IVUS, which enables the delineation of the lumen contour without ambiguity and can detect microvasculature infused with an ultrasound contrast agent.

Moving back to an IVUS catheter design where the ultrasound beam gets deflected by a rotating mirror could also present significant advantages. Since the travel path of IVUS pulses inside the catheter would increase, transducer ring-down effects could be reduced and IVUS images of arterial wall structures in direct contact with the catheter sheath could be generated. Moreover, such a design would enable the transmission of longer coded excitations. Other academic IVUS innovations such as IVUS flow or 3D IVUS palpography could be easily implemented, and might prove to be valuable in characterize shearing stress in coronary arteries. In conclusion, by merging in a single sequence all the existing modalities derived from the analysis of IVUS radiofrequency signals, one would significantly augment the prognostic value of IVUS and its capacity to guide interventions at a low cost.

References

[1] L. S. Lilly, ***Pathophysiology of the heart disease***. 4th Edition, Lippincott Williams & Wilkins (2006).

[2] P. Libby, P. M. Ridker, G. K. Hansson, **Progress and challenges in translating the biology of atherosclerosis**. *Nature* **473**, 317-325 (2011).

[3] W. E. Hellings, W. Peeters, F. L. Moll, S. R. Piers, J. van Setten, P. J. Van der Spek, J. P. de Vries, K. A. Seldenrijk, P. C. De Bruin, A. Vink, E. Velema, D. P. de Kleijn, G. Pasterkamp, **Composition of carotid atherosclerotic plaque is associated with cardiovascular outcome: a prognostic study**. *Circulation* **121**, 1941-1950 (2010).

[4] P. Libby, **Atherosclerosis: the new view**. *Scientific American* **286**, 46-55 (May, 2002).

[5] E. Falk, P. K. Shah, V. Fuster, **Coronary plaque disruption**. *Circulation* **92**, 657-671 (1995).

[6] J. E. Muller, G. H. Tofler, P. H. Stone, **Circadian variation and triggers of onset of acute cardiovascular disease**. *Circulation* **79**, 733-743 (1989).

[7] J. A. Schaar, J. E. Muller, E. Falk, R. Virmani, V. Fuster, P. W. Serruys, A. Colombo, C. Stefanadis, S. Ward Casscells, P. R. Moreno, A. Maseri, A. F. van der Steen, **Terminology for high-risk and vulnerable coronary artery plaques. Report of a meeting on the vulnerable plaque, June 17 and 18, 2003, Santorini, Greece**. *European heart journal* **25**, 1077-1082 (2004).

[8] D. Vancraeynest, A. Pasquet, V. Roelants, B. L. Gerber, J.-L. J. Vanoverschelde, **Imaging the Vulnerable Plaque**. *Journal of the American College of Cardiology* **57**, 1961-1979 (2011).

[9] K. Sakakura, M. Nakano, F. Otsuka, E. Ladich, F. D. Kolodgie, R. Virmani, **Pathophysiology of Atherosclerosis Plaque Progression**. *Heart, Lung and Circulation*, (2013).

[10] P. Stolzmann, S. Subramanian, A. Abdelbaky, P. Horvat-Maurovich, H. Scheffel, A. Tawakol, U. Hoffmann, **Complementary value of cardiac FDG PET and CT for the characterization of atherosclerotic disease**. *Radiographics* **31**, 1255-1269 (2011).

[11] F. Tavora, N. Cresswell, L. Li, D. Fowler, A. Burke, **Frequency of acute plaque ruptures and thin cap atheromas at sites of maximal stenosis**. *Arquivos brasileiros de cardiologia* **94**, 143-159, (2010).

[12] L. H. Piers, R. Dikkers, T. P. Willems, B. J. G. L. De Smet, M. Oudkerk, F. Zijlstra, R. A. Tio, **Computed tomographic angiography or conventional coronary angiography in therapeutic decision-making**. *European heart journal* **29**, 2902-2907 (2008).

[13] S. Glagov, E. Weisenberg, C. K. Zarins, R. Stankunavicius, G. J. Kolettis, **Compensatory Enlargement of Human Atherosclerotic Coronary Arteries**. *New England Journal of Medicine* **316**, 1371-1375 (1987).

[14] P. W. Serruys, J. A. Ormiston, Y. Onuma, E. Regar, N. Gonzalo, H. M. Garcia-Garcia, K. Nieman, N. Bruining, C. Dorange, K. Miquel-Hébert, S. Veldhof, M. Webster, L. Thuesen, D. Dudek, **A bioabsorbable everolimus-eluting coronary stent system (ABSORB): 2-year outcomes and results from multiple imaging methods**. *The Lancet* **373**, 897-910 (2009).

[15] S. E. Nissen, **Application of intravascular ultrasound to characterize coronary artery disease and assess the progression or regression of atherosclerosis**. *The American Journal of Cardiology* **89**, 24-31 (2002).

[16] N. Bom, C. T. Lancee, **Apparatus for ultrasonically examining a hollow organ**. UK Patent no. 1402192 (1972).

[17] S. J. Park, J. M. Ahn, S. J. Kang, **Paradigm shift to functional angioplasty: New insights for fractional flow reserve-and intravascular ultrasound-guided percutaneous coronary intervention**. *Circulation* **124**, 951-957 (2011).

[18] G. W. Stone, A. Maehara, A. J. Lansky, B. De Bruyne, E. Cristea, G. S. Mintz, R. Mehran, J. McPherson, N. Farhat, S. P. Marso, H. Parise, B. Templin, R. White, Z. Zhang, P. W. Serruys, **A prospective natural-history study of coronary atherosclerosis**. *New England Journal of Medicine* **364**, 226-235 (2011).

[19] J. B. Lee, G. S. Mintz, J. B. Lisauskas, S. G. Biro, J. Pu, S. T. Sum, S. P. Madden, A. P. Burke, J. Goldstein, G. W. Stone, R. Virmani, J. E. Muller, A. Maehara, **Histopathologic validation of the intravascular ultrasound diagnosis of calcified coronary artery nodules**. *American Journal of Cardiology* **108**, 1547-1551 (2011).

[20] M. J. Davies, **Stability and instability: two faces of coronary atherosclerosis The Paul Dudley White Lecture 1995**. *Circulation* **94**, 2013-2020 (1996).

[21] W. Li, A. F. van der Steen, C. T. Lancée, I. Céspedes, N. Bom, **Blood flow imaging and volume flow quantitation with intravascular ultrasound**. *Ultrasound in Medicine & Biology* **24**, 203-214 (1998).

[22] S. G. Carlier, W. Li, E. I. Cespedes, A. F. W. v. d. Steen, J. N. Hamburger, N. Bom, P. W. J. C. Serruys, **Simultaneous Morphological and Functional Assessment of a Renal Artery Stent Intervention With Intravascular Ultrasound**. *Circulation (Baltimore)* **97**, 2575-2576 (1998).

[23] J. Schaar, C. d. Korte, F. Mastik, R. Baldewsing, E. Regar, P. d. Feyter, C. Slager, A. W. v. d. Steen, P. Serruys, **Intravascular palpography for high-risk vulnerable plaque assessment**. *Herz* **28**, 488-495 (2003).

[24] E. Céspedes, C. de Korte, A. van der Steen, **Intraluminal ultrasonic palpation: assessment of local and cross-sectional tissue stiffness**. *Ultrasound in Medicine & Biology* **26**, 385-396 (2000).

[25] P. W. Serruys, H. M. García-García, P. Buszman, P. Erne, S. Verheye, M. Aschermann, H. Duckers, O. Bleie, D. Dudek, H. E. Bøtker, **Effects of the direct lipoprotein-associated phospholipase A2 inhibitor darapladib on human coronary atherosclerotic plaque**. *Circulation* **118**, 1172-1182 (2008).

[26] M. J. Mulligan-Kehoe, **The vasa vasorum in diseased and nondiseased arteries**. *Am. J. Physiol.-Heart Circul. Physiol.* **298**, 295-305 (2010).

[27] E. L. Ritman, A. Lerman, **The dynamic vasa vasorum**. *Cardiovasc. Res.* **75**, 649-658 (2007).

[28] M. Gössl, D. Versari, H. A. Hildebrandt, T. Bajanowski, G. Sangiorgi, R. Erbel, E. L. Ritman, L. O. Lerman, A. Lerman, **Segmental heterogeneity of vasa vasorum neovascularization in human coronary atherosclerosis**. *JACC: Cardiovascular Imaging* **3**, 32-40 (2010).

[29] S. Carlier, I. A. Kakadiaris, N. Dib, M. Vavuranakis, S. M. O'Malley, K. Gul, C. J. Hartley, R. Metcalfe, R. Mehran, C. Stefanadis, E. Falk, G. Stone, M. Leon, M. Naghavi, **Vasa vasorum imaging: a new window to the clinical detection of vulnerable atherosclerotic plaques**. *Curr Atheroscler Rep* **7**, 164-169 (2005).

[30] S. O'Malley, M. Vavuranakis, M. Naghavi, I. Kakadiaris, **Intravascular ultrasound-based imaging of vasa vasorum for the detection of vulnerable atherosclerotic plaque**. *Medical Image Computing and Computer-Assisted Intervention–MICCAI 2005*, 343-351 (2005).

[31] D. E. Goertz, M. E. Frijlink, D. Tempel, L. C. van Damme, R. Krams, J. A. Schaar, F. J. Ten Cate, P. W. Serruys, N. de Jong, A. F. van der Steen, **Contrast harmonic intravascular ultrasound: a feasibility study for vasa vasorum imaging**. *Invest Radiol* **41**, 631-638 (2006).

[32] D. E. Goertz, M. E. Frijlink, D. Tempel, V. Bhagwandas, A. Gisolf, R. Krams, N. de Jong, A. F. W. van der Steen, **Subharmonic Contrast Intravascular Ultrasound for Vasa Vasorum Imaging**. *Ultrasound in Medicine & Biology* **33**, 1859-1872 (2007).

[33] R. Bekeredjian, P. A. Grayburn, R. V. Shohet, **Use of ultrasound contrast agents for gene or drug delivery in cardiovascular medicine**. *Journal of the American College of Cardiology* **45**, 329-335 (2005).

[34] P. A. Dijkmans, L. J. Juffermans, R. J. Musters, A. van Wamel, F. J. ten Cate, W. van Gilst, C. A. Visser, N. de Jong, O. Kamp, **Microbubbles and ultrasound: from diagnosis to therapy**. *Eur J Echocardiogr* **5**, 245-256 (2004).

[35] D. H. Simpson, P. N. Burns, M. A. Averkiou, **Techniques for perfusion imaging with microbubble contrast agents**. *IEEE transactions on ultrasonics, ferroelectrics, and frequency control* **48**, 1483-1494 (2001).

[36] R. J. Eckersley, C. T. Chin, P. N. Burns, **Optimising phase and amplitude modulation schemes for imaging microbubble contrast agents at low acoustic power**. *Ultrasound in Medicine & Biology* **31**, 213-219 (2005).

[37] D. H. Simpson, C. T. Chin, P. N. Burns, **Pulse inversion Doppler: a new method for detecting nonlinear echoes from microbubble contrast agents**. *IEEE transactions on ultrasonics, ferroelectrics, and frequency control* **46**, 372-382 (1999).

[38] K. Cheung, O. Couture, P. D. Bevan, P. N. Burns, F. S. Foster, **The effect of bubble size distribution and driving frequency on the "subharmonic" response from Definity microbubbles**. *IEEE Ultrasonics Symposium*, 850-853 (2005).

[39] D. E. Goertz, M. Frijlink, A. Bouakaz, C. T. Chin, N. de Jong, A. F. van der Steen, **The effect of bubble size on nonlinear scattering from microbubbles at high frequencies**. *IEEE Ultrasonics Symposium*, 1503-1506 (2003).

[40] D. E. Goertz, N. de Jong, A. F. van der Steen, **Attenuation and Size Distribution Measurements of Definity(Tm) and Manipulated Definity(Tm) Populations**. *Ultrasound in Medicine & Biology* **33**, 1376-1388 (2007).

[41] D. E. Goertz, M. E. Frijlink, N. de Jong, A. F. W. van der Steen, **High frequency nonlinear scattering from a micrometer to submicrometer sized lipid encapsulated contrast agent**. *Ultrasound in Medicine & Biology* **32**, 569-577 (2006).

[42] S. Feinstein, **The powerful microbubble: from bench to bedside, from intravascular indicator to therapeutic delivery system, and beyond**. *Am J Physiol Heart Circ Physiol* **287**, 450-457 (2004).

[43] J. Hohmann, T. Albrecht, C. W. Hoffmann, K. J. Wolf, **Ultrasonographic detection of focal liver lesions: increased sensitivity and specificity with microbubble contrast agents**. *European Journal of Radiology* **46**, 147-159 (2003).

[44] D. Maresca, K. Jansen, G. Renaud, G. van Soest, X. Li, Q. Zhou, N. De Jong, K. K. Shung, A. F. W. van der Steen, **Intravascular ultrasound chirp imaging**. *Applied Physics Letters* **100**, (2012).

[45] J. Alter, C. A. Sennoga, D. M. Lopes, R. J. Eckersley, D. J. Wells, **Microbubble Stability Is a Major Determinant of the Efficiency of Ultrasound and Microbubble Mediated in Vivo Gene Transfer**. *Ultrasound in Medicine & Biology* **35**, 976-984 (2009).

[46] H. J. Vos, M. Emmer, N. de Jong, **Oscillation of single microbubbles at room versus body temperature**. In *IEEE Ultrasonics Symposium Proceedings*, pp. 982-984 (2008).

[47] A. Bouakaz, N. de Jong, **WFUMB safety symposium on echo-contrast agents: nature and types of ultrasound contrast agents**. *Ultrasound in Medicine & Biology* **33**, 187-196 (2007).

[48] J. R. Lindner, J. Song, A. R. Jayaweera, J. Sklenar, S. Kaul, **Microvascular rheology of definity microbubbles after intra-arterial and intravenous administration**. *J. Am. Soc. Echocardiogr.* **15**, 396-403 (2002).

[49] D. Adam, M. Sapunar, E. Burla, **On the relationship between encapsulated ultrasound contrast agent and pressure**. *Ultrasound in Medicine & Biology* **31**, 673-686 (May, 2005).

[50] V. L. Newhouse, P. Mohana Shankar, **Bubble size measurements using the nonlinear mixing of two frequencies**. *J. Acoust. Soc. Am.* **75**, 1473-1477 (1984).

[51] D. Cathignol, J. Y. Chapelon, V. L. Newhouse, P. M. Shankar, **Bubble Sizing with High Spatial-Resolution**. *IEEE transactions on ultrasonics, ferroelectrics, and frequency control* **37**, 30-37 (Jan, 1990).

[52] P. J. Magari, R. J. Kline-Schoder, B. H. Stoedefalke, B. D. Butler, **A non-invasive, in-vivo, bubble sizing instrument**. In *IEEE Ultrasonics Symposium Proceedings,* pp. 1205-1210 (1997).

[53] T. G. Leighton, A. D. Phelps, D. G. Ramble, D. A. Sharpe, **Comparison of the abilities of eight acoustic techniques to detect and size a single bubble**. *Ultrasonics* **34**, 661-667 (1996).

[54] C. C. Coussios, C. K. Holland, L. Jakubowska, S. L. Huang, R. C. MacDonald, A. Nagaraj, D. D. McPherson, **In vitro characterization of liposomes and Optison (R) by acoustic scattering at 3.5 MHz**. *Ultrasound in Medicine & Biology* **30**, 181-190 (2004).

[55] S. Rossi, G. Waton, M. P. Krafft, **Phospholipid-Coated Gas Bubble Engineering: Key Parameters for Size and Stability Control, as Determined by an Acoustical Method**. *Langmuir* **26**, 1649-1655 (2010).

[56] J. Sijl, E. Gaud, P. J. Frinking, M. Arditi, N. de Jong, D. Lohse, M. Versluis, **Acoustic characterization of single ultrasound contrast agent microbubbles**. *The Journal of the Acoustical Society of America* **124**, 4091-4097 (2008).

[57] H. Medwin, **Counting bubbles acoustically: a review**. *Ultrasonics* **15**, 7-13 (1977).

[58] T. G. Leighton, ***The acoustic bubble***. Academic Press Limited, London, (1994).

[59] P. van Neer, G. Matte, J. Sijl, J. M. G. Borsboom, N. de Jong, **Transfer functions of US transducers for harmonic imaging and bubble responses**. *Ultrasonics* **46**, 336-340 (2007).

[60] J. A. Jensen, N. B. Svendsen, **Calculation of Pressure Fields from Arbitrarily Shaped, Apodized, and Excited Ultrasound Transducers**. *IEEE transactions on ultrasonics, ferroelectrics, and frequency control* **39**, 262-267 (1992).

[61] E. G. Radulescu, P. A. Lewin, A. Goldstein, A. Nowicki, **Hydrophone spatial averaging corrections from 1 to 40 MHz**. *IEEE transactions on ultrasonics, ferroelectrics, and frequency control* **48**, 1575-1580 (2001).

[62] P. Marmottant, S. van der Meer, M. Emmer, M. Versluis, N. de Jong, S. Hilgenfeldt, D. Lohse, **A model for large amplitude oscillations of coated bubbles accounting for buckling and rupture**. *The Journal of the Acoustical Society of America* **118**, 3499-3505 (2005).

[63] M. Emmer, H. J. Vos, M. Versluis, N. de Jong, **Radial Modulation of Single Microbubbles**. *IEEE transactions on ultrasonics, ferroelectrics, and frequency control* **56**, 2370-2379 (2009).

[64] S. P. Qin, D. E. Kruse, K. W. Ferrara, **Transmitted ultrasound pressure variation in micro blood vessel phantoms**. *Ultrasound in Medicine & Biology* **34**, 1014-1020 (2008).

[65] A. L. Klibanov, P. T. Rasche, M. S. Hughes, J. K. Wojdyla, K. P. Galen, J. H. Wible, G. H. Brandenburger, **Detection of individual microbubbles of an ultrasound contrast agent: Fundamental and pulse inversion imaging**. *Acad. Radiol.* **9**, S279-S281 (2002).

[66] A. C. Barger, R. Beeuwkes, L. L. Lainey, K. J. Silverman, **Hypothesis: Vasa Vasorum and Neovascularization of Human Coronary Arteries**. *New England Journal of Medicine* **310**, 175-177 (1984).

[67] C. Veltmann, S. Lohmaier, T. Schlosser, S. Shai, A. Ehlgen, C. Pohl, H. Becher, K. Tiemann, **On the design of a capillary flow phantom for the evaluation of ultrasound contrast agents at very low flow velocities**. *Ultrasound in Medicine & Biology* **28**, 625-634 (2002).

[68] M. O. Culjat, D. Goldenberg, P. Tewari, R. S. Singh, **A review of tissue substitutes for ultrasound imaging**. *Ultrasound in Medicine & Biology* **36**, 861-873 (2010).

[69] A. Kharine, S. Manohar, R. Seeton, R. G. Kolkman, R. A. Bolt, W. Steenbergen, F. F. de Mul, **Poly(vinyl alcohol) gels for use as tissue phantoms in photoacoustic mammography**. *Physics in Medicine & Biology* **48**, 357-370 (2003).

[70] F. S. Foster, C. J. Pavlin, K. A. Harasiewicz, D. A. Christopher, D. H. Turnbull, **Advances in ultrasound biomicroscopy**. *Ultrasound in Medicine & Biology* **26**, 1-27 (2000).

[71] D. E. Goertz, M. E. Frijlink, N. de Jong, A. F. W. van der Steen, **Nonlinear intravascular ultrasound contrast imaging**. *Ultrasound in Medicine & Biology* **32**, 491-502 (2006).

[72] J. Yuan, S. Rhee, X. N. Jiang, **60 MHz PMN-PT based 1-3 composite transducer for IVUS imaging**. *IEEE Ultrasonics Symposium*, pp. 682-685 (2008).

[73] J.-B. Michel, R. Virmani, E. Arbustini, G. Pasterkamp, **Intraplaque haemorrhages as the trigger of plaque vulnerability**. *European heart journal* **32**, 1977-1985 (2011).

[74] J. Mamou, O. Aristizabal, R. H. Silverman, J. A. Ketterling, D. H. Turnbull, **High-Frequency Chirp Ultrasound Imaging with an Annular Array for Ophthalmologic and Small-Animal Imaging**. *Ultrasound in Medicine & Biology* **35**, 1198-1208 (2009).

[75] A. Novell, S. van der Meer, M. Versluis, N. de Jong, A. Bouakaz, **Contrast agent response to chirp reversal: simulations, optical observations, and acoustical verification**. *IEEE transactions on ultrasonics, ferroelectrics, and frequency control* **56**, 1199-1206 (2009).

[76] D. H. Thomas, P. Looney, R. Steel, N. Pelekasis, W. N. McDicken, T. Anderson, V. Sboros, **Acoustic detection of microbubble resonance**. *Applied Physics Letters* **94**, (2009).

[77] Q. F. Zhou, X. C. Xu, E. J. Gottlieb, L. Sun, J. M. Cannata, H. Ameri, M. S. Humayun, P. D. Han, K. K. Shung, **PMN-PT single crystal, high-frequency ultrasonic needle transducers for pulsed-wave Doppler application**. *IEEE transactions on ultrasonics, ferroelectrics, and frequency control* **54**, 668-675 (2007).

[78] C. J. P. M. Teirlinck, R. A. Bezemer, C. Kollmann, J. Lubbers, P. R. Hoskins, P. Fish, K.-E. Fredfeldt, U. G. Schaarschmidt, **Development of an example flow test object and comparison of five of these test objects, constructed in various laboratories**. *Ultrasonics* **36**, 653-660 (1998).

[79] N. de Jong, L. Hoff, T. Skotland, N. Bom, **Absorption and scatter of encapsulated gas filled microbubbles: theoretical considerations and some measurements**. *Ultrasonics* **30**, 95-103 (1992).

[80] T. Misaridis, J. A. Jensen, **Use of modulated excitation signals in medical ultrasound. Part II: Design and performance for medical imaging applications**. *IEEE transactions on ultrasonics, ferroelectrics, and frequency control* **52**, 192-207 (2005).

[81] Z. A. Fayad, V. Mani, V. Fuster, **The time has come for clinical cardiovascular trials with plaque characterization as an endpoint**. *European heart journal* **33**, 160-161 (2012).

[82] J. C. Sluimer, M. J. Daemen, **Novel concepts in atherogenesis: Angiogenesis and hypoxia in atherosclerosis**. *Journal of Pathology* **218**, 7-29 (2009).

[83] N. Bom, C. T. Lancée, F. C. Van Egmond, **An ultrasonic intracardiac scanner**. *Ultrasonics* **10**, 72-76 (1972).

[84] C. L. de Korte, H. H. G. Hansen, A. F. W. van der Steen, **Vascular ultrasound for atherosclerosis imaging**. *Interface Focus* **1**, 565-575 (2011).

[85] M. Vavuranakis, I. A. Kakadiaris, S. M. O'Malley, T. G. Papaioannou, E. A. Sanidas, M. Naghavi, S. Carlier, D. Tousoulis, C. Stefanadis, **A new method for assessment of plaque vulnerability based on vasa vasorum imaging, by using contrast-enhanced intravascular ultrasound and differential image analysis**. *International Journal of Cardiology* **130**, 23-29 (2008).

[86] M. E. Frijlink, D. E. Goertz, H. J. Vos, E. Tesselaar, G. Blacquiere, A. Gisolf, R. Krams, A. F. van der Steen, **Harmonic intravascular ultrasound imaging with a dual-frequency catheter**. *Ultrasound in Medicine & Biology* **32**, 1649-1654 (2006).

[87] H. J. Vos, M. E. Frijlink, E. Droog, D. E. Goertz, G. Blacquiere, A. Gisolf, N. De Jong, A. F. Van der Steen, **Transducer for harmonic intravascular ultrasound imaging**. *IEEE transactions on ultrasonics, ferroelectrics, and frequency control* **52**, 2418-2422 (2005).

[88] D. E. Goertz, E. Cherin, A. Needles, R. Karshafian, A. S. Brown, P. N. Burns, F. S. Foster, **High frequency nonlinear B-scan imaging of microbubble contrast agents**. *IEEE transactions on ultrasonics, ferroelectrics, and frequency control* **52**, 65-79 (2005).

[89] G. L. t. Kate, G. G. J. Renaud, Z. Akkus, S. C. H. v. d. Oord, F. J. t. Cate, V. Shamdasani, R. R. Entrekin, E. J. G. Sijbrands, N. d. Jong, J. G. Bosch, A. F. L. Schinkel, A. F. W. van der Steen, **Far-wall pseudoenhancement during contrast-enhanced ultrasound of the carotid arteries: clinical description and in vitro reproduction**. *Ultrasound in Medicine & Biology* **38**, 593-600 (2012).

[90] M. Pasovic, M. Danilouchkine, T. Faez, P. van Neer, C. Cachard, A. F. W. van der Steen, O. Basset, N. de Jong, **Second harmonic inversion for ultrasound contrast harmonic imaging**. *Physics in Medicine & Biology* **56**, 3163-3180 (2011).

[91] M.-X. Tang, N. Kamiyama, R. J. Eckersley, **Effects of nonlinear propagation in ultrasound contrast agent imaging**. *Ultrasound in Medicine & Biology* **36**, 459 (2010).

[92] H. H. G. Hansen, R. G. P. Lopata, T. Idzenga, C. L. de Korte, **Full 2D displacement vector and strain tensor estimation for superficial tissue using beam-steered ultrasound imaging**. *Physics in Medicine & Biology* **55**, 3201-3218 (2010).

[93] M. F. Giannoni, E. Vicenzini, M. Citone, M. C. Ricciardi, L. Irace, A. Laurito, L. F. Scucchi, V. Di Piero, B. Gossetti, A. Mauriello, L. G. Spagnoli, G. L. Lenzi, F. B. Valentini, **Contrast Carotid Ultrasound for the Detection of Unstable Plaques with Neoangiogenesis: A Pilot Study**. *European Journal of Vascular and Endovascular Surgery* **37**, 722-727 (2009).

[94] P. J. Frinking, A. Bouakaz, J. Kirkhorn, F. J. Ten Cate, N. de Jong, **Ultrasound contrast imaging: current and new potential methods**. *Ultrasound in Medicine & Biology* **26**, 965-975 (2000).

[95] Y. Sun, D. E. Kruse, K. W. Ferrara, **Contrast imaging with chirped excitation**. *IEEE transactions on ultrasonics, ferroelectrics, and frequency control* **54**, 520-529 (2007).

[96] R. Virmani, F. D. Kolodgie, A. P. Burke, A. V. Finn, H. K. Gold, T. N. Tulenko, S. P. Wrenn, J. Narula, **Atherosclerotic plaque progression and vulnerability to rupture: Angiogenesis as a source of intraplaque hemorrhage**. *Arteriosclerosis, thrombosis, and vascular biology* 25, 2054-2061 (2005).

[97] D. Maresca, G. Renaud, G. van Soest, X. Li, Q. Zhou, K. K. Shung, N. de Jong, A. F. W. van der Steen, **Contrast-Enhanced Intravascular Ultrasound Pulse Sequences for Bandwidth-Limited Transducers**. *Ultrasound in Medicine & Biology* 39, 706-713 (2013).

[98] E. Mace, G. Montaldo, I. Cohen, M. Baulac, M. Fink, M. Tanter, **Functional ultrasound imaging of the brain**. *Nature Methods*, (2011).

[99] P. N. Burns, **Instrumentation for contrast echocardiography**. *Echocardiography* 19, 241-258 (2002).

[100] B. Kuersten, T. H. Murthy, P. Li, Z. Liu, E. Locricchio, C. Baisch, P. Rafter, M. Vannan, **Ultraharmonic myocardial contrast imaging: In vivo experimental and clinical data from a novel technique**. *J. Am. Soc. Echocardiogr.* 14, 910-916 (2001).

[101] T. Shiogai, N. Takayasu, T. Mizuno, M. Nakagawa, H. Furuhata, **Comparison of transcranial brain tissue perfusion images between ultraharmonic, second harmonic, and power harmonic imaging**. *Stroke* 35, 687-693 (2004).

[102] C. Sun, S. D. Pye, J. E. Browne, A. Janeczko, B. Ellis, M. B. Butler, V. Sboros, A. J. W. Thomson, M. P. Brewin, C. H. Earnshaw, C. M. Moran, **The Speed of Sound and Attenuation of an IEC Agar-Based Tissue-Mimicking Material for High Frequency Ultrasound Applications**. *Ultrasound in Medicine & Biology* 38, 1262-1270 (2012).

[103] M. E. Frijlink, D. E. Goertz, A. Bouakaz, A. F. van der Steen, **A simulation study on tissue harmonic imaging with a single-element intravascular ultrasound catheter**. *The Journal of the Acoustical Society of America* 120, 1723-1731 (2006).

[104] C. Vinegoni, I. Botnaru, E. Aikawa, M. A. Calfon, Y. Iwamoto, E. J. Folco, V. Ntziachristos, R. Weissleder, P. Libby, F. A. Jaffer, **Indocyanine green enables near-infrared fluorescence imaging of lipid-rich, inflamed atherosclerotic plaques**. *Science Translational Medicine* 3, 84ra45 (2011).

[105] V. Hamburger, H. L. Hamilton, **A series of normal stages in the development of the chick embryo**. *Developmental Dynamics* 195, 231-272 (1992).

[106] D. Staub, M. B. Patel, A. Tibrewala, D. Ludden, M. Johnson, P. Espinosa, B. Coll, K. A. Jaeger, S. B. Feinstein, **Vasa vasorum and plaque neovascularization on contrast-enhanced carotid ultrasound imaging correlates with cardiovascular disease and past cardiovascular events**. *Stroke* 41, 41-47 (2010).

[107] M. A. Schellpfeffer, G. L. Kolesari, **Microbubble Contrast Imaging of the Cardiovascular System of the Chick Embyro**. *Ultrasound in Medicine & Biology* **38**, 504-510 (2012).

[108] M. Frijlink, D. E. Goertz, L. C. A. van Damme, R. Krams, A. F. van der Steen, **Intravascular ultrasound tisse harmonic imaging in vivo**. *IEEE transactions on ultrasonics, ferroelectrics, and frequency control* **53**, 1844-1852 (2006).

[109] B. Latour, ***Science in action: How to follow scientists and engineers through society***. Harvard university press (1987).

[110] W. Tsai, **Knowledge transfer in intraorganizational networks: effects of network position and absorptive capacity on business unit innovation and performance**. *Academy of management journal* **44**, 996-1004 (2001)

[111] S. P. Borgatti, M. G. Everett, L. C. Freeman, **Ucinet for Windows: Software for social network analysis**. (2002).

[112] R. D. Luce, A. D. Perry, **A method of matrix analysis of group structure**. *Psychometrika* **14**, 95-116 (1949).

[113] S. Nissen, J. Gurley, C. Grines, D. Booth, R. McClure, M. Berk, C. Fischer, A. DeMaria, **Intravascular ultrasound assessment of lumen size and wall morphology in normal subjects and patients with coronary artery disease**. *Circulation* **84**, 1087-1099 (1991).

[114] T. Venturini, **Diving in magma: How to explore controversies with actor-network theory**. *Public understanding of science* **19**, 258-273 (2010).

[115] T. Kubo, T. Akasaka, **What is the optimal imaging tool for coronary atherosclerosis?** in *Coronary atherosclerosis: current management and treatment* (eds. Arampatzis, C, McFadden, EP, Michalis, LK, Virmani, R, Serruys, PW) 250-8 (Informa Healthcare, London, UK, 2012)

[116] E. J. Gussenhoven, P. A. V. Frietman, S. H. K. The, R. J. van Suylen, F. C. van Egmond, C. T. Lancée, H. van Urk, J. R. T. C. Roelandt, T. Stijnen, N. Bom, **Assessment of medial thinning in atherosclerosis by intravascular ultrasound**. *The American Journal of Cardiology* **68**, 1625-1632 (1991).

[117] C. Chandrana, N. Kharin, G. D. Vince, S. Roy, A. J. Fleischman, **Demonstration of second-harmonic IVUS feasibility with focused broadband miniature transducers**. *IEEE transactions on ultrasonics, ferroelectrics, and frequency control* **57**, 1077-1085 (2010).

[118] E. Regar, M. Gnanadesigan, A. F. W. van der Steen, G. van Soest, **Quantitative Optical Coherence Tomography Tissue-Type Imaging for Lipid-Core Plaque Detection**. *JACC: cardiovascular interventions* (2013).

[119] K. Jansen, A. F. W. van der Steen, H. M. M. van Beusekom, J. W. Oosterhuis, G. van Soest, **Intravascular photoacoustic imaging of human coronary atherosclerosis**. *Optics Letters* **36**, 597-599 (2011)

[120] A. Rosenthal, F. A. Jaffer, V. Ntziachristos, **Intravascular multispectral optoacoustic tomography of atherosclerosis: prospects and challenges**. *Imaging in Medicine* **4**, 299-310 (2012).

[121] Tonino, P. A. *et al.* **Fractional flow reserve versus angiography for guiding percutaneous coronary intervention**. *New England Journal of Medicine* **360**, 213-224 (2009).

[122] M. Frijlink, ***Harmonic intravascular ultrasound***, Ph.D. Thesis. Erasmus University, the Netherlands (2006).

[123] X. Li, J. Yin, C. Hu, Q. Zhou, K. K. Shung, Z. Chen, **High-resolution coregistered intravascular imaging with integrated ultrasound and optical coherence tomography probe**. *Applied Physics Letters* **97**, 133702-133702-133703 (2010).

[124] B. L. Helfield, E. Cherin, F. S. Foster, D. E. Goertz, **Investigating the Subharmonic Response of Individual Phospholipid Encapsulated Microbubbles at High Frequencies: A Comparative Study of Five Agents**. *Ultrasound in Medicine & Biology* **38**, 846-863 (2012).

[125] J. A. Ketterling, O. Aristizábal, D. H. Turnbull, F. L. Lizzi, **Design and fabrication of a 40-MHz annular array transducer**. *IEEE transactions on ultrasonics, ferroelectrics, and frequency control* **52**, 672-681 (2005).

SUMMARY

IMAGING MICROVASCULAR NETWORKS DEEP IN THE HEART

In 2011, an international team of researchers examined more than 50 ancient Egyptian mummies from the Middle Kingdom to the Greco-Roman dynasty with a medical X-ray scanner, in search for evidence of a major cardiovascular disease: atherosclerosis*. Conclusion: "atherosclerosis is commonplace in mummified ancient Egyptians."

It is safe to say that since antiquity and probably earlier, people are confronted with atherosclerosis, a deadly affliction leading to heart attacks and sudden death. In 2008, 7.3 million people worldwide died of a heart attack according to the world health organization.

The heart is a central organ that ensures the perpetual transportation of blood and oxygen throughout the entire body. What we often forget is that the heart itself requires blood and oxygen to maintain its function. This supply is ensured by blood vessels running along the heart surface called coronary arteries. Cardiologists now recognize that it is the development of atherosclerosis in the coronary arteries that causes heart attacks. To date, the early identification of patient presenting a high risk of cardiovascular accident remains a central issue in medicine.

Because a good understanding of diseases at a microscopic scale often leads to new diagnostics and treatments, a clear role exists for a medical tool able to visualize coronary atherosclerosis in humans.

Since 1972, researchers of the Erasmus Medical Centre in Rotterdam have been developing echography at the tip of a catheter, a technique to navigate inside coronary arteries and image the arterial wall with a great level of detail. This technique was named intravascular ultrasound (abbreviated as IVUS) and was the first to reveal the shapes and dimensions of atherosclerotic lesions nested in the coronary artery wall. 40 years later, external imaging techniques, such as echocardiography, MRI and CT, still lack the resolution to image coronary artery wall structures, which are too small and lie too deep in the body.

Diving deeper and deeper, people realized that the coronary arteries, whose function is to supply heart muscle cells with blood and oxygen, were nourished themselves by a network of microvessels that penetrate the layers of the arterial wall. This network is called the vasa vasorum, which literally means "the vessels of the vessels". Recent findings indicate that the presence of vasa vasorum inside an atherosclerotic coronary lesion was associated with future risks of a heart attack.
Unfortunately, even IVUS does not have a sufficient resolution to detect the vasa vasorum, which exhibits vessel diameters ranging from 200 microns (the diameter of a human hair) down to 5 microns (the diameter of a single red blood cell).
To predict the risk of heart attacks, cardiologists need a tool that can detect coronary vasa vasorum in humans. In addition, the method should prove to be safe, reliable and affordable.

Scientists of the Biomedical Engineering department of Erasmus Medical Centre introduced the following concept: by injecting microscopic bubbles of the dimension of red blood cells in the blood stream, these would eventually enter the vasa vasorum. If one can track with IVUS the signals of these bubbles, one could indirectly detect the presence and extent of coronary vasa vasorum.

In this thesis, we present the development of microbubble detection methods for clinical IVUS catheters and evaluation of their capacity to detect vasa vasorum sized channels in controlled experiments.

The first method relied on chirps, bio-inspired acoustic signals of increasing or decreasing frequency. Chirps are widely used by animals like dolphins or bats for echolocation purposes. Scientists noticed that, contrary to biological tissue, a microbubble could generate different echoes in response to an up-sweep chirp and an identically shaped down-sweep chirp, through a phenomenon called transient resonance. Therefore, by transmitting pairs of up-sweep and down-sweep chirps with IVUS, we were able to sort areas filled with microbubbles from areas filled with tissue. *In vivo*, such an ultrasound detection method will permit to image vascular networks infused with microbubbles, while hiding surrounding biological structures.

The second method reported relied on the excitation of unique microbubble echoes called "ultraharmonics". Ultraharmonics arise at a frequency which is 1.5 times higher than the transmitted frequency and can only be generated by microbubbles. Therefore, imaging microbubble ultraharmonics with IVUS is another method to disentangle blood from tissue. In practice, microbubble echoes comprise mostly transmit frequency content, which shadows completely the weaker ultraharmonic content. Yet, we could extract the ultraharmonic echo's thanks to a dedicated ultrasound pulse sequence and in this manner visualize the microbubbles.

We compared both methods and observed that ultraharmonic IVUS imaging was more successful than IVUS chirp imaging at detecting of vasa vasorum sized microchannels. We pursued with *in vivo* experiments and demonstrated that ultraharmonic IVUS could successfully image a microvascular network of vasa vasorum dimension, below the detection limit of conventional IVUS. The ultraharmonic IVUS image showed an excellent agreement with a photograph of the microvascular region of interest.

Ultraharmonic IVUS imaging is a method capable of detecting intricate microvascular networks invisible with conventional IVUS catheters and could turn into a promising tool for coronary vasa vasorum detection in humans. Ultimately, we hope that ultraharmonic IVUS imaging of microvascularization will help cardiologists to identify early coronary atherosclerotic lesions presenting risks of heart attacks, and therefore limit vast losses of productive life years in our societies.

Beyond the scope of IVUS, the implementation of ultraharmonic ultrasound on conventional ultrasound scanners could allow doctors to assess the microvasculature density and therefore the inflammatory status of important diseases like atherosclerosis or rheumatoid arthritis.

* A. H. Allam, R. C. Thompson, L. S. Wann, M. I. Miyamoto, A. e.-H. Nur el-Din, G. A. el-Maksoud, M. Al-Tohamy Soliman, I. Badr, H. A. el-Rahman Amer, M. L. Sutherland, J. D. Sutherland, G. S. Thomas, **Atherosclerosis in Ancient Egyptian Mummies: The Horus Study**. *JACC: Cardiovascular Imaging* 4, 315-327 (2011).

SAMENVATTING

AFBEELDEN VAN MICROVASCULAIRE NETWERKEN DIEP IN HET HART

In 2011 lichtte een internationaal team van onderzoekers meer dan 50 oude Egyptische mummies van het Middenrijk tot het Grieks-Romeins Rijk door met een röntgenapparaat, op zoek naar bewijs van een belangrijke hart- en vaatziekte: atherosclerose*. Hun conclusie luidde: "atherosclerose is gemeengoed in gemummificeerde oude Egyptenaren."

Al sinds de oudheid worden mensen geconfronteerd met atherosclerose, een dodelijke aandoening die kan leiden tot hartaanvallen en plotselinge dood. Volgens de World Health Organization stierven in 2008 wereldwijd 7,3 miljoen mensen aan een hartaanval.

Het hart is het centrale orgaan, dat zorgt voor het continue transport van bloed en zuurstof door het hele lichaam. Wat we vaak vergeten is dat het hart zelf ook bloed en zuurstof nodig heeft voor het handhaven van zijn functie. Deze voeding wordt geleverd door de bloedvaten die over het hartoppervlak lopen en de kransslagaders worden genoemd. Het is algemeen erkend dat de ontwikkeling van atherosclerose in de kransslagaders de veroorzaker van hartaanvallen is. De vroegtijdige identificatie van de patiënt met een verhoogd risico op een hartaanval blijft echter tot op heden een centraal vraagstuk binnen de geneeskunde.

Een goed begrip van ziekten op een microscopische schaal leidt vaak tot nieuwe diagnostiek en behandelingen en daarom is er een duidelijke rol weggelegd voor een medisch hulpmiddel dat atherosclerose in de menselijke kransslagaders kan afbeelden.

Sinds 1972 houden onderzoekers van het Erasmus Medisch Centrum in Rotterdam zich bezig met het ontwikkelen van echografie aan het uiteinde van een katheter, om van binnenuit de wand van de kransslagaders gedetailleerd in beeld te brengen. Deze techniek wordt intravasculair ultrageluid (IVUS) genoemd en was als eerste in staat de vormen en afmetingen van atherosclerotische laesies in de wand van de kransslagaders te onthullen. Nu, veertig jaar later, hebben externe beeldvormende technieken, zoals

echocardiografie, MRI en CT, nog steeds niet de benodigde resolutie om de structuren in de vaatwand van de kransslagaders in beeld te brengen omdat ze zo klein zijn en erg diep in het lichaam liggen.

Dieper en dieper kijkend, besefte men dat de kransslagaders die de hartspiercellen van bloed en zuurstof voorzien, op hun beurt weer gevoed worden door een netwerk van zeer kleine vaatjes die de arteriële wand binnendringen. Dit netwerk wordt vasa vasorum genoemd, wat Latijn is voor "de vaten van de vaten". Recente bevindingen wijzen erop dat de aanwezigheid van vasa vasorum binnen een atherosclerotische laesie in de kransslagaders verband houdt met het toekomstige risico op een hartaanval.

Helaas beschikt zelfs IVUS niet over voldoende resolutie om vasa vasorum te detecteren, dat in diameter varieert van 200 micron (de diameter van een menselijke haar) tot 5 micron (de diameter van een enkele rode bloedcel).

Om het risico op een hartaanval te kunnen voorspellen, hebben cardiologen een hulpmiddel nodig dat vasa vasorum in de kransslagaders van de mens detecteren kan. De methode moet bovendien veilig, betrouwbaar en betaalbaar zijn.

Wetenschappers van de afdeling Biomedische Technologie van het Erasmus Medisch Centrum hebben het volgende concept geïntroduceerd: in de bloedstroom geïnjecteerde microscopische gasbellen (microbellen), in de orde van grootte van rode bloedcellen, zullen uiteindelijk in de vasa vasorum terecht komen. Als met IVUS de signalen van deze bellen opgevangen kunnen worden, kan indirect de aanwezigheid en omvang van vasa vasorum in de wand van de kransslagaders gedetecteerd worden.

In dit proefschrift beschrijven we de ontwikkeling van twee microbeldetectiemethoden voor klinische IVUS katheters en de evaluatie van hun vermogen om kanalen van hetzelfde formaat als vasa vasorum te detecteren in gecontroleerde experimenten.

De eerste methode is gebaseerd op tjirps, akoestische signalen, geïnspireerd door de natuur, van oplopende of aflopende frequentie. Tjirps worden veel gebruikt door dieren, zoals dolfijnen of vleermuizen, voor echolocatie doeleinden. Wetenschappers hebben ontdekt dat een microbel, in tegenstelling tot biologisch weefsel, verschillend reageert op een oplopende tjirp en een aflopende tjirp, via een verschijnsel dat transiënte resonantie genoemd wordt. Door nu met IVUS paren van oplopende en aflopende tjirps te verzenden konden we gebieden met microbellen onderscheiden van biologisch weefsel. Met deze techniek kunnen we in vivo plaatjes maken waarop de met microbellen gevulde vasa vasorum netwerken duidelijk zichtbaar zijn, terwijl de echo's van omringende biologische structuren onderdrukt worden.

De tweede methode die beschreven wordt, gebruikt unieke trillingen van microbellen die gegenereerd worden in reactie op ultrageluid. Deze trillingen hebben een frequentie die anderhalf keer hoger is dan de verzonden frequentie en worden alleen gegenereerd door microbellen. Ze worden "ultraharmonische echo's" genoemd. Het afbeelden van deze ultraharmonische trillingen met IVUS is dus een andere methode om de bloedvaten van weefsel te onderscheiden. In de praktijk bevatten microbel echo's echter voornamelijk de verzendfrequentie signalen, die de zwakkere ultraharmonische signalen volledig overschaduwen. Dankzij een speciale reeks echografie pulsen waren we toch in staat om de microbel ultraharmonische echo's te onderscheiden en op deze manier de microbellen zichtbaar te maken.

We vergeleken beide methoden en constateerden dat de ultraharmonische IVUS methode succesvoller was dan de IVUS tjirp methode in het opsporen van kanaaltjes van dezelfde dimensies als vasa vasorum. We hebben vervolgens in vivo experimenten uitgevoerd en aangetoond dat ultraharmonische IVUS beeldvorming een netwerk van kleine vaten ter grootte van vasa vasorum, en dus onder de detectiegrens van conventionele IVUS, met succes in beeld kan brengen. De ultraharmonisch IVUS afbeelding vertoonde een voortreffelijke overeenstemming met een foto van het in beeld gebrachte gebied.

Ultraharmonische IVUS beeldvorming is een methode voor het opsporen van ingewikkelde netwerken van kleine bloedvaten die onzichtbaar zijn voor conventionele IVUS katheters. Deze nieuwe techniek is een potentieel veelbelovend instrument voor vasa vasorum detectie in de kransslagaders van de mens. Wij hopen dat ultraharmonische IVUS beeldvorming van vasa vasorum, cardiologen uiteindelijk zal helpen bij het vroegtijdig identificeren van atherosclerotische laesies in de kransslagaders, die het risico op een hartaanval verhogen, en daarmee grote verliezen van productieve levensjaren in onze samenleving zal beperken.

Buiten het kader van IVUS kan de uitvoering van ultraharmonische echografie op conventionele echografie apparaten het artsen mogelijk maken om de dichtheid van kleine bloedvaten en daarmee de ontstekingsstatus van belangrijke ziekten zoals atherosclerose of reumatoïde artritis te bepalen.

* A. H. Allam, R. C. Thompson, L. S. Wann, M. I. Miyamoto, A. e.-H. Nur el-Din, G. A. el-Maksoud, M. Al-Tohamy Soliman, I. Badr, H. A. el-Rahman Amer, M. L. Sutherland, J. D. Sutherland, G. S. Thomas, **Atherosclerosis in Ancient Egyptian Mummies: The Horus Study**. *JACC: Cardiovascular Imaging* 4, 315-327 (2011).

Acknowledgements

Soon after my arrival in the Netherlands, where I started my career as a young scientist, I visited the Kröller-Müller museum and its sculpture garden nested in the national park of the Hoge Veluwe. I became quite perplexed when I came across the painting of a red and green Pegasus, as I could clearly remember myself gazing at this image as a child. Later on, talking on the phone with my parents, I realized that we had visited the museum 20 years ago. This is my first memory in the Netherlands, a vivid and colourful one.

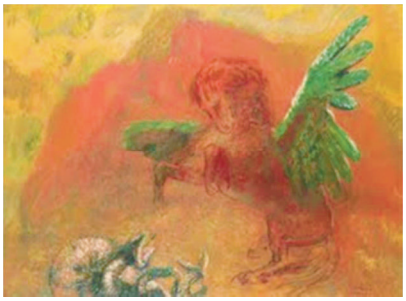

Reproduction of the painting by Odilon Redon

I would like to thank my parents, Jacqueline et Bruno, for their love, guidance and care and all the wonders we came across when travelling together. It shaped my curiosity and nourished my imagination, which helps me tremendously today. Thanks to them, leaving Paris for the Netherlands felt somewhat familiar.

I would like to thank my grandma Poutchett and my sister Marie for being always available and supportive in the course of my journey in the Netherlands, for the visits and the phone calls, the days spent in Rome and our week end escapes.

I have a special thought for Aude, who helped me finding my first internship at Philips in the Netherlands. Without you, I would not be here today!

I am grateful to Freek and Szabolcs who welcomed me warmly as a member of their team at Philips Research and gave me the confidence to pursue a scientific career.

I am thankful to Ton, Nico, Hans and Gijs who offered me the opportunity to pursue a PhD at the Biomedical Engineering Department. It has been an honour to work in group with so much history, and a pleasure to interact with you in Rotterdam and at conferences abroad.

Thank you Robert for been so welcoming, for walking me around the laboratory the day of my interview. Thank you Marie for handing the work you initiated, as well as your studio. Thank you Paul, for taking me to kung-fu lessons when I had just arrived. Thank you Marcia, Telli, Guillaume, Pieter, for your friendship and for lending an ear to my issues. It great to have your around! Thank you Ilya, Alex, Verya for your enthusiasm and all the fun, I am going to miss you guys. And also Kim and Kim and Lambert and Ali and Klazina, Yin, Tom, Zeynettin, Jacopo, Mehri, and all the others who make the lab such a friendly and tolerant workplace. Thank you Samantha, Frits, Charles, for your knowledgeable insights, your help and our discussions. Thank you Geert and Michiel for building anything and everything from sketches for me.

Thank you Min, Muthu, Tianshi, the 22nd floor extension of the group is a little eastern paradise thanks to you. It is definitely our lab's best kept secret, with a breath-taking view. But time is counted...

I would like to address special thanks to Mieke and Gracia, you have been always available, smiling and helpful with me, merci beaucoup.

Merci Laurent, Sara, Sophie, Thierry, Thibault, Christophe, Gillaume, Juliette, Pascal, Isabelle, et tous ceux qui sont restés proches malgré la distance. Aline and Anja in particular since our splendid semester down under.

Merci à mes cousins, Anne-Laure, Myriam, Nicolas, Gabriel, Emmanuel et à toute la famille pour votre amitié et vos encouragements depuis de longues années.

Merci Sylvain de m'avoir accueilli et fait découvrir Nantes. Merci Anne, Michel et Antonin pour tous les Noëls passés ensembles.

Thank you Micha, Xabi, Mattia, Jacqueline for the fun at Ragnar, on the road from Milan to Rotterdam, or at the Irish Pub!

Lia, Piet, Bregit, Arwen, Cindy, Frank, Erwin, Magda, Jaya and Bin, thanks a million for making a warm place for me in your family!

Pavlov and Harriet, thank you for the barking and the loving. I even thought about you as paranymphs, but you cannot read...

And you Krista, well, I would simply like to thank you for being by my side day and night for three years now, you're wonderful.

David
Blijdorp, Rotterdam
2013

CURRICULUM VITAE

David Maresca was born in Paris on June 16, 1983. He followed his secondary education at the Lycée Claude Monet from 1994 to 2001. In 2003, he started his university education in Physics at the University Paris Diderot. In the frame of his studies, he completed various assignments at the interface of physics and other disciplines such as astronomy (Hα kinematics of isolated galaxies), journalism (brief news items for *Sciences et Avenir* magazine), philosophy (epistemology, evolutionary theories), art (pigment analysis of the Mona Lisa with near infrared spectroscopy) and medicine (transcranial hyperthermia with ultrasound). He received a Master of Science in Ultrasound Physics in 2007 after the completion of his master's thesis, entitled "Single element ultrasonic imaging based on a variable refractive structure", at Philips High Tech Campus, Eindhoven, the Netherlands. Subsequently, he was appointed for a year as research scientist in experimental echocardiography at Philips Research and co-authored a patent on an acoustic fluid lens for ultrasound imaging. In October 2008, he joined the Thorax Centre Department of Biomedical Engineering of Erasmus University Medical Centre, Rotterdam, the Netherlands, to carry out a PhD in harmonic intravascular ultrasound imaging under the supervision of Nico de Jong and Antonius F. W. van der Steen.

Dates

16 June 1983	- Birth in Paris, France.
2001	- Baccalauréat Scientifique, Lycée Claude Monet, Paris, France.
2001-2003	- Classes préparatoires Physique, Chimie, Sciences de l'Ingénieur, Lycée Pierre-Gilles de Gennes – ENCPB, Paris, France.
2003	- Entered the Magistère de Physique program of the University Paris Diderot, Paris, France.
2004	- Exchange program at the University of New South Wales, Sydney, Australia.
2007	- Master of Science in Ultrasound Physics of the University Paris Diderot. Magistère de Physique of the University Paris Diderot.
2007-2008	- Research Scientist in Experimental Echocardiography at Philips Research, Eindhoven High Tech Campus, the Netherlands.
2008-2012	-PhD in Experimental Echocardiography at the Thorax Centre Department of Biomedical Engineering, Erasmus University Medical Centre, Rotterdam, the Netherlands.

Publications

Articles

D. Maresca, M. Emmer, P. L. van Neer, H. J. Vos, M. Versluis, M. Muller, N. de Jong, A. F. W. van der Steen, **Acoustic Sizing of an Ultrasound Contrast Agent**. *Ultrasound in Medicine & Biology* 36, 1713-1721 (2010).

D. Maresca, K. Jansen, G. Renaud, G. Van Soest, X. Li, Q. Zhou, N. De Jong, K. K. Shung, A. F. W. van der Steen, **Intravascular Ultrasound Chirp Imaging**. *Applied Physics Letters* **100**, (2012).

D. Maresca, G. Renaud, G. van Soest, X. Li, Q. Zhou, K. K. Shung, N. de Jong, A. F. W. van der Steen, **Contrast-Enhanced Intravascular Ultrasound Pulse Sequences for Bandwidth-Limited Transducers**. *Ultrasound in Medicine & Biology* **39**, 706-713 (2013).

D. Maresca, I. Skachkov, G. Renaud, K. Jansen, G. van Soest, N. de Jong, A. F. W. van der Steen, **Imaging Microvasculature with Contrast-Enhanced Ultraharmonic Ultrasound**. *Submitted*.

D. Maresca, S. Adams, B. Maresca, A. F. W van der Steen, **Lessons learned through a Sociological Study of IVUS Innovation**. *Submitted*

Conference presentations

D. Maresca, M. Muller, M. Emmer, H. J. Vos, N. de Jong, A. F. W. van der Steen, **Acoustic size distribution analyzer for microbubbles**. *Proceedings of the 2009 IEEE International Ultrasonics Symposium (IUS),* 1809-1812 (2009).

D. Maresca, M. Emmer, G. Springeling, F. Mastik, G. van Soest, N. de Jong, A. F. van der Steen, **Contrast-enhanced intravascular ultrasound 3D reconstruction of a vasa vasorum mimicking model**. *Proceedings of the 2010 IEEE International Ultrasonics Symposium (IUS),* 2364-2367 (2010).

A. van der Steen, G. van Soest, M. Emmer, D. Maresca, K. Jansen, F. Mastik, P. Serruys, E. Regar, **Intravascular ultrasound: Assessment of atherosclerosis**. *Proceedings of the 2010 Biomedical Imaging Symposium: From Nano to Macro,* 281-281 (2010).

D. Maresca, K. Jansen, G. Renaud, W. Den Dekker, G. Van Soest, X. Li, Q. Zhou, J. Cannata, K. K. Shung, A. F. W. Van Der Steen, **Intravascular ultrasound chirp imaging**.. *Proceedings of the 2011 IEEE International Ultrasonics Symposium (IUS)*, 2110-2113 (2011).

D. Maresca, G. Renaud, G. van Soest, N. de Jong, A. F. W. van der Steen, **Contrast-enhanced intravascular ultrasound imaging**. *Acoustics 2012, Congrès Français d'Acoustique (CFA)*, (2012).

D. Maresca, G. Renaud, G. van Soest, X. Li, Q. Zhou, K. K. Shung, N. de Jong, A. F. W. van der Steen, **Two contrast detection sequences for bandwidth-limited intravascular ultrasound transducers**. *Proceedings of the 2012 IEEE International Ultrasonics Symposium (IUS)*, (2012).

D. Maresca, I. Skachkov, G. Renaud, X. Li, Q. Zhou, K. K. Shung, G. van Soest, N. de Jong, A. F. W. van der Steen, ***In vivo* ultraharmonic contrast intravascular ultrasound observation of microvascular circulation**. *2012 IEEE International Ultrasonics Symposium (IUS)*, (2012).

Invited talks

D. Maresca, M. Emmer, P. L. van Neer, H. J. Vos, M. Versluis, M. Muller, N. de Jong, A. F. W. van der Steen, **Acoustic sizing of an ultrasound contrast agent**. *15th European symposium on Ultrasound Contrast Imaging*, (2010).

D. Maresca, K. Jansen, G. Renaud, W. Den Dekker, G. Van Soest, X. Li, Q. Zhou, J. Cannata, K. K. Shung, A. F. W. Van Der Steen, **Intravascular ultrasound chirp imaging***. *Proceedings of the 2011 IEEE International Ultrasonics Symposium (IUS)*, 2110-2113 (2011). ***student competition finalist, student travel support award**

D. Maresca, G. Renaud, G. van Soest, N. de Jong, A. F. W. van der Steen, **Contrast-enhanced intravascular ultrasound chirp imaging**. In *17th European symposium on Ultrasound Contrast Imaging*, (2012).

D. Maresca, I. Skachkov, G. Renaud, X. Li, Q. Zhou, K. K. Shung, G. van Soest, N. de Jong, A. F. W. van der Steen, **IVUS chirps for vasa vasorum imaging**. *8th International Conference on Ultrasonic Biomedical Microscanning*, (2012).

D. Maresca, T. Bore, R. Pillay, C. Lahanier, **The original Mona Lisa**. *Lustrum symposium of the Interuniversity Cardiology Institute of the Netherlands (ICIN)*, (2012).

PhD Portfolio

International conference attendance

	Date	ECTs
• IEEE International Ultrasonics Symposium, Beijing, China	11/2008	1.20
• 15th Ultrasound Contrast Imaging symposium, Rotterdam, the Netherlands	01/2009	0.60
• Vulnerable Plaque Meeting, Athens, Greece	06/2009	0.90
• IEEE International Ultrasonics Symposium, Rome, Italy	09/2009	1.20
• 16th Ultrasound Contrast Imaging symposium, Rotterdam, the Netherlands	01/2010	0.60
• IEEE International Ultrasonics Symposium, San Diego, USA	10/2010	1.20
• 17th Ultrasound Contrast Imaging symposium, Rotterdam, the Netherlands	01/2011	0.60
• IEEE International Ultrasonics Symposium, Orlando, USA	10/2011	1.20
• 1st Optics in Cardiology symposium 2011, Rotterdam, the Netherlands	12/2011	0.60
• 18h Ultrasound Contrast Imaging symposium, Rotterdam, the Netherlands	01/2012	0.60
• Acoustics 2012, Nantes, France	04/2012	1.50
• Ultrasonic Biomedical Microscanning conference, Saint Paulin, Canada	09/2012	1.20
• IEEE International Ultrasonics Symposium, Dresden, Germany	10/2012	1.20
• 19th Ultrasound Contrast Imaging symposium, Rotterdam, the Netherlands	01/2013	0.60
• 2nd Optics in Cardiology symposium 2013, Rotterdam, the Netherlands	03/2013	0.60

Conference Presentations

• Poster presentation - IEEE International Ultrasonics Symposium	09/2009	0.50
• Oral presentation - Ultrasound Contrast Imaging symposium	01/2010	1.00
• Poster presentation - IEEE International Ultrasonics Symposium	10/2010	0.50
• Student competition Poster - IEEE International Ultrasonics Symposium	10/2011	1.00
• Student competition Oral - IEEE International Ultrasonics Symposium	10/2011	2.00
• Oral presentation - Dutch Society for Medical Ultrasound meeting	11/2011	1.00
• Oral presentation - Ultrasound Contrast Imaging symposium	01/2012	1.00
• Oral presentation - Acoustics 2012	04/2012	1.00

- Oral presentation - Ultrasonic Biomedical Microscanning conference 2012 09/2012 1.00
- Oral presentation - IEEE International Ultrasonics Symposium 2012 10/2012 1.00
- **Poster** presentation - IEEE International Ultrasonics Symposium 2012 10/2012 0.50

Courses

- **Photoacoustics** - IEEE International Ultrasonics Symposium (IUS) 2008 11/2008 0.15
- **Ultrasound Contrast Agents** - IEEE IUS 2008 11/2008 0.15
- **Piezoelectric Transducer Fundamentals** - IEEE IUS 2009 09/2009 0.15
- **CMUTs: Theory, Technology and Applications** - IEEE IUS 2009 09/2009 0.15
- **The Art of Presenting Science** – FOM Foundation 12/2009 2.00
- **Cardiovascular Imaging and Diagnostics** - COEUR postgraduate school 04/2010 1.50
- **Ultrasound Signal Compression** - IEEE IUS 2010 10/2010 0.15
- **Medical ultrasound transducers** - IEEE IUS 2010 10/2010 0.15
- **Photoshop and Illustrator** - MolMed postgraduate school 03/2011 0.30
- **InDesign Workshop** - MolMed postgraduate school 05/2011 0.20
- **Ultrasound Imaging Systems** - IEEE IUS 2011 10/2011 0.15
- **Ultrafast Ultrasonic Imaging** - IEEE IUS 2012 10/2012 0.15

Research Seminars

- Dutch Society for Medical Ultrasound meeting, Rotterdam, the Netherlands 05/2009 0.30
- COEUR research seminar – Therapeutic use of microbubbles 07/2009 0.40
- COEUR keynote lecture – Angiogenesis and myocardial Ischemia 10/2009 0.15
- Dutch Society for Medical Ultrasound meeting, Twente, the Netherlands 04/2010 0.30
- COEUR research seminar – Imaging of atherosclerosis 12/2010 0.40
- COEUR research seminar – Detection of early atherosclerosis 03/2011 0.40
- Dutch Society for Medical Ultrasound meeting, Eindhoven, the Netherlands 11/2011 0.30
- Sound Light Symposium - Twente University, the Netherlands 11/2011 0.30

Total ECTs 32.05